Check for updates

Angewandte Chemie International Edition

Angewandte International Edition Chemie

How to cite: *Angew. Chem. Int. Ed.* **2026**, e2501228
doi.org/10.1002/anie.2501228

RESEARCH ARTICLE

Bioorthogonal Vitamin C Probes Enable Cellular Profiling and Investigation of Lysine Vitcylation

Wanting Wang[1] | Baoli Ding[2] | Shuqiao Yang[1] | Xuejie Li[1] | Jiawei Yang[1] | Zhiwan Zhou[1] | Sidong Xiao[1] | Xiadi He[3] | Cheng-Liang Zhu[2] | Shuai Zhang[1]

[1]Hubei Hongshan Laboratory, College of Biomedicine and Health, College of Life Science and Technology, Huazhong Agricultural University, Wuhan, China | [2]College of Pharmaceutical Sciences, Zhejiang University, Hangzhou, China | [3]Department of Endocrine and Metabolic Diseases, Shanghai Institute of Endocrine and Metabolic Diseases, National Clinical Research Center for Metabolic Diseases (Shanghai), Key Laboratory for Endocrine and Metabolic Diseases of the National Health Commission of the PR China, Lifecycle Health Management Center, Ruijin Hospital, Shanghai Jiao Tong University School of Medicine, Shanghai, China

Correspondence: Xiadi He (xiadi_he@shsmu.edu.cn) | Cheng-Liang Zhu (chengliangzhu@zju.edu.cn) | Shuai Zhang (shuaizhang@mail.hzau.edu.cn)

Received: 2 March 2026 | **Revised:** 4 October 2026 | **Accepted:** 5 October 2026

Keywords: biochemistry | bioorthogonal chemistry | cell biology | chemistry | intracellular | lysine | proteomics | proteome | ribosome biogenesis

ABSTRACT

Vitamin C is an essential micronutrient, yet its direct chemical engagement with the proteome remains poorly defined. Here, we develop and experimentally benchmark a bioorthogonal probe platform for labeling, profiling, and imaging of lysine vitcylation, a recently identified vitamin C-derived post-translational modification, in living cells. Chemoproteomic analysis and fluorescence imaging reveal a candidate vitcylome enriched in nucleolar proteins associated with ribonucleoprotein biogenesis and RNA processing, and reporter-derived lysine adducts on selected targets were validated by mass spectrometry. Time-resolved analyses demonstrate that intracellular vitcylation undergoes unexpectedly rapid remodeling, indicating active cellular regulation. Furthermore, a genome-wide CRISPR-Cas9 screen identifies glutathione S-transferase P1 (GSTP1) as an upstream regulator of global vitamin C-derived protein modification, linking vitcylation remodeling to cellular electrophile handling and redox homeostasis. Collectively, this platform provides a chemical framework for profiling, visualizing, and investigating protein vitcylation in living cells, and reveals vitcylation as a dynamic, spatially organized and regulated metabolic modification.

1 | Introduction

Metabolites are increasingly recognized as active chemical signals that regulate protein function through covalent post-translational modifications (PTMs) [1, 2]. Lysine acylations derived from metabolic intermediates [3], such as acetylation [4, 5], aminoacylation [6], succinylation [7], lactylation [8–10], and pyruvylation [11] have emerged as key mechanisms linking metabolic state to chromatin regulation, transcription, and cellular signaling. Their discovery and mechanistic analysis have been accelerated by selective antibodies and, critically, by chemical biology approaches that enable the visualization, enrichment, and direct characterization of metabolite-protein conjugates [12, 13].

Vitamin C (ascorbate) is an essential micronutrient with best-known roles as a cofactor for prolyl hydroxylases in collagen maturation [14] and for Fe^{2+}/α-ketoglutarate-dependent dioxygenases, including the ten-eleven translocation (TET) family of DNA demethylases [15]. Notably, under physiological conditions,

Wanting Wang, Baoli Ding, Shuqiao Yang, and Xuejie Li contributed equally to this work.

All rights reserved, including rights for text and data mining and training of artificial intelligence technologies or similar technologies.
© 2026 Wiley-VCH GmbH

active uptake through sodium-dependent vitamin C transporters (SVCTs) can maintain intracellular ascorbate at millimolar concentrations in certain tissues and cell types, including the brain, adrenal gland, and immune cells [16]. Beyond these canonical functions, ascorbate has recently been found to form a covalent lysine modification, termed vitcylation, through reaction of its electrophilic lactone moiety with protein nucleophiles [17]. This finding raises the intriguing possibility that vitamin C directly encodes metabolic information onto the proteome. However, the biological scope, subcellular organization, and regulatory principles of vitcylation have remained essentially unexplored, largely due to the absence of selective detection and enrichment strategies.

Chemical biology provides a powerful framework for overcoming such limitations [13, 18]. Bioorthogonal metabolic labeling—wherein a tagged metabolite analog is incorporated into biomolecules and subsequently visualized or enriched via click chemistry—has transformed the study of glycosylation [19, 20], lipidation [21–25], and diverse metabolite-derived protein modifications [26–31]. Whether vitamin C-derived PTMs are similarly accessible to metabolic tagging has remained an open question.

Here we describe and experimentally benchmark a bioorthogonal vitamin C probe platform for investigating lysine vitcylation in living cells. We first developed **VC-1**, an alkyne-functionalized ascorbate analog that forms lysine adducts similar to those generated by vitamin C in vitro. To overcome the limited membrane permeability of this probe, we synthesized a per-O-acetylated derivative (**VC-2**) that undergoes intracellular ester hydrolysis to release the free vitamin C reporter [32, 33]. This platform supports quantitative chemoproteomics and high-resolution imaging, revealing candidate vitcylation targets enriched in the nucleus, especially nucleolus, including proteins involved in ribonucleoprotein biogenesis and RNA processing. Time-resolved labeling uncovered that intracellular vitcylation is highly dynamic, undergoing rapid remodeling despite the intrinsic chemical stability of the vitcyl-lysine linkage. By integrating chemical profiling with a genome-wide CRISPR-Cas9 screen, we identified GSTP1 as an upstream metabolic regulator of global protein vitcylation. Collectively, this work establishes a bioorthogonal chemical framework for studying vitamin C-derived lysine modification and reveals vitcylation as a dynamic, spatially organized, and regulated metabolic modification.

2 | Results

2.1 | Development of Vitcylation Chemical Reporter

To investigate the landscape of vitamin C-mediated protein modification, we developed a bioorthogonal chemical reporter for protein vitcylation profiling. We designed and synthesized **VC-1**, an alkyne-functionalized analogue featuring a compact propargyl ether moiety at the C3 hydroxyl group of vitamin C (Figure 1a). **VC-1** retains the lactone-containing ascorbate scaffold while enabling subsequent conjugation to fluorophores or affinity handles through Cu(I)-catalyzed azide-alkyne cycloaddition (CuAAC).

We first characterized the lysine reactivity of **VC-1** using the synthetic peptide substrate Ac-YAPVAKDLASR. Tandem mass spectrometric analysis identified a **VC-1**-derived lysine adduct with a mass shift of +214.04774 Da (Figure 1b). Under analogous conditions, native ascorbate generated the corresponding +175.0242 Da lysine adduct (Figure S1a), where the mass difference of 39.02354 Da is consistent with the propargyl substituent introduced in **VC-1**. These results demonstrate that **VC-1** recapitulates the lysine-directed conjugation chemistry of native vitamin C in vitro.

Having established its reactivity, we next evaluated **VC-1** labeling in a complex proteome. Incubation of cell lysates with **VC-1**, followed by CuAAC with TAMRA-azide, revealed concentration-dependent protein labeling (Figure 1c). Importantly, this labeling was attenuated by competition with excess sodium ascorbate (NaVC) (Figure 1d), indicating that **VC-1** and vitamin C compete for protein modification.

We next evaluated the utility of **VC-1** for global chemoproteomic profiling. Probe-labeled proteins were conjugated to biotin-azide through click chemistry, enriched using streptavidin beads, and subjected to LC–MS/MS analysis. Quantitative proteomic analysis identified 2446 **VC-1**-enriched candidate proteins compared with the DMSO control (Figure 1e and Table S1). To increase the confidence of target identification, we performed a competition-based quantitative chemoproteomics in the presence of excess vitamin C, which prioritized 1094 competition-sensitive candidate vitcylation targets, including the previously reported substrate STAT1 (Figure 1f and Table S1) [17]. Together, these results establish **VC-1** as a chemical reporter for enrichment and chemoproteomic profiling of candidate vitamin C-modified proteins.

To assess whether the observed labeling behavior was unique to the 3-O reporter topology, we also synthesized the C6-O-propargyl regioisomer **6O-VC-1** (Figure S1b). This probe likewise produced concentration-dependent protein labeling in cell lysates, which was attenuated by excess NaVC (Figure S1c,d). These results indicate that the C6-O regioisomeric probe also supports vitamin C-derived protein labeling in cell lysates and provides an orthogonal comparator for assessing reporter-topology effects.

Although **VC-1** and **6O-VC-1** produced robust labeling in cell lysates, both showed negligible labeling in intact cells under the tested conditions (Figure S1e,f). This limited cellular labeling may reflect impaired recognition of the modified ascorbate scaffolds by SVCTs, together with limited cellular uptake due to their high polarity, thereby motivating the development of an O-acetylated pro-probe strategy for live-cell experiments.

2.2 | VC-2 Probe Enables Live-Cell Profiling of Candidate Vitcylation Targets

To overcome the limited cellular uptake of **VC-1** probe, we adopted a "pro-probe" strategy analogous to that used for bioorthogonal glycan reporters [32]. We synthesized **VC-2** by acetylating the hydroxyl groups of the **VC-1** scaffold to facilitate membrane permeation. Following cellular uptake, endogenous

15213773, 0, Downloaded from https://onlinelibrary.wiley.com/doi/10.1002/anie.2501228 by University Of British Columbia, Wiley Online Library on [12/10/2026]. See the Terms and Conditions (https://onlinelibrary.wiley.com/terms-and-conditions) on Wiley Online Library for rules of use; OA articles are governed by the applicable Creative Commons License

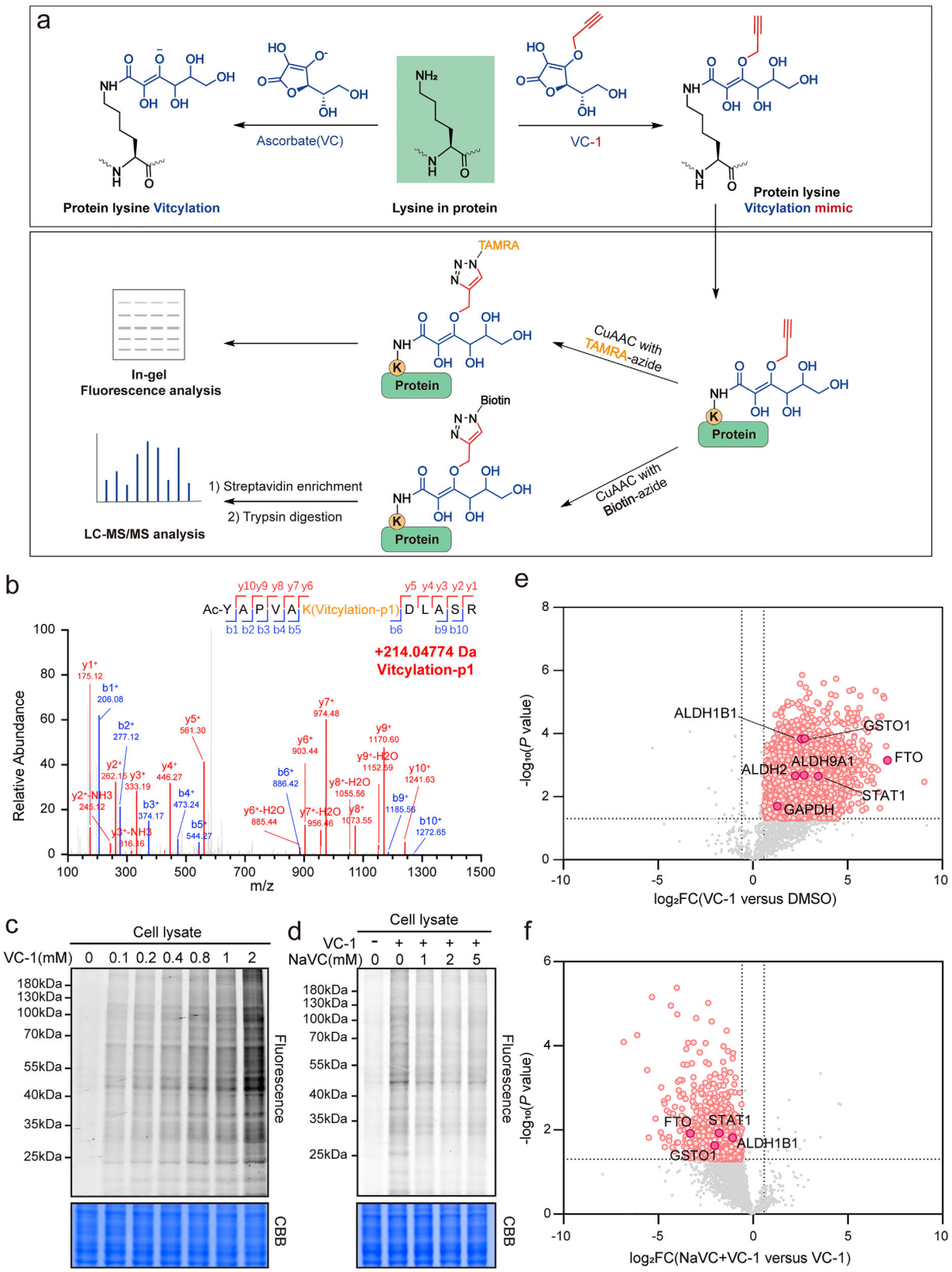


FIGURE 1 | **VC-1** is an alkyne-tagged vitcylation probe. (a) Schematic representation of native lysine vitcylation and the **VC-1** reporter workflow. Protein lysine vitcylation mimic can be conjugated to TAMRA-azide for in-gel fluorescence analysis or to biotin-azide for streptavidin enrichment and LC–MS/MS analysis. (b) Representative MS/MS spectrum of Ac-YAPVAKDLASR carrying a **VC-1**-derived lysine adduct (Vitcylation-p1, **VC-1**) with a mass shift of +214.0477 Da. The modified lysine is highlighted in orange, and the annotated b- and y-type fragment ions support site localization. (c) Concentration-dependent **VC-1** labeling in HEK293T cell lysates. Lysates were treated with the indicated concentrations of **VC-1** (3 h, 37°C). CBB staining served as a total-protein loading control. A representative gel from three independent experiments ($n = 3$) is shown. (d) NaVC competition of **VC-1** labeling in HEK293T cell lysates. Lysates were treated with **VC-1** (1 mM, 3 h, 37°C) in the presence of the indicated concentrations of NaVC (1 h,

15213773, 0, Downloaded from https://onlinelibrary.wiley.com/doi/10.1002/anie.2501228 by University Of British Columbia, Wiley Online Library on [12/10/2026]. See the Terms and Conditions (https://onlinelibrary.wiley.com/terms-and-conditions) on Wiley Online Library for rules of use; OA articles are governed by the applicable Creative Commons License

esterases are expected to hydrolyze the masking groups [33], regenerating **VC-1** probe in situ (Figure 2a). In contrast to the negligible labeling observed with **VC-1** in intact cells, **VC-2** produced robust, concentration-dependent protein labeling in living cells (Figure 2b). Importantly, this labeling was attenuated by pretreatment with excess vitamin C (Figure 2c), indicating that a measurable fraction of **VC-2**-derived protein labeling is sensitive to vitamin C competition. The weaker competition observed in intact cells than in lysates may reflect differences in uptake and intracellular processing: **VC-2** is delivered through a transporter-independent pro-probe strategy, whereas native vitamin C uptake is mediated by SVCTs [16, 34]. Notably, the same pro-probe strategy also enabled intracellular labeling with **6O-VC-2** (Figure S1g), the C6-modified analogue derived from **6O-VC-1** (Figure S1b). Moreover, **VC-2** efficiently labeled proteins across multiple mammalian cell lines, demonstrating its broad applicability for studying vitamin C-derived protein modification in living cells (Figure S1h).

To determine whether **VC-2** could report modification at a native vitcylation site, we performed LC–MS/MS analysis of STAT1, a previously reported vitcylation substrate. Following metabolic labeling of STAT1–FLAG-expressing cells and subsequent immunoprecipitation, LC–MS/MS analysis identified a +214.04774 Da modification on Lys298 (Figure 2d), corresponding to the deacetylated **VC-1** adduct. This result supports intracellular deacetylation of **VC-2** to regenerate **VC-1** reporter and demonstrates modification of the same STAT1 lysine residue previously reported for endogenous vitamin C-derived vitcylation. Consistent with this site-level evidence, **VC-2** also promoted STAT1 phosphorylation (Figure S2a), supporting its ability to reproduce a reported functional effect associated with vitamin C-derived STAT1 modification [17].

Leveraging the improved cellular permeability of **VC-2**, we next performed quantitative chemoproteomic profiling in living cells. Initial analysis identified 2663 VC-probe-enriched candidate proteins relative to the DMSO control (Figure 2e and Table S2). To increase the confidence of target identification and minimize probe-specific background, we incorporated competition-based quantitative chemoproteomics using excess vitamin C as an additional specificity filter. This analysis prioritized 1615 competition-sensitive candidate vitcylation targets, including the previously reported substrate STAT1 (Figure 2f and Table S2). Among competition-sensitive proteins, the median competition effect was smaller for **VC-2** in living cells (log2FC = −1.008) than for **VC-1** in lysates (log2FC = −1.527), consistent with the weaker global competition observed by in-gel fluorescence. Functional annotation of these candidate targets revealed significant enrichment in ribonucleoprotein complex biogenesis, noncoding RNA processing, and RNA splicing (Figure 2g and Table S3), suggesting a potential connection between vitamin C-derived protein modification and RNA metabolism.

2.3 | Biochemical Validation of VC-probe-enriched Candidate Vitcylation Targets

To validate the chemoproteomic results, we selected representative candidate target proteins for biochemical analysis. HEK293T cells expressing individual FLAG-tagged proteins were metabolically labeled with **VC-2**, followed by immunoprecipitation and Cu(I)-catalyzed azide–alkyne cycloaddition (CuAAC) with TAMRA-azide (Figure 3a). In-gel fluorescence analysis confirmed **VC-2**-dependent labeling of multiple candidates (Figure S2b). We further examined representative proteins by competition with excess native vitamin C, including several candidates showing strong competition in the quantitative chemoproteomic dataset, and observed corresponding reductions in **VC-2** labeling (Figure 3b), whereas the additional candidates examined showed smaller changes under the same conditions (Figure S2c). Together, these biochemical validation experiments were consistent with the chemoproteomic results and supported the reliability of the candidate identification workflow.

To obtain residue-level evidence, we performed LC–MS/MS analysis on immunoprecipitated target proteins. **VC-1**-modified adducts were identified at FTO Lys211/409, ALDH1B1 Lys414, ALDH9A1 Lys246/249/389, GSTO1 Lys114, and IMPDH1 Lys206/208 (Figures 3c,d and S3). These results provide direct evidence for covalent modification of specific lysine residues by the vitcylation reporter and establish a subset of VC-probe-enriched proteins as site-validated candidate targets.

To estimate the extent of protein modification, we performed complementary semi-quantitative enrichment analysis [35] and site-specific LC–MS/MS occupancy measurements for representative targets. Enrichment-based analysis (Figure S4a) indicated low apparent protein-level labeling occupancy on tested candidates, with estimated occupancy of approximately 1.12% for GSTO1 and below 1% for ALDH1B1, IMPDH1, and ALDH2 (Figure S4b). Consistently, targeted LC–MS/MS analysis estimated site-specific modification occupancies of 5.71% for GSTO1 Lys114 and 0.28% for ALDH1B1 Lys414 (Figure S4c). These measurements indicate that VC-derived lysine modifications occur at substoichiometric levels on the tested proteins and sites, consistent with the low occupancy commonly observed for many metabolically driven lysine acylations [36], which can nevertheless exert regulatory effects.

As a preliminary functional assessment, we examined the effect of vitamin C on the activity of GAPDH, which was identified as a VC-probe-enriched candidate vitcylation target in our chemopro-

37°C). A representative gel from three independent experiments ($n = 3$) is shown. (e) Volcano plot comparing proteins enriched from HEK293T cell lysates treated with **VC-1** (1 mM) versus DMSO. Proteins significantly enriched by **VC-1** ($\log_2$FC > 0.5849 and $p < 0.05$) are shown in red. Data were obtained from three biological replicates per group ($n = 3$), and p values were calculated using two-tailed Student's t-test. (f) Volcano plot comparing protein enriched from HEK293T cell lysates treated with **VC-1** (1 mM) in the presence versus absence of excess competing NaVC (5 mM). Negative values indicate proteins whose **VC-1**-dependent enrichment was attenuated by NaVC. NaVC-competitive candidates meeting the thresholds $\log_2$FC < −0.5849 and $p < 0.05$ are shown in red. Data were obtained from three biological replicates per group ($n = 3$), and p values were calculated using two-tailed Student's t-test.

15213773, 0, Downloaded from https://onlinelibrary.wiley.com/doi/10.1002/anie.202501228 by University Of British Columbia, Wiley Online Library on [12/10/2026]. See the Terms and Conditions (https://onlinelibrary.wiley.com/terms-and-conditions) on Wiley Online Library for rules of use; OA articles are governed by the applicable Creative Commons License

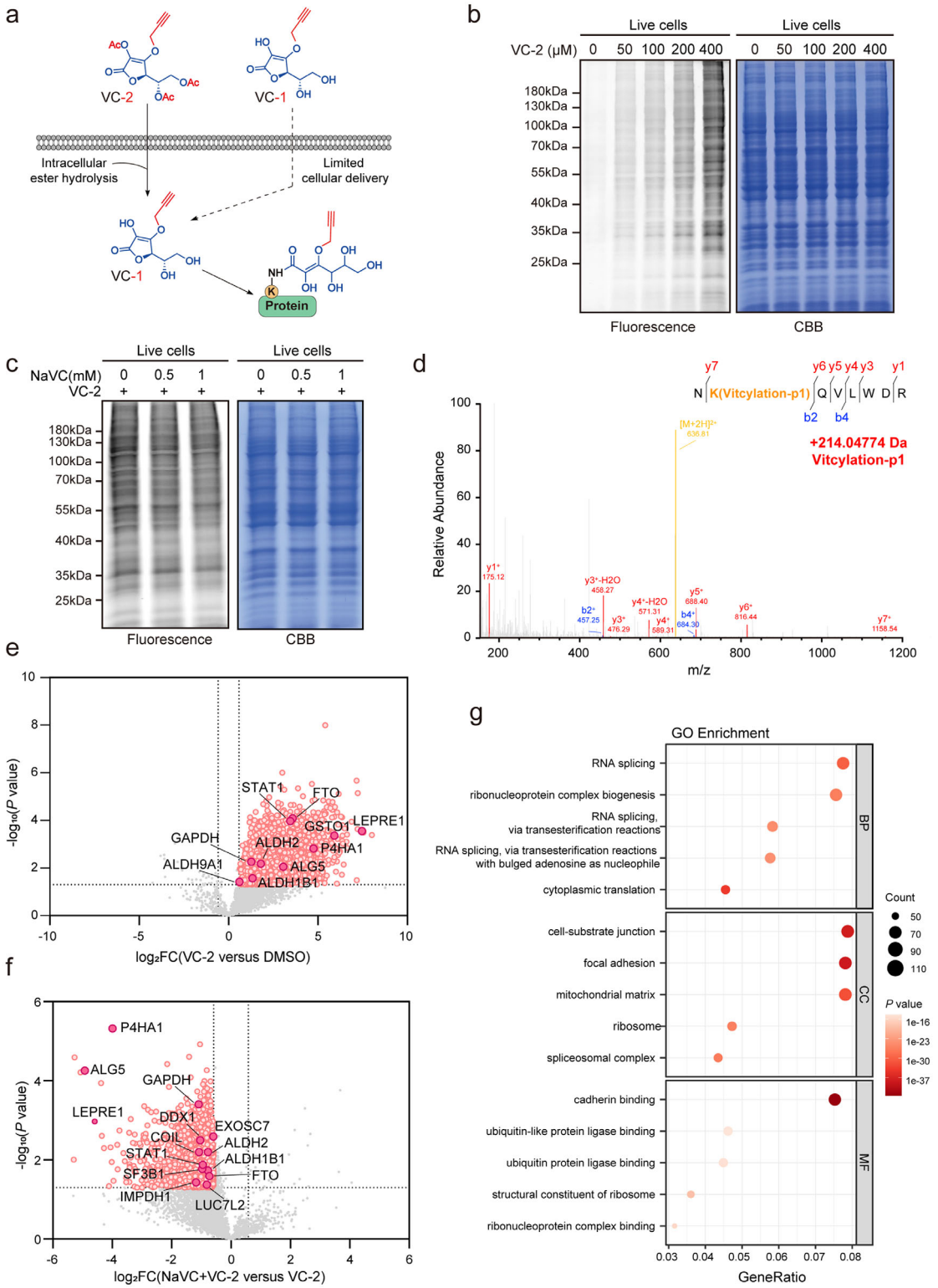


FIGURE 2 | **VC-2** probe enables live-cell profiling of candidate vitcylation targets. (a) Proposed cell-delivery and intracellular-unmasking strategy for **VC-2**. O-acetyl ester masking in **VC-2** improves cellular delivery and is expected to undergo intracellular ester hydrolysis to unmask the clickable vitcylation reporter. (b) Concentration-dependent **VC-2** labeling in HEK293T cells. Cells were treated with the indicated concentrations of **VC-2**, followed by CuAAC with TAMRA-azide and in-gel fluorescence analysis. Coomassie Brilliant Blue (CBB) staining served as a total-protein loading control. A representative gel from three independent experiments is shown. (c) NaVC competition of **VC-2**-derived labeling in intact HEK293T cells. Cells were treated with **VC-2** (200 μM, 1 h) in the absence or presence of NaVC (500 or 1000 μM, 16 h). CBB staining served as a total-protein loading control. (d) Representative MS/MS spectrum of the STAT1 peptide carrying a VC-reporter-derived lysine adduct at Lys298 with a mass shift of +214.0477 Da from **VC-2**-treated HEK293T cells expressing FLAG-tagged STAT1. The modified lysine is highlighted in orange, and annotated fragment ions support site localization. (e) Volcano plot comparing proteins enriched from HEK293T cells treated with **VC-2** (400 μM) versus DMSO. Proteins significantly enriched

15213773, 0, Downloaded from https://onlinelibrary.wiley.com/doi/10.1002/anie.2501228 by University Of British Columbia, Wiley Online Library on [12/10/2026]. See the Terms and Conditions (https://onlinelibrary.wiley.com/terms-and-conditions) on Wiley Online Library for rules of use; OA articles are governed by the applicable Creative Commons License

teomic analysis. LC–MS/MS further identified Lys194 (K194) as a vitcylation site on GAPDH (Figure S5a). In an in vitro enzymatic assay, exposure to NaVC reduced GAPDH activity across the tested pH range, with more pronounced effects at pH 7.8 and 8.0 (Figure S5b). Notably, the K194R mutant retained enzymatic activity but showed partial resistance to NaVC-induced inhibition compared with wild-type GAPDH (Figure 3e), suggesting that modification at K194 contributes to the vitamin C-dependent regulation of GAPDH activity. Although the incomplete protection afforded by K194R indicates that additional sites or other vitamin C-dependent mechanisms may also contribute, these findings provide site-specific evidence linking K194 modification to the modulation of GAPDH activity by vitamin C under defined conditions.

2.4 | Nucleolar Enrichment of the Candidate Vitcylome is Associated With RNA-Processing Pathways

To define the subcellular organization of the vitamin C-derived protein modification, we performed high-resolution fluorescence imaging of cells metabolically labeled with **VC-2**. We observed a striking compartmentalization: while a basal signal was detectable in the cytosol, the **VC-2**-derived labeling signal was predominantly enriched within the nucleus (Figure 4a). To ensure that this localization was not an artifact of the metabolic labeling workflow, we performed a parallel control using the established S-palmitoylation probe, Alk-14 [22]. In contrast to **VC-2**, Alk-14 exhibited characteristic membrane localization, confirming that the nuclear signal is specific to the probe scaffold. Notably, the nuclear **VC-2**-derived labeling signal was more concentrated into 2–4 bright, spherical condensates—morphology characteristic of liquid-liquid phase separation (LLPS) [37, 38]. Co-staining with the marker Fibrillarin (FBL) confirmed that these dense puncta represent the nucleolus (Figure 4b).

To determine whether this enrichment relies on active ribosomal RNA transcription—the primary function of the nucleolus—we perturbed nucleolar architecture using Actinomycin D (ActD) [39, 40]. In vehicle-treated cells, the **VC-2**-derived labeling signal colocalized well with FBL. However, following ActD-induced transcriptional arrest, we observed a dramatic spatial divergence. While FBL underwent characteristic dispersion from nucleolus, the **VC-2**-derived labeling signal remained intact as distinct nuclear puncta (Figure 4c).

This unexpected resistance to ActD-induced disassembly suggests that vitcylation does not merely tag transiently associating RNA-binding proteins. Instead, it also appears to mark a stable structural scaffold or a specific phase-separated core within the nucleolus. Consistent with this observation, our VC-probe-enriched candidate vitcylation targets are strongly enriched in RNA splicing and ribonucleoprotein complex biogenesis (Figure 2g). Representative candidates include core spliceosomal components (e.g., SRSF1, SF3B1, PRPF8, and U2AF2), nucleolar structural proteins (NPM1 and COIL), RNA helicases (DDX1, DDX17, and DHX9), and RNA exosome subunits (EXOSC2, EXOSC7, and EXOSC9). Many of these proteins function as structural or assembly factors that remain stably associated with preribosomal complexes and RNA-processing machinery rather than behaving as transient enzymatic clients [38, 41, 42]. Together, the preferential enrichment of these structural and RNA-processing proteins provides a plausible explanation for the persistence of **VC-2**-positive condensates following ActD treatment. Although further studies will be required to determine which of these proteins undergo endogenous vitcylation, these findings suggest that **VC-2**-derived labeling preferentially associates with nucleolar structural and RNA-processing networks.

To provide biological context for the chemoproteomic findings, we performed RNA sequencing (RNA-seq) following vitamin C treatment. We observed minimal fluctuations in global transcript abundance (Figure S6 and Table S4). In contrast, vitamin C treatment induced widespread alterations in alternative splicing events (Figure 4d and Table S5). Although these transcriptional responses cannot be directly attributed to protein vitcylation, they are consistent with our chemoproteomic observation that VC-probe-enriched candidate vitcylation targets are highly enriched in RNA splicing and ribonucleoprotein complex biogenesis.

Gene Ontology (GO) analysis of the alternatively spliced transcripts revealed enrichment in pathways involved in RNA metabolism and chromatin regulation, including ncRNA and tRNA processing, endoribonuclease activity, RNA turnover, and histone acetyltransferase (HAT) and deacetylase complexes (Figure 4e and Table S6). Notably, these functional categories substantially overlap with those identified by chemoproteomic profiling of the candidate vitcylome. While the transcriptomic changes likely reflect the combined biological activities of vitamin C, their concordance with the proteomic dataset supports the hypothesis that vitcylation may contribute to the regulation of nucleolar RNA-processing networks. Selective perturbation of vitcylation globally or at defined proteins will be required to test a causal relationship.

2.5 | VC-2-Derived Protein Labeling Changes Over Time and is Modulated by GSTP1

To delineate time-dependent changes in intracellular **VC-2**-derived protein labeling, we performed time-dependent labeling

by **VC-2** ($\log_2$FC > 0.5849 and $p < 0.05$) are shown in red. Data were obtained from three biological replicates per group (n = 3). *P* values were calculated using two-tailed Student's t-test. (f) Volcano plot comparing protein enriched from HEK293T cells treated with **VC-2** (400 μM) in the presence versus absence of excess competing NaVC (4 mM). Negative values indicate proteins whose **VC-2**-dependent enrichment was attenuated by NaVC. NaVC-competitive candidates meeting the thresholds $\log_2$FC < −0.5849 and $p < 0.05$ are shown in red. Data were obtained from three biological replicates per group ($n = 3$). *P* values were calculated using two-tailed Student's *t*-test. (g) Gene Ontology (GO) enrichment analysis of the NaVC-competitive candidate set. Dot size indicates the number of proteins, color indicates enrichment significance, and the x-axis indicates GeneRatio. BP, biological process; CC, cellular component; MF, molecular function.

15213773, 0, Downloaded from https://onlinelibrary.wiley.com/doi/10.1002/anie.202501228 by University Of British Columbia, Wiley Online Library on [12/10/2026]. See the Terms and Conditions (https://onlinelibrary.wiley.com/terms-and-conditions) on Wiley Online Library for rules of use; OA articles are governed by the applicable Creative Commons License

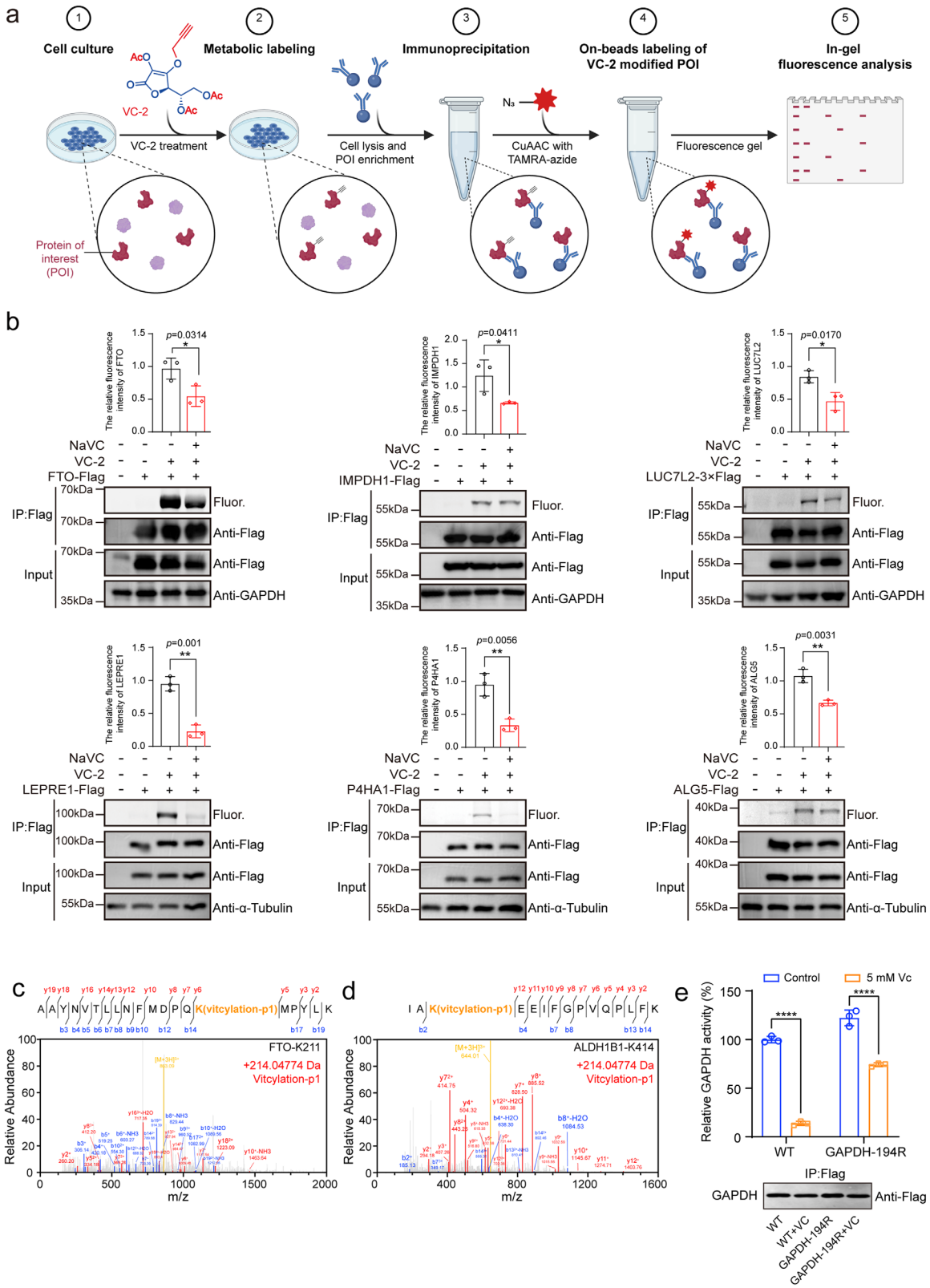


FIGURE 3 | Biochemical and site-level validation of representative VC-probe-enriched candidates. (a) Workflow for immunoprecipitation-coupled fluorescence analysis of **VC-2**-derived labeling. Cells expressing a Flag-tagged protein of interest were labeled with **VC-2**, lysed, and subjected to anti-Flag immunoprecipitation. Immunoprecipitated proteins were labeled on beads by CuAAC with TAMRA-azide and analyzed by in-gel fluorescence. Workflow created with BioRender.com. (b) Vitamin C competition of **VC-2**-derived labeling for selected candidate proteins. HEK293T cells expressing the indicated Flag-tagged proteins were treated with **VC-2** (200 μM, 1 h) in the absence or presence of excess NaVC (4 mM, 16 h) followed by anti-Flag immunoprecipitation, on-beads CuAAC with TAMRA-azide, and in-gel fluorescence analysis. Fluorescent signals were normalized to the immunoprecipitated protein signal. Data are shown as mean ± SEM from three independent biological replicates. *p* values are indicated above the bar

15213773, 0, Downloaded from https://onlinelibrary.wiley.com/doi/10.1002/anie.2501228 by University Of British Columbia, Wiley Online Library on [12/10/2026]. See the Terms and Conditions (https://onlinelibrary.wiley.com/terms-and-conditions) on Wiley Online Library for rules of use; OA articles are governed by the applicable Creative Commons License

experiments using the **VC-2** probe. We observed a distinct biphasic labeling profile: the signal accumulated rapidly, peaking at 1–2 h, but underwent a sharp decline by 4 h, returning to near-baseline levels by 24 h. Notably, this biphasic profile was consistently observed in both Huh7 and HEK293T cell lines (Figures 5a and S7a), indicating the generality of the phenomenon. This time-dependent loss of labeling contrasts with the persistence of stable chemical adducts such as protein glycation [43], suggesting the existence of active regulatory mechanisms. Crucially, this time-dependent loss of signal was unique to the live-cell environment. Incubation of **VC-1** or **VC-2** with cell lysates, either under native (1% NP-40) or denaturing (2% SDS) conditions, resulted in stable labeling with no appreciable decay over time (Figure S7b–d). Similarly, **VC-1** labeling of lysates from cells overexpressing individual substrate proteins remained stable (Figure S7e). In parallel, western blot analysis showed no appreciable changes in the protein abundance labeled by **VC-2** during the chase period in cells (Figure S7f). However, unchanged total protein abundance does not exclude turnover of a selectively modified subpopulation. Consistently, inhibition of proteasomal degradation by MG132 or lysosomal degradation by chloroquine (CQ) produced slight increases in fluorescence under some conditions but did not prevent the time-dependent decline in **VC-2**-derived protein labeling (Figure S7g,h), suggesting that the observed decrease in labeling signal is unlikely to be primarily driven by global turnover of modified proteins. This discrepancy indicates that the decline of **VC-2**-derived protein labeling is not due to intrinsic chemical instability of the vitcyl-lysine bond or the modified proteins, but is potentially driven by active cellular regulatory mechanisms.

We next examined whether canonical lysine deacylation pathways contribute to the decline in **VC-2**-derived labeling. Pharmacological inhibition of histone deacetylases (HDACs) and sirtuins using trichostatin A (TSA) [44] and nicotinamide (NAM) (Figure 5b,c) [45], as well as inhibition of O-GlcNAcase with Thiamet G (TMG) (Figure S7i) [46], failed to delay the decline in labeling. Combined inhibition of HDACs and sirtuins did not further attenuate the decline in labeling (Figure S7j). These data suggest that **VC-2**-derived labeling is not regulated by the canonical enzymatic machinery governing acetylation or glycosylation, and the molecular processes responsible for the signal decline remain to be determined.

To systematically identify factors controlling this dynamic modification cycle, we conducted a fluorescence-activated cell sorting (FACS)-based genome-wide CRISPR-Cas9 screen (Figure 5d). Huh7 cells were transduced with a lentiviral whole-genome sgRNA library and, after puromycin selection, labeled with **VC-2**. After cell fixation, **VC-2**-labeled proteins were fluorescently tagged via CuAAC with TAMRA-azide, and cells were sorted into high labeling (top 5%), low labeling (bottom 5%), and unchanged (middle 50%) populations. Enriched sgRNAs were quantified by next-generation sequencing and analyzed using MAGeCK [47, 48].

This screen revealed metabolic and regulatory factors associated with **VC-2**-derived labeling. Among the top-enriched hits whose disruption increased the labeling signal were *GSTP1*, *RPTOR*, *DGAT2*, and *MBTPS1* (Figure 5e,f and Table S7). In contrast, the low labeling population was enriched for genes including *PSMB3*, *DDX6*, and *PLCG1* (Figure S8a,b and Table S8). The screen did not reveal an obvious candidate hydrolase or deacylase among the strongest hits. Instead, the prominent enrichment of GSTP1, a glutathione S-transferase involved in electrophile detoxification and redox regulation [49], implicated cellular electrophile-handling capacity as an upstream regulator of protein vitcylation.

Consistent with the screen results, GSTP1 depletion increased global **VC-2** labeling (Figure 5g) while overexpression of GSTP1 decreased the labeling (Figure 5h). Although no commercial or broadly validated pan-vitcyllysine antibody is currently available, an in-house antibody detected increased native vitamin C-induced vitcyllysine signal upon GSTP1 depletion, providing orthogonal support for its effect on cellular vitamin C-derived lysine modification (Figure S8c). Interestingly, time-course experiments showed that GSTP1 loss not only increased the overall **VC-2** labeling level but also delayed the decline of the labeling signal (Figures 5i and S8d). However, in pulse-chase experiments, although GSTP1-deficient cells exhibited a higher initial post-pulse labeling intensity, the relative decay kinetics after probe removal were not substantially altered (Figures 5j and S8e). These results indicate that GSTP1 primarily influences the formation or accumulation of vitamin C-derived modification rather than directly controlling its subsequent decay.

Together with the established role of GSTP1 in electrophile detoxification, these findings support a model in which GSTP1 modulates the availability, reactivity, or lifetime of reactive vitamin C-derived species upstream of protein vitcylation modification.

3 | Discussion

In this study, we developed and experimentally benchmarked a bioorthogonal vitamin C reporter platform for labeling, visualizing, and profiling vitamin C-derived lysine modification in living cells. The probes preserve the core chemistry of vitamin C-derived lysine modification while incorporating a bioorthogonal handle for imaging and affinity enrichment. By integrating probe design, vitamin C competition, quantitative chemoproteomics, imaging,

graphs and were calculated using unpaired two-tailed Student's *t*-test. Differences with $p < 0.05$ were considered statistically significant. *$p < 0.05$, ** $p < 0.01$. (c) Representative MS/MS spectrum identifying a VC-reporter-derived lysine adduct (Vitcylation-p1, **VC-1**) at FTO Lys211 from **VC-2**-treated HEK293T cells expressing FLAG-tagged FTO. (d) Representative MS/MS spectrum identifying a VC-reporter-derived lysine adduct (Vitcylation-p1, **VC-1**) at ALDH1B1 Lys414 from **VC-2**-treated HEK293T cells expressing FLAG-tagged ALDH1B1. (e) HEK293T cells overexpressing FLAG-tagged GAPDH WT or K194R were treated with vehicle or 5 mM NaVC for 2 h. GAPDH was immunoprecipitated with anti-FLAG antibody, and its activity was measured by NADH oxidation at 340 nm. Data are shown as mean ± SEM from three independent experiments. Statistical significance was evaluated using Two-way ANOVA. Differences with $p < 0.05$ were considered statistically significant. ****$p < 0.0001$.

15213773, 0, Downloaded from https://onlinelibrary.wiley.com/doi/10.1002/anie.202501228 by University Of British Columbia, Wiley Online Library on [12/10/2026]. See the Terms and Conditions (https://onlinelibrary.wiley.com/terms-and-conditions) on Wiley Online Library for rules of use; OA articles are governed by the applicable Creative Commons License

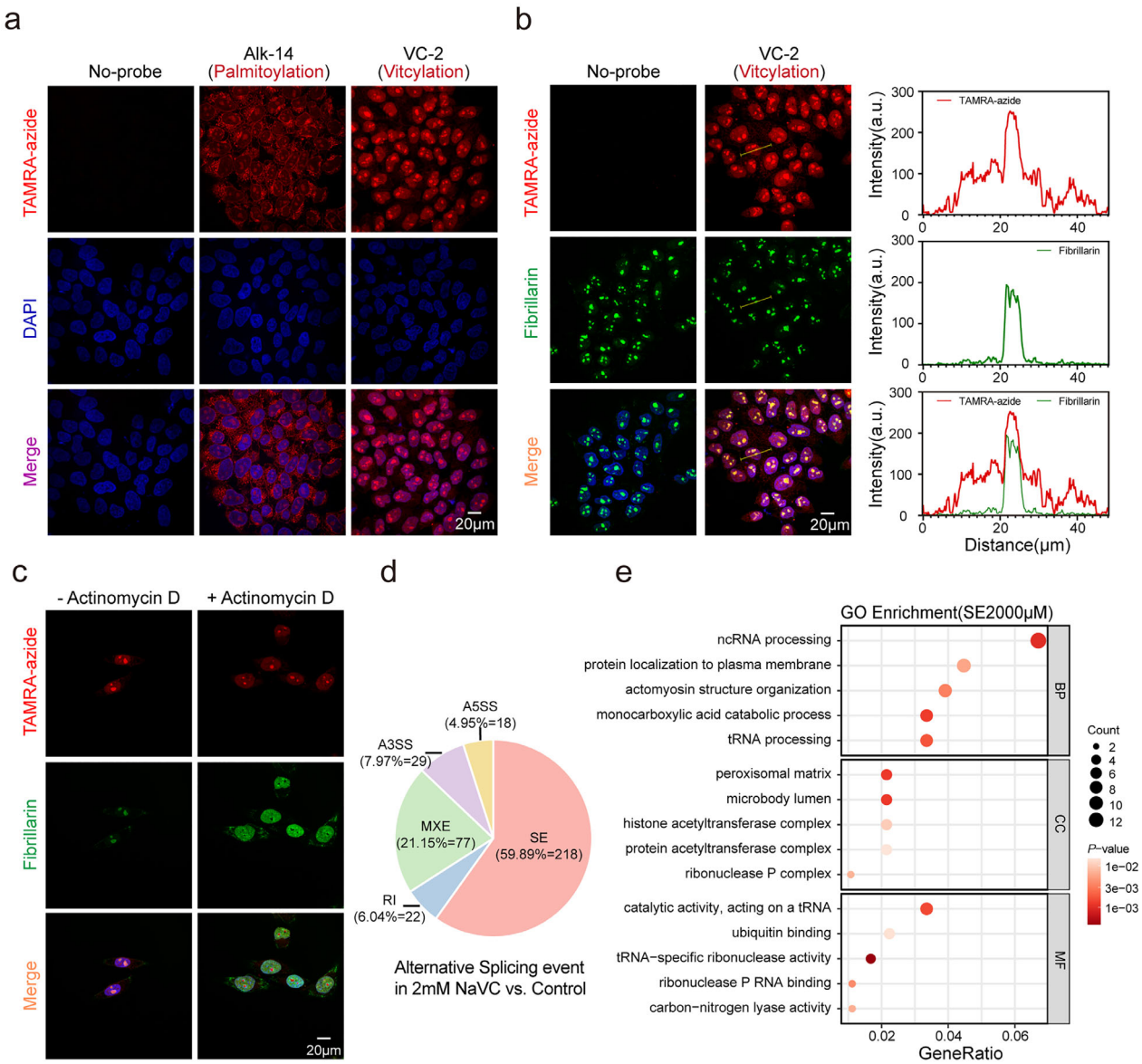


FIGURE 4 | **VC-2**-derived labeling persists in nucleolar structures. (a) Fluorescence imaging of **VC-2**-derived labeling in HeLa cells. Alk-14, an S-palmitoylation reporter, and DMSO treatment were included as controls. Nuclei were stained with DAPI. $n = 3$ independent biological replicates. (b) Colocalization of **VC-2**-derived labeling (red) with the nucleolar marker fibrillarin (green) in HeLa cells. Representative line-scan intensity profiles are shown. $n = 3$ independent biological replicates. (c) Effect of actinomycin D (ActD, 10 μg/mL) on fibrillarin localization and **VC-2**-derived labeling patterns in HeLa cells. $n = 3$ independent biological replicates. (d) Distribution of alternative splicing events in HEK293T cells treated with 2 mM NaVC versus control. Data were obtained from three biological replicates per group ($n = 3$). (e) Gene Ontology (GO) enrichment analysis of alternatively spliced transcripts, grouped by biological process (BP), cellular component (CC), and molecular function (MF).

and functional genomics, we provide a practical framework for studying the cellular organization and regulation of protein vitcylation.

Using this platform, we generated a proteome-wide map of VC-probe-enriched candidate vitcylation targets, validated representative proteins by in-gel fluorescence analysis, and identified some modification sites by LC–MS/MS. These candidates showed a pronounced enrichment in ribonucleoprotein biogenesis, noncoding RNA processing, and RNA splicing, revealing a previously unexplored connection between vitamin C chemistry and RNA-associated cellular processes. However, as for other metabolite-derived PTM discovery efforts, probe-based enrichment provides a candidate discovery resource rather than a definitive inventory of endogenous vitcylation substrates. Probe-specific behavior, intracellular probe exposure, and indirect enrichment may also contribute to the dataset and its limited overlap with native vitcylation datasets. Future studies integrating endogenous modification detection, site-specific validation, and mechanistic characterization will be essential to determine the physiological roles of individual vitcylation events.

Spatially, **VC-2**-derived protein labeling exhibits a striking enrichment within the nucleus, particularly in the nucleolus. Proteomic and imaging analyses converge on a model in which **VC-2** preferentially labels stable nucleolar assemblies involved in ribosome

15213773, 0, Downloaded from https://onlinelibrary.wiley.com/doi/10.1002/anie.202501228 by University Of British Columbia, Wiley Online Library on [12/10/2026]. See the Terms and Conditions (https://onlinelibrary.wiley.com/terms-and-conditions) on Wiley Online Library for rules of use; OA articles are governed by the applicable Creative Commons License

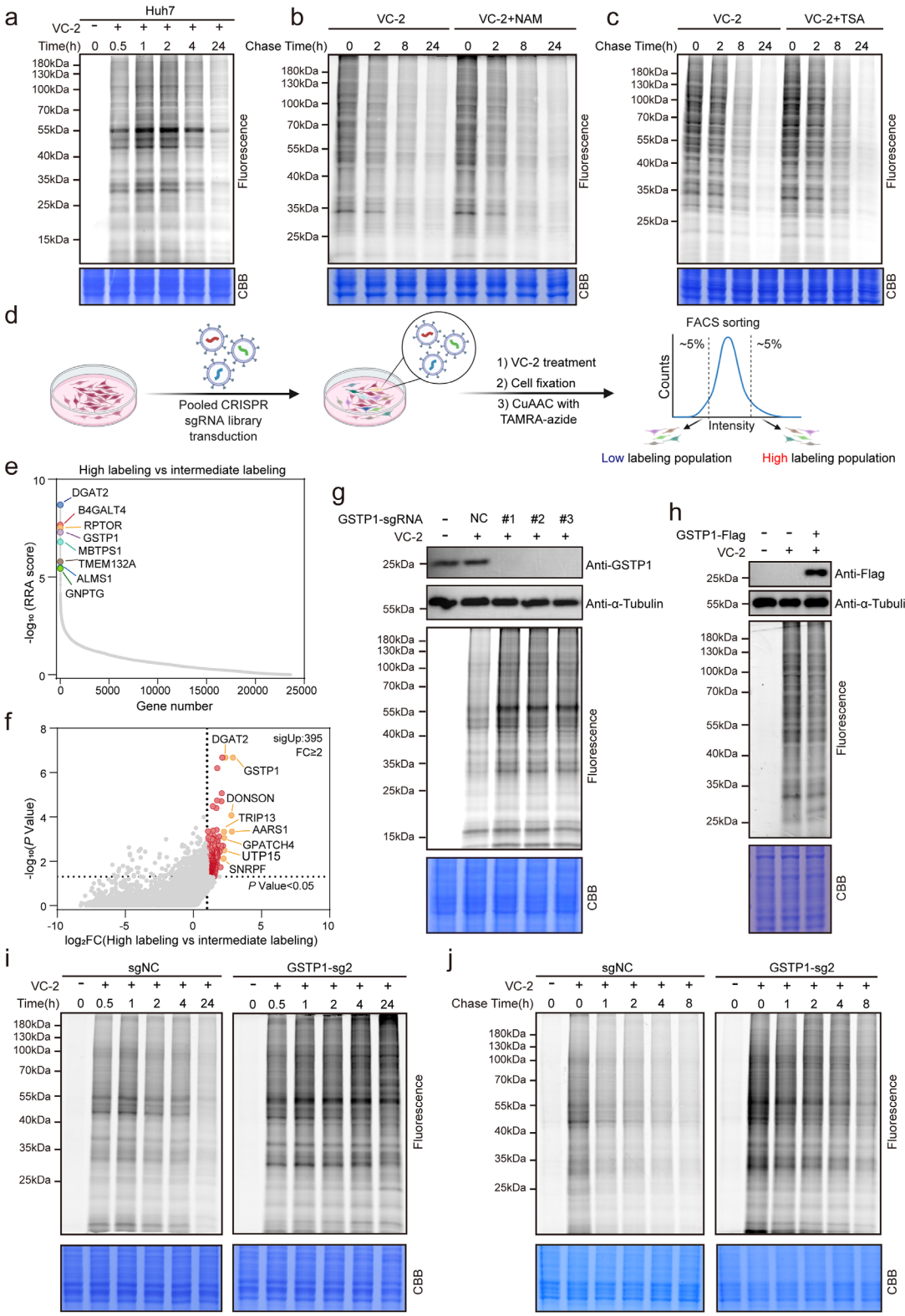


FIGURE 5 | GSTP1 modulates cellular vitamin C-derived lysine modification. (a) Time-dependent protein labeling with **VC-2** (200 μM) in Huh7 cells. (b–c) Pulse-chase analysis of **VC-2**-derived labeling dynamics in HEK293T cells treated with NAM (2 mM; b) or TSA (0.4 μM; c). HEK293T cells were labeled with **VC-2** (200 μM, 1 h), washed, and chased for the indicated times. (d) Schematic overview of the FACS-based genome-wide CRISPR screening workflow in Huh7 cells to identify regulators of vitcylation dynamics. Workflow created with BioRender.com. (e) Robust rank aggregation (RRA) analysis of genes enriched in the high labeling population. (f) Volcano plot depicting the screening hits. The x-axis represents gene-level $\log_2$ fold change (LFC) of high labeling versus unchanged populations. The y-axis shows the -log10(*p* value) calculated by MAGeCK. (g) GSTP1 knockout increases **VC-2** labeling in Huh7 cells. (h) GSTP1 overexpression decreases **VC-2** labeling in HEK293T cells. (i) Time-dependent protein labeling with **VC-2** in *GSTP1* KO Huh7 cells. (j) Pulse-and-chase analysis of **VC-2** labeling dynamics in *GSTP1* KO Huh7 cells.

15213773, 0, Downloaded from https://onlinelibrary.wiley.com/doi/10.1002/anie.2501228 by University Of British Columbia, Wiley Online Library on [12/10/2026]. See the Terms and Conditions (https://onlinelibrary.wiley.com/terms-and-conditions) on Wiley Online Library for rules of use; OA articles are governed by the applicable Creative Commons License

biogenesis, including components of the SSU processome, RNA exosome, and associated architectural factors. The persistence of nucleolar labeling following transcriptional inhibition by actinomycin D further suggests that these modifications are associated with relatively stable ribonucleoprotein scaffolds rather than transient RNA-binding interactions. These observations raise the possibility that vitamin C-derived lysine modification contributes to the organization of ribonucleoprotein biogenesis and RNA-processing machineries.

An unexpected finding of this study is the time-dependent remodeling of intracellular **VC-2**-derived protein labeling. Despite the chemical stability of the vitcyl-lysine bond in vitro, vitcylation labeling signals declined in living cells, suggesting active cellular control of the modified state. Inhibitors of HDACs, sirtuins, and O-GlcNAcase did not substantially alter this decay, and our genome-wide CRISPR screen did not identify a dedicated devitcylase or acylase pathway. Instead, the screen revealed GSTP1 as a key regulator of this modification landscape: GSTP1 depletion increased, whereas GSTP1 overexpression decreased, global protein vitcylation. Pulse-and-chase analysis further showed that GSTP1 primarily affects the initial abundance of the modified state rather than its subsequent decay kinetics. Given the established role of GSTP1 in glutathione-dependent electrophile detoxification and redox buffering, these findings support a model in which GSTP1 may regulate vitamin C-derived lysine modification by controlling the availability, lifetime, or reactivity of reactive ascorbate species.

More broadly, our findings expand the conceptual landscape of vitamin C biology. In addition to serving as an enzymatic cofactor and antioxidant, vitamin C directly encodes metabolic information onto the proteome via covalent modification. Vitcylation thus joins a growing class of metabolite-derived PTMs that blur the classical distinction between metabolism and signaling. The chemical platform described here provides a foundation for future studies aimed at dissecting the physiological roles of vitcylation in development, stress adaptation, and disease, and raises the possibility that nutritional vitamin C status may exert regulatory effects through direct proteomic wiring.

In summary, we developed an experimentally benchmarked bioorthogonal chemical strategy for interrogating vitamin C-derived lysine modification in living systems. Application of this platform revealed a spatially organized and dynamically modulated landscape of protein vitcylation and identified GSTP1 as an upstream metabolic regulator. Together, these findings provide a versatile chemical biology platform for studying vitamin C-derived protein modification and lay the groundwork for defining the physiological functions of vitcylation in health and disease.

Author Contributions

S.Z., C.-L.Z., and X.H. conceived of the study and supervised the research. W.W. performed most of the experiments. B.D. synthesized chemical probes developed in this study. S.Y. performed proteomic and bioinformatics analyses. X.L. performed the CRISPR-Cas9 screen. J.Y. and Z.Z. contributed to plasmid construction. S.X. contributed to biochemical experiments. S.Z., W.W., C.-L.Z., and X.H. wrote the paper with input from all authors. All authors prepared the figures and edited the manuscript.

Acknowledgments

We are grateful to Prof. Fan Yao (Huazhong Agricultural University) for his generous help with the CRISPR screen experiments and insightful suggestions. Fluorescence gel results were acquired at the National Key Laboratory of Agricultural Microbiology Core facility. Mass spectrometry experiments were conducted with the assistance of the Multi-Omics Mass Spectrometry Core at the Biomedical Research Core Facilities (BRCF), Shenzhen Bay Laboratory. This work was supported by the Fundamental Research Funds for the Central Universities (2662024SYPY002 to S.Z.), the Natural Science Foundation of Zhejiang Province (LZ25H300002 to C.-L.Z.) and the National Natural Science Foundation of China (32541021 to X.H.).

Conflicts of Interest

The authors declare the following competing financial interest: A patent application has been filed by Zhejiang University and Deep PTM Biotechnology Limited related to the compounds and methods described in this manuscript, on which C.-L.Z., S.Z., B.D., W.W., S.Y., and X.H. are listed as inventors. The remaining authors declare no conflicts of interest.

Data Availability Statement

The data that support the findings of this study are available in the supplementary material of this article. The mass spectrometry proteomics data have been deposited to the ProteomeXchange Consortium via iProX under accession PXD081327/IPX0018333000. The RNA-seq transcriptomic data have been deposited in the Gene Expression Omnibus (GEO) database under accession number GSE339167.

References

1. B. Zhang and F. C. Schroeder, "Mechanisms of Metabolism-Coupled Protein Modifications," *Nature Chemical Biology* 21 (2025): 819–830, https://doi.org/10.1038/s41589-024-01805-z.

2. D. Zhang, Z. Tang, H. Huang, et al., "Metabolic Regulation of Gene Expression by Histone Lactylation," *Nature* 574 (2019): 575–580, https://doi.org/10.1038/s41586-019-1678-1.

3. K. Huang, Y. Wang, B. Li, et al., "Acylation Modification-Mediated Metabolism Reprogramming in Cancer," *iScience* 28 (2025): 113883.

4. E. Verdin and M. Ott, "50 years of Protein Acetylation: From Gene Regulation to Epigenetics, Metabolism and Beyond," *Nature Reviews Molecular Cell Biology* 16 (2015): 258–264, https://doi.org/10.1038/nrm3931.

5. A. Eftekhari, U. Sabir, and T. Kasumov, "The Role of Lysine Acetylation in Metabolic Sensing and Proteostasis," *Pharmacology & Therapeutics* 274 (2025): 108908, https://doi.org/10.1016/j.pharmthera.2025.108908.

6. X.-D. He, W. Gong, J.-N. Zhang, et al., "Sensing and Transmitting Intracellular Amino Acid Signals Through Reversible Lysine Aminoacylations," *Cell Metabolism* 27 (2018): 151–166.e6, https://doi.org/10.1016/j.cmet.2017.10.015.

7. K. F. Kubatzky, Y. Gao, and D. Yu, "Post-Translational Modulation of Cell Signalling Through Protein Succinylation," *Exploration of Targeted Anti-Tumor Therapy* 4 (2023): 1260–1285, https://doi.org/10.37349/etat.2023.00196.

8. H. Ren, Y. Tang, and D. Zhang, "The Emerging Role of Protein L-lactylation in Metabolic Regulation and Cell Signalling," *Nature Metabolism* 7 (2025): 647–664, https://doi.org/10.1038/s42255-025-01259-0.

9. Z. Lin, F. Long, J. Liu, et al., "Metabolic Reprogramming Promotes Apoptosis Resistance in Acute Lymphoblastic Leukemia Through CASP3 Lactylation," *Molecular cancer* 24 (2025): 204, https://doi.org/10.1186/s12943-025-02392-w.

15213773, 0, Downloaded from https://onlinelibrary.wiley.com/doi/10.1002/anie.202501228 by University Of British Columbia, Wiley Online Library on [12/10/2026]. See the Terms and Conditions (https://onlinelibrary.wiley.com/terms-and-conditions) on Wiley Online Library for rules of use; OA articles are governed by the applicable Creative Commons License

10. X. Sheng, H. Lin, P. A. Cole, and Y. Zhao, "Biochemistry and Regulation of Histone Lysine L-Lactylation," *Nature Reviews Molecular Cell Biology* 27 (2026): 95–109, https://doi.org/10.1038/s41580-025-00876-7.

11. X. Song, P. Peng, H. Zheng, et al., "Lysine Pyruvylation Couples Glycolytic Flux to Epigenetic Regulation," *Nature Metabolism* 8 (2026): 1495–1507.

12. M. Grammel and H. C. Hang, "Chemical Reporters for Biological Discovery," *Nature Chemical Biology* 9 (2013): 475–484, https://doi.org/10.1038/nchembio.1296.

13. C. G. Parker and M. R. Pratt, "Click Chemistry in Proteomic Investigations," *Cell* 180 (2020): 605–632, https://doi.org/10.1016/j.cell.2020.01.025.

14. J. M. Pullar, A. C. Carr, and M. C. M. Vissers, "The Roles of Vitamin C in Skin Health," *Nutrients* 9 (2017): 866, https://doi.org/10.3390/nu9080866.

15. J. I. Young, S. Züchner, and G. Wang, "Regulation of the Epigenome by Vitamin C," *Annual Review of Nutrition* 35 (2015): 545–564, https://doi.org/10.1146/annurev-nutr-071714-034228.

16. M. Doseděl, E. Jirkovský, K. Macáková, et al., "Vitamin C—Sources, Physiological Role, Kinetics, Deficiency, Use, Toxicity, and Determination," *Nutrients* 13 (2021): 615, https://doi.org/10.3390/nu13020615.

17. X. He, Q. Wang, X. Cheng, et al., "Lysine Vitcylation Is a Vitamin C-derived Protein Modification That Enhances STAT1-Mediated Immune Response," *Cell* 188 (2025): 1858–1877.e21, https://doi.org/10.1016/j.cell.2025.01.043.

18. J. A. Prescher and C. R. Bertozzi, "Chemistry in Living Systems," *Nature Chemical Biology* 1 (2005): 13–21, https://doi.org/10.1038/nchembio0605-13.

19. M. M. Mukherjee, D. Biesbrock, L. K. Abramowitz, et al., "Selective Bioorthogonal Probe for *N*-Glycan Hybrid Structures," *Nature Chemical Biology* 21 (2025): 681–692, https://doi.org/10.1038/s41589-024-01756-5.

20. M. Kufleitner, L. M. Haiber, S. Li, et al., "Next-Generation Metabolic Glycosylation Reporters Enable Detection of Protein O−GlcNAcylation in Living Cells Without S -Glyco Modification," *Angewandte Chemie International Edition* 63 (2024): e202320247, https://doi.org/10.1002/anie.202320247.

21. B. R. Martin and B. F. Cravatt, "Large-Scale Profiling of Protein Palmitoylation in Mammalian Cells," *Nature Methods* 6 (2009): 135–138, https://doi.org/10.1038/nmeth.1293.

22. G. Charron, M. M. Zhang, J. S. Yount, et al., "Robust Fluorescent Detection of Protein Fatty-Acylation With Chemical Reporters," *Journal of the American Chemical Society* 131 (2009): 4967–4975, https://doi.org/10.1021/ja810122f.

23. H. C. Hang and M. E. Linder, "Exploring Protein Lipidation With Chemical Biology," *Chemical Reviews* 111 (2011): 6341–6358, https://doi.org/10.1021/cr2001977.

24. E. Thinon, R. A. Serwa, M. Broncel, et al., "Global Profiling of Co- and Post-Translationally *N*-Myristoylated Proteomes in Human Cells," *Nature Communications* 5 (2014): 4919, https://doi.org/10.1038/ncomms5919.

25. T. Peng, E. Thinon, and H. C. Hang, "Proteomic Analysis of Fatty-Acylated Proteins," *Current Opinion in Chemical Biology* 30 (2016): 77–86, https://doi.org/10.1016/j.cbpa.2015.11.008.

26. Y. Sun, Y. Chen, and T. Peng, "A Bioorthogonal Chemical Reporter for the Detection and Identification of Protein Lactylation," *Chemical Science* 13 (2022): 6019–6027, https://doi.org/10.1039/D2SC00918H.

27. Y.-Y. Yang, J. M. Ascano, and H. C. Hang, "Bioorthogonal Chemical Reporters for Monitoring Protein Acetylation," *Journal of the American Chemical Society* 132 (2010): 3640–3641, https://doi.org/10.1021/ja908871t.

28. Q. Tang, Y. Guo, L. Meng, and X. Chen, "Chemical Tagging of Protein Lipoylation," *Angewandte Chemie International Edition* 60 (2021): 4028–4033, https://doi.org/10.1002/anie.202010981.

29. Y.-F. Zhou, S. Yuan, B. Ma, J. Gao, and C. Wang, "Chemical Proteomic Profiling of Lysine Crotonylation Using Minimalist Bioorthogonal Probes in Mammalian Cells," *Chemical Science* 16 (2025): 2843–2849, https://doi.org/10.1039/D4SC06745B.

30. M. Gao, Q. Wan, S. Zhou, P. Wu, W. Nie, and S. Chen, "Chemoselective Tagging of Protein Methacrylation," *Journal of the American Chemical Society* 147 (2025): 43699–43706, https://doi.org/10.1021/jacs.5c13826.

31. X. Bao, Q. Zhao, T. Yang, Y. M. E. Fung, and X. D. Li, "A Chemical Probe for Lysine Malonylation," *Angewandte Chemie International Edition* 52 (2013): 4883–4886, https://doi.org/10.1002/anie.201300252.

32. B. Cheng, Q. Tang, C. Zhang, and X. Chen, "Glycan Labeling and Analysis in Cells and In Vivo," *Annual Review of Analytical Chemistry* 14 (2021): 363–387, https://doi.org/10.1146/annurev-anchem-091620-091314.

33. N. Barlow, D. K. Chalmers, B. J. Williams-Noonan, P. E. Thompson, and R. S. Norton, "Improving Membrane Permeation in the Beyond Rule-of-Five Space by Using Prodrugs to Mask Hydrogen Bond Donors," *ACS Chemical Biology* 15 (2020): 2070–2078, https://doi.org/10.1021/acschembio.0c00218.

34. H. Tsukaguchi, T. Tokui, B. Mackenzie, et al., "A Family of Mammalian na+-Dependent L-Ascorbic Acid Transporters," *Nature* 399 (1999): 70–75, https://doi.org/10.1038/19986.

35. P. Li, Y. Zhang, C. Kim, and Y. Yu, "A Large-Scale Method to Measure the Stoichiometries of Protein Poly-ADP-Ribosylation," *ACS Chemical Biology* 21 (2026): 527–545, https://doi.org/10.1021/acschembio.5c00817.

36. B. K. Hansen, R. Gupta, L. Baldus, et al., "Analysis of Human Acetylation Stoichiometry Defines Mechanistic Constraints on Protein Regulation," *Nature Communications* 10 (2019): 1055, https://doi.org/10.1038/s41467-019-09024-0.

37. B. R. Sabari, A. Dall'Agnese, and R. A. Young, "Biomolecular Condensates in the Nucleus," *Trends in Biochemical Sciences* 45 (2020): 961–977, https://doi.org/10.1016/j.tibs.2020.06.007.

38. D. L. J. Lafontaine, J. A. Riback, R. Bascetin, and C. P. Brangwynne, "The Nucleolus as a Multiphase Liquid Condensate," *Nature Reviews Molecular Cell Biology* 22 (2021): 165–182, https://doi.org/10.1038/s41580-020-0272-6.

39. R. P. Perry and D. E. Kelley, "Inhibition of RNA Synthesis by Actinomycin D: Characteristic Dose-Response of Different RNA Species," *Journal of Cellular Physiology* 76 (1970): 127–139, https://doi.org/10.1002/jcp.1040760202.

40. M. Chen and P. Jiang, "Altered Subcellular Distribution of Nucleolar Protein Fibrillarin by Actinomycin D in HEp-2 Cells," *Acta Pharmacologica Sinica* 25 (2004): 902–906.

41. M. R. Puno and C. D. Lima, "Structural Basis for RNA Surveillance by the Human Nuclear Exosome Targeting (NEXT) Complex," *Cell* 185 (2022): 2132–2147.e26, https://doi.org/10.1016/j.cell.2022.04.016.

42. G.-Q. Zhu, Z. Tang, T.-H. Chu, et al., "Targeting SRSF1 Improves Cancer Immunotherapy by Dually Acting on CD8+T and Tumor Cells," *Signal Transduction Targeted Therapy* 10 (2025): 25, https://doi.org/10.1038/s41392-024-02118-2.

43. M. S. Martin, J. W. Jacob-Dolan, V. T. T. Pham, N. M. Sjoblom, and R. A. Scheck, "The Chemical Language of Protein Glycation," *Nature Chemical Biology* 21 (2025): 324–336, https://doi.org/10.1038/s41589-024-01644-y.

44. D. M. Vigushin, S. Ali, P. E. Pace, et al., "Trichostatin a is a Histone Deacetylase Inhibitor With Potent Antitumor Activity Against Breast Cancer In Vivo," *Clinical Cancer Research* 7 (2001): 971–976.

45. A. A. Sauve, C. Wolberger, V. L. Schramm, and J. D. Boeke, "The Biochemistry of Sirtuins," *Annual Review of Biochemistry* 75 (2006): 435–465, https://doi.org/10.1146/annurev.biochem.74.082803.133500.

46. M. S. Macauley and D. J. Vocadlo, "Increasing O-GlcNAc Levels: An Overview of Small-Molecule Inhibitors of O-GlcNAcase," *Biochimica Et Biophysica Acta* 1800 (2010): 107–121, https://doi.org/10.1016/j.bbagen.2009.07.028.

15213773, 0, Downloaded from https://onlinelibrary.wiley.com/doi/10.1002/anie.2501228 by University Of British Columbia, Wiley Online Library on [12/10/2026]. See the Terms and Conditions (https://onlinelibrary.wiley.com/terms-and-conditions) on Wiley Online Library for rules of use; OA articles are governed by the applicable Creative Commons License

47. B. Wang, M. Wang, W. Zhang, et al., "Integrative Analysis of Pooled CRISPR Genetic Screens Using MAGeCKFlute," *Nature Protocols* 14 (2019): 756–780, https://doi.org/10.1038/s41596-018-0113-7.

48. W. Li, H. Xu, T. Xiao, et al., "MAGeCK Enables Robust Identification of Essential Genes From Genome-Scale CRISPR/Cas9 Knockout Screens," *Genome Biology* 15 (2014): 554, https://doi.org/10.1186/s13059-014-0554-4.

49. A. Chatterjee and S. Gupta, "The Multifaceted Role of Glutathione S-Transferases in Cancer," *Cancer Letters* 433 (2018): 33–42, https://doi.org/10.1016/j.canlet.2018.06.028.

Supporting Information

Additional supporting information can be found online in the Supporting Information section.

Supporting File 1: anie75289-sup-0001-SuppMat.docx.

Supporting File 2: anie75289-sup-0002-S1.xlsx.

Supporting File 3: anie75289-sup-0003-S2.xlsx.

Supporting File 4: anie75289-sup-0004-S3-S4.xlsx.

Supporting File 5: anie75289-sup-0005-S5.xlsx.

Supporting File 6: anie75289-sup-0006-S6-S9.xlsx.

Supporting File 7: anie75289-sup-0007-SuppMat.pdf.

Supporting File 8: anie75289-sup-0008-SuppMat.xlsx.

15213773, 0, Downloaded from https://onlinelibrary.wiley.com/doi/10.1002/anie.2501228 by University Of British Columbia, Wiley Online Library on [12/10/2026]. See the Terms and Conditions (https://onlinelibrary.wiley.com/terms-and-conditions) on Wiley Online Library for rules of use; OA articles are governed by the applicable Creative Commons License

Supporting Information

Bioorthogonal Vitamin C Probes Enable Cellular Profiling and Investigation of Lysine Vitcylation

Wanting Wang[1#], Baoli Ding[2#], Shuqiao Yang[1#], Xuejie Li[1#], Jiawei Yang[1], Zhiwan Zhou[1], Sidong Xiao[1], Xiadi He[3*], Cheng-Liang Zhu[2*], Shuai Zhang[1*]

Affiliations:

[1]Hubei Hongshan Laboratory, College of Biomedicine and Health, College of Life Science and Technology, Huazhong Agricultural University, Wuhan, 430070, China.

[2]College of Pharmaceutical Sciences, Zhejiang University, Hangzhou, 310058, China.

[3]Department of Endocrine and Metabolic Diseases, Shanghai Institute of Endocrine and Metabolic Diseases, National Clinical Research Center for Metabolic Diseases (Shanghai), Key Laboratory for Endocrine and Metabolic Diseases of the National Health Commission of the PR China, Lifecycle Health Management Center, Ruijin Hospital, Shanghai Jiao Tong University School of Medicine, Shanghai 200025, China.

[#]These authors contributed equally to this work.

*Correspondence to: shuaizhang@mail.hzau.edu.cn, chengliangzhu@zju.edu.cn, xiadi_he@shsmu.edu.cn

Table of Contents

1. Chemical Synthesis and Characterization 4

1.1 Synthesis of VC-1 (3O-VC-1) 4

1.2 Synthesis of VC-2 (3O-VC-2) 6

1.3 Synthesis of 6O-VC-1 7

1.4 Synthesis of 6O-VC-2 10

2. Biological Experimental Methods 12

2.1 Cell culture and transfection 12

2.2 CuAAC click reaction and in-gel fluorescence analysis 12

2.3 Protein labeling in cell lysates using VC probes 12

2.4 Metabolic labeling in mammalian cells with VC-2 13

2.5 Chemoproteomic profiling of vitcylated proteins 13

2.6 LC-MS/MS analysis 14

2.7 LC-MS/MS and PRM-based targeted analysis of Lysine Vitcylation-p1 15

2.8 Plasmid construction 17

2.9 Site-directed mutagenesis 17

2.10 Generation of GSTP1 knockout Huh7 cells 18

2.11 Immunoprecipitation and immunoblot assays 18

2.12 Western blot analysis 19

2.13 VC-1 labeling of overexpressed proteins in cell lysates 19

2.14 Sample Preparation for Stoichiometry Measurement 20

2.15 Immunofluorescence microscopy 21

2.16 FACS-based CRISPR screening 21

2.17 GAPDH activity assay 22

2.18 Flow cytometry 23

2.19 RNA-seq and data analysis 23

2.20 Bioinformatic Analysis 24

2.21 Statistical Analysis 24

3. Supplementary Figures 25

4. Supplementary Tables 36

5. Source Data 36

6. NMR Spectra, HPLC and HRMS Reports 36

6.1 NMR Spectra 37

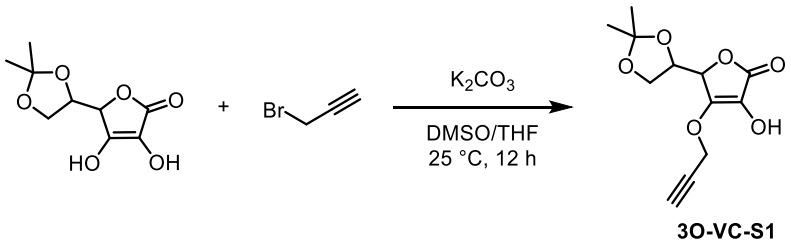
6.2 HPLC and HRMS Analysis Reports 45

7. Reference 48

1. Chemical Synthesis and Characterization

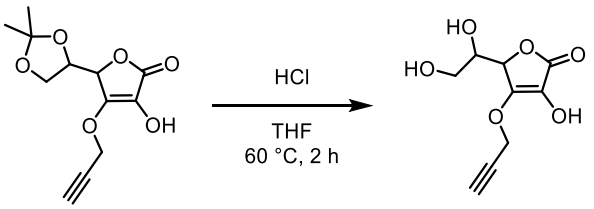
Unless otherwise noted, reagents and solvents were used as received. Column chromatography was performed on silica gel unless otherwise specified. ^{1}H and ^{13}C NMR spectra were recorded at the indicated field strengths. Chemical shifts (δ) are reported in ppm and coupling constants (*J*) are reported in Hz.

1.1 Synthesis of VC-1 (3O-VC-1)



5,6-*O*-Isopropylidene-*L*-ascorbic acid (5.00 g, 23.0 mmol, 1.0 equiv.) and K_2CO_3 (1.60 g, 11.5 mmol, 0.5 equiv.) were dissolved in a mixed solvent of DMSO (26 mL) and THF (24 mL). The mixture was stirred at room temperature for 20 min, and propargyl bromide (2.70 g, 23.0 mmol, 1.0 equiv.) was added dropwise. The reaction mixture was stirred at room temperature for 12 h. After completion as monitored by TLC, the reaction was quenched with water (50 mL) and extracted with EtOAc (50 mL × 3). The combined organic layers were dried over anhydrous Na_2SO_4, filtered, and concentrated under reduced pressure. The crude residue was purified by silica gel column chromatography (EtOAc/hexanes = 1:6) to afford **3O-VC-S1** as a white solid (1.73 g, 30% yield).

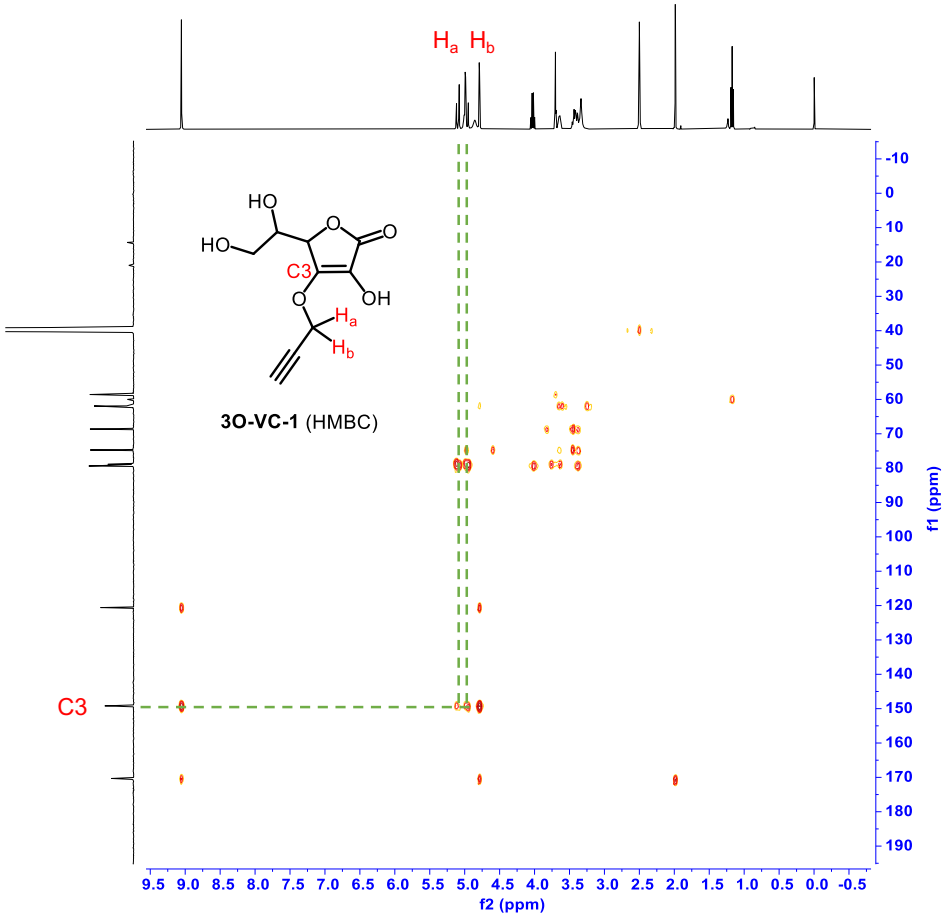
3-*O*-Propargyl-5,6-*O*-isopropylidene-*L*-ascorbic acid (3O-VC-S1): ^{1}H NMR (400 MHz, DMSO-d_6) δ 9.26 (s, 1H), 5.08 (dd, *J* = 15.6, 2.4 Hz, 1H), 5.01 (dd, *J* = 15.6, 2.4 Hz, 1H), 4.84 (d, *J* = 2.8 Hz, 1H), 4.22 (ddd, *J* = 7.1, 6.0, 2.8 Hz, 1H), 4.10 (dd, *J* = 8.5, 7.0 Hz, 1H), 3.86 (dd, *J* = 8.5, 6.1 Hz, 1H), 3.72 (t, *J* = 2.4 Hz, 1H), 1.26 (s, 3H), 1.25 (s, 3H). ^{13}C NMR (100 MHz, DMSO-d_6) δ 169.8, 148.6, 120.8, 109.4, 79.6, 78.7, 74.4, 73.5, 65.0, 58.7, 26.0, 25.5. LC-MS (ESI, m/z): calcd for $C_{12}H_{15}O_6^+$, $[M + H]^+$ 255.08, found 254.90.



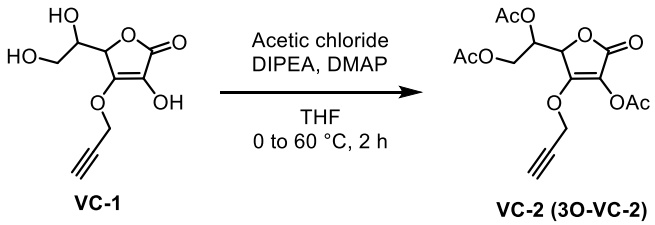
3O-VC-S1 **VC-1 (3O-VC-1)**

Compound **3O-VC-S1** (2.34 g, 9.20 mmol, 1.0 equiv.) was dissolved in THF (23 mL), and 12 *N* HCl (2.3 mL) was added. The reaction mixture was heated at 60 °C for 2 h. After completion as monitored by TLC, the solvent was removed under reduced pressure, and the crude residue was purified by silica gel column chromatography (EtOAc/hexanes = 1:1) to afford **VC-1 (3O-VC-1)** as pale brown oil (1.72 g, 87% yield).

3-*O*-Propargyl-*L*-ascorbic acid (VC-1, **3O-VC-1):** ^{1}H NMR (400 MHz, DMSO-d_6) δ 9.05 (s, 1H), 5.10 (dd, J = 15.5, 2.4 Hz, 1H), 5.02–4.95 (m, 2H), 4.86 (s, 1H), 4.79 (d, J = 1.4 Hz, 1H), 3.70 (t, J = 2.4 Hz, 1H), 3.68–3.61 (m, 1H), 3.47–3.38 (m, 2H). ^{13}C NMR (100 MHz, DMSO-d_6) δ 170.3, 149.2, 120.6, 79.4, 78.9, 74.7, 68.6, 61.9, 58.6. HRMS (APCI, m/z): calcd for $C_9H_{11}O_6^+$, $[M + H]^+$ 215.0550, found 215.0553. Note: the regiochemistry of **VC-1 (3O-VC-1)** was established by HMBC (H7a/7b and C3 HMBC correlations shown below).

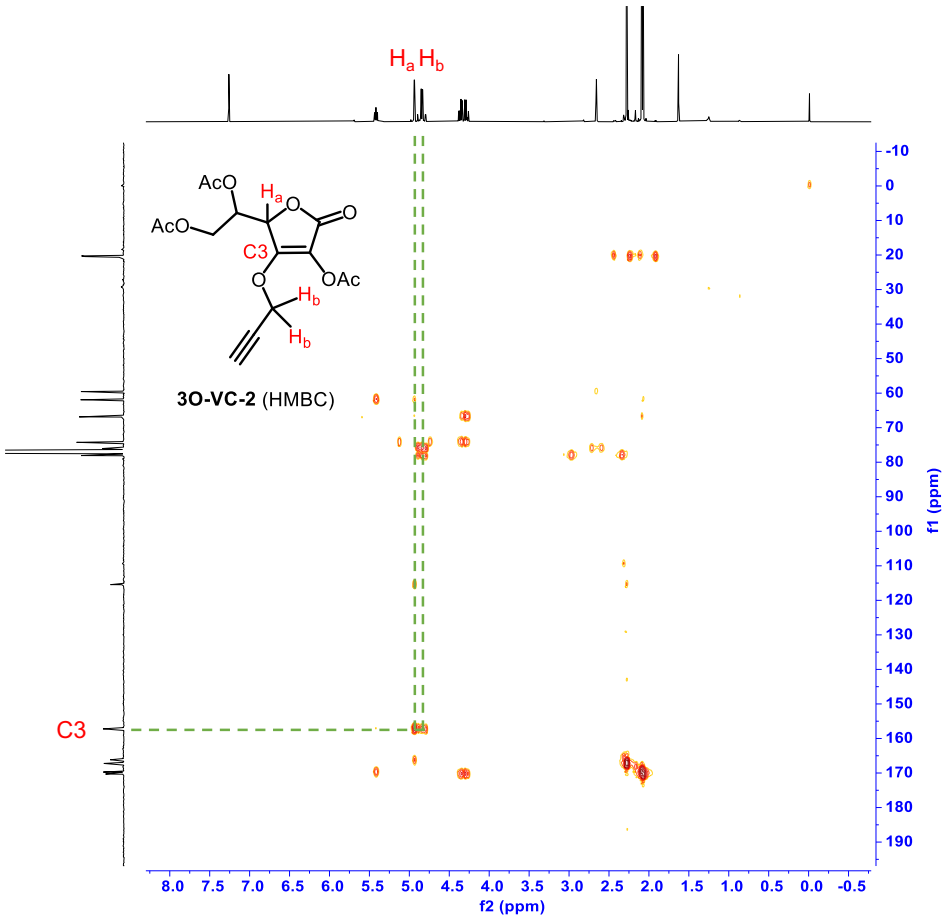


1.2 Synthesis of VC-2 (3O-VC-2)

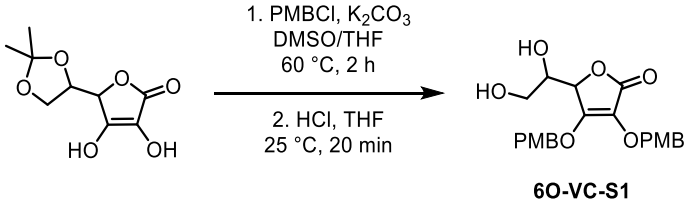


Compound **VC-1** (1.20 g, 5.60 mmol, 1.0 equiv.) and DMAP (68 mg, 0.56 mmol, 0.1 equiv.) were dissolved in anhydrous THF (12 mL). Acetyl chloride (2.2 mL, 30.8 mmol, 5.5 equiv.) and DIPEA (3.1 mL, 17.9 mmol, 3.2 equiv.) were added sequentially at 0 °C. The reaction mixture was warmed to room temperature and stirred for 30 min, then heated at 60 °C for 2 h. After completion as monitored by TLC, the solvent was removed under reduced pressure, and the residue was quenched with water (15 mL) and extracted with CH_2Cl_2 (15 mL × 3). The combined organic layers were dried over anhydrous Na_2SO_4, filtered, and concentrated. The crude residue was purified by silica gel column chromatography (EtOAc/hexanes = 1:4) to afford **VC-2** (**3O-VC-2**) as yellow oil (1.21 g, 64% yield).

2,5,6-Tri-*O*-acetyl-3-*O*-propargyl-*L*-ascorbic acid (VC-2, 3O-VC-2): ^{1}H NMR (400 MHz, $CDCl_3$) δ 5.42 (ddd, *J* = 7.0, 6.0, 1.7 Hz, 1H), 4.94 (d, *J* = 1.7 Hz, 1H), 4.87 (dd, *J* = 15.6, 2.4 Hz, 1H), 4.82 (dd, *J* = 15.6, 2.5 Hz, 1H), 4.36 (dd, *J* = 11.5, 6.0 Hz, 1H), 4.28 (dd, *J* = 11.5, 6.9 Hz, 1H), 2.66 (t, *J* = 2.4 Hz, 1H), 2.28 (s, 3H), 2.09 (s, 3H), 2.07 (s, 3H). ^{13}C NMR (100 MHz, $CDCl_3$) δ 170.3, 169.7, 167.2, 166.2, 157.2, 115.4, 78.1, 76.0, 74.2, 66.9, 61.9, 59.5, 20.6, 20.4, 20.3. HRMS(APCI, m/z): calcd for $C_{15}H_{17}O_9^+$, $[M + H]^+$ 341.0867, found 341.0878. Note: the O-3 connectivity of **VC-2 (3O-VC-2)** was supported by HMBC correlations between the propargylic methylene protons H7b/H7b (δ4.87/4.82 ppm) and C3 (δC157.2 ppm) as shown below.



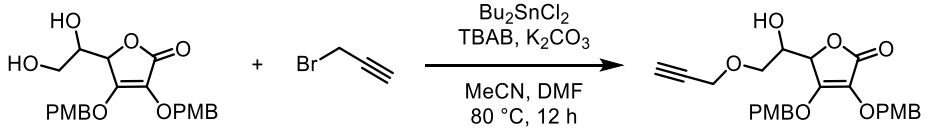
1.3 Synthesis of 6O-VC-1



5,6-*O*-Isopropylidene-*L*-ascorbic acid (2.00 g, 9.26 mmol, 1.0 equiv.) and 4-

methoxybenzyl chloride (3.46 g, 22.2 mmol, 2.4 equiv.) were dissolved in a mixed solvent of DMSO (10.4 mL) and THF (9.6 mL). K_2CO_3 (3.07 g, 22.2 mmol, 2.4 equiv.) was added, and the reaction mixture was heated at 60 °C for 2 h. After completion as monitored by TLC, the mixture was filtered. The filtrate was quenched with ice-water (20 mL) and extracted with EtOAc (20 mL × 3). The combined organic layers were dried over anhydrous Na_2SO_4, filtered, and concentrated. The residue was dissolved in THF (30 mL), and 12 *N* HCl (3 mL) was added. The reaction mixture was stirred at room temperature for 20 min. After completion as monitored by TLC, saturated aqueous $NaHCO_3$ was added at 0 °C to adjust the pH to basic, and the mixture was extracted with EtOAc (30 mL × 3). The combined organic layers were dried over anhydrous Na_2SO_4, filtered, and concentrated. The crude residue was purified by neutral alumina column chromatography ($MeOH/CH_2Cl_2$ = 1:20) to afford **6O-VC-S1** as yellow oil (1.50 g, 40% yield).

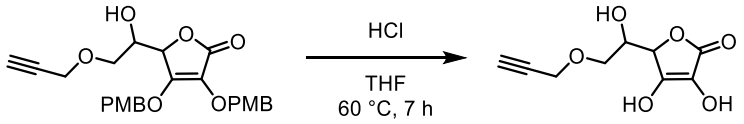
2,3-Di-*O*-(4-methoxybenzyl)-*L*-ascorbic acid (6O-VC-S1): ^1H NMR (400 MHz, Chloroform-*d*) δ 7.33 (d, *J* = 8.1 Hz, 2H), 7.15 (d, *J* = 8.1 Hz, 2H), 6.93 – 6.84 (m, 4H), 5.14 – 5.03 (m, 4H), 4.64 (s, 1H), 3.91 – 3.85 (m, 1H), 3.81 (s, 3H), 3.80 (s, 3H), 3.78 – 3.69 (m, 2H). ^{13}C NMR (100 MHz, Chloroform-*d*) δ 169.7, 160.0, 160.0, 157.6, 130.9, 129.9, 128.0, 127.3, 120.7, 114.0, 114.0, 76.0, 73.5, 73.4, 69.9, 63.3, 55.3. LC-MS (ESI, m/z): calcd for $C_{22}H_{25}O_8^+$, $[M + H]^+$ 417.15, found 416.90.



Compound **6O-VC-S1** (2.50 g, 6.08 mmol, 1.0 equiv.) and dibutyltin dichloride (185 mg, 0.608 mmol, 0.1 equiv.) were dissolved in a mixed solvent of MeCN (30 mL) and DMF (3 mL). Tetrabutylammonium bromide (196 mg, 0.608 mmol, 0.1 equiv.) and K_2CO_3 (1.26 g, 9.12 mmol, 1.5 equiv.) were added, followed by portion-wise addition of propargyl bromide (1.43 g, 12.16 mmol, 2.0 equiv.). The reaction mixture was heated at 80 °C for 12 h. After completion as monitored by TLC, the reaction was quenched with water (30 mL) and extracted with EtOAc (30 mL × 3). The combined organic

layers were dried over anhydrous Na_2SO_4, filtered, and concentrated. The crude residue was purified by silica gel column chromatography (EtOAc/hexanes = 1:4.7) to afford **6O-VC-S2** as yellow oil (946 mg, 34% yield).

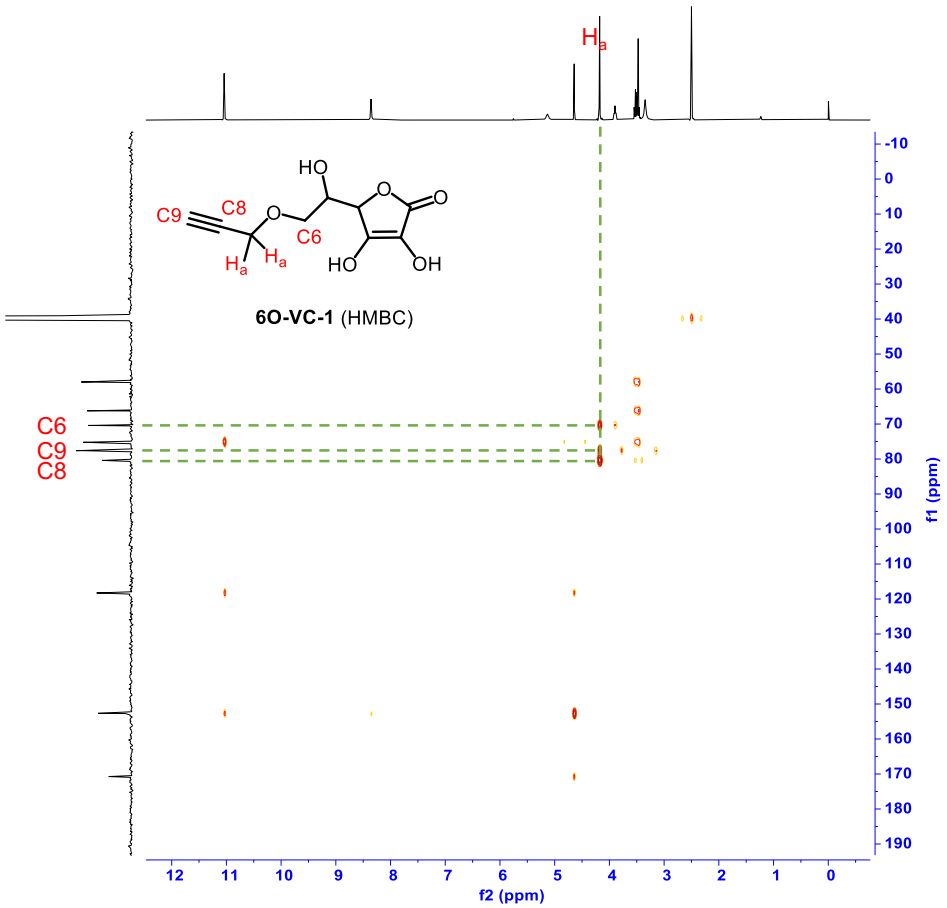
2,3-Di-*O*-(4-methoxybenzyl)-6-*O*-propargyl-*L*-ascorbic acid (6O-VC-S2): ^{1}H NMR (400 MHz, $CDCl_3$) δ 7.35–7.32 (m, 2H), 7.17–7.14 (m, 2H), 6.91–6.85 (m, 4H), 5.13–5.04 (m, 4H), 4.67 (d, *J* = 2.2 Hz, 1H), 4.16 (d, *J* = 2.4 Hz, 2H), 4.04–3.98 (m, 1H), 3.82 (s, 3H), 3.81 (s, 3H), 3.66 (dd, J = 6.1, 2.2 Hz, 2H), 2.43 (t, J = 2.4 Hz, 1H). ^{13}C NMR (100 MHz, $CDCl_3$) δ 169.6, 160.0, 157.3, 130.9, 129.9, 128.1, 127.4, 120.7, 114.0, 79.0, 75.1, 75.0, 73.5, 73.3, 69.9, 68.2, 58.6, 55.3. LC-MS (ESI, m/z): calcd for $C_{25}H_{27}O_8^+$, $[M + H]^+$ 455.17, found 454.90.



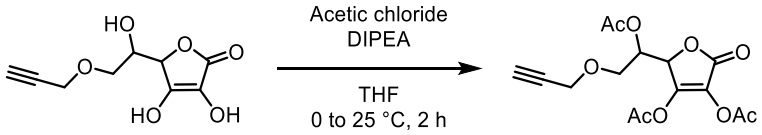
6O-VC-S2 **6O-VC-1**

Compound **6O-VC-S2** (2.93 g, 6.44 mmol, 1.0 equiv.) was dissolved in THF (30 mL), and 12 *N* HCl (6 mL) was added. The reaction mixture was heated at 60 °C for 7 h. After completion as monitored by TLC, the solvent was removed under reduced pressure, and the crude residue was purified by silica gel column chromatography (EtOAc/hexanes = 3:2) to afford **6O-VC-1** as a white solid (705 mg, 51% yield).

6-*O*-Propargyl-*L*-ascorbic acid (6O-VC-1): ^{1}H NMR (400 MHz, DMSO-d_6) δ 11.04 (s, 1H), 8.36 (s, 1H), 5.13 (s, 1H), 4.65 (d, *J* = 1.5 Hz, 1H), 4.18 (d, *J* = 2.4 Hz, 2H), 3.90 (t, *J* = 6.9 Hz, 1H), 3.55–3.46 (m, 3H). ^{13}C NMR (100 MHz, DMSO-d_6) δ 170.7, 152.7, 118.3, 80.4, 77.6, 75.2, 70.4, 66.2, 58.0. HRMS (ESI, m/z): calcd for $C_9H_9O_6^-$, $[M - H]^-$ 213.0405, found 213.0431. Note: the regiochemistry of **6O-VC-1** was established by HMBC (see below).



1.4 Synthesis of 6O-VC-2

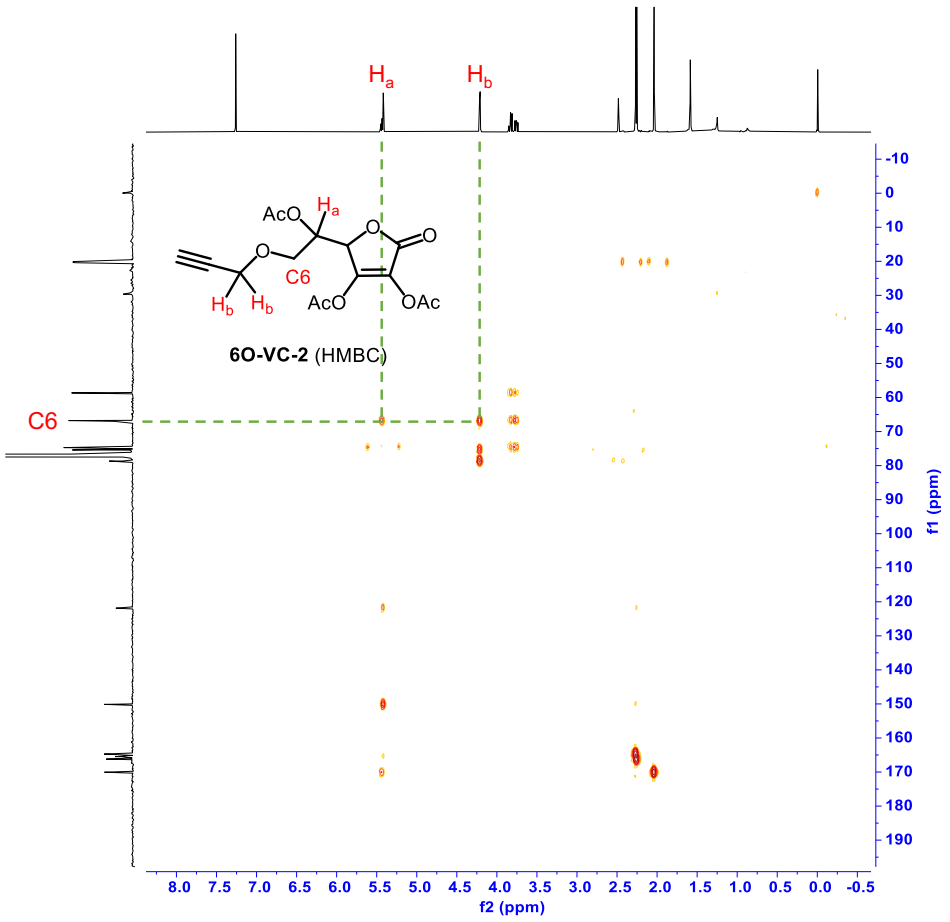


6O-VC1 **6O-VC-2**

Compound **6O-VC-1** (400 mg, 1.87 mmol, 1.0 equiv.) was dissolved in anhydrous THF (5 mL). Acetyl chloride (528 µL, 7.48 mmol, 4.0 equiv.) and DIPEA (1.3 mL, 7.48 mmol, 4.0 equiv.) were added sequentially at 0 °C. The reaction mixture was warmed to room temperature and stirred for 2 h. Additional acetyl chloride (264 µL, 3.74 mmol, 2.0 equiv.) was added, and the mixture was stirred for another 5 min. After completion as monitored by TLC, the solvent was removed under reduced pressure, and the crude residue was purified by silica gel column chromatography (EtOAc/hexanes = 1:6) to afford **6O-VC-2** as yellow oil (370 mg, 58% yield).

2,3,5-Tri-*O*-acetyl-6-*O*-propargyl-*L*-ascorbic acid (6O-VC-2): ^{1}H NMR (400 MHz, $CDCl_3$) δ 5.45–5.41 (m, 2H), 4.21 (dd, J = 2.3, 0.8 Hz, 2H), 3.86–3.81 (m, 1H), 3.78–3.73 (m, 1H), 2.48 (t, J = 2.4 Hz, 1H), 2.27 (s, 3H), 2.25 (s, 3H), 2.04 (s, 3H). ^{13}C NMR

(100 MHz, $CDCl_3$) δ 170.0, 166.2, 165.5, 164.7, 150.1, 121.9, 78.7, 75.4, 74.7, 67.0, 66.8, 58.6, 20.4, 20.4, 20.1. HRMS (APCI, m/z): calcd for $C_{15}H_{17}O_9^+$, $[M + H]^+$ 341.0867, found 341.0879. Note: the regiochemistry of **6O-VC-2** was established by HMBC (see below).



2. Biological Experimental Methods

2.1 Cell culture and transfection

HEK293T (RRID: CVCL_0063), HeLa (RRID: CVCL_0030), Huh7 (RRID: CVCL_0336) and NIH3T3 (RRID: CVCL_0594) cells were maintained in DMEM (Gibco, C11995500BT) supplemented with 10% Fetal bovine serum (Gibco, A5256701), 100 U/mL penicillin and 100 μg/mL streptomycin (Solarbio, P1400) at 37 °C in a humidified atmosphere with 5% CO_2. The commercial cell lines, HEK293T, Huh7 and HeLa, were obtained from the American Type Culture Collection (ATCC). The NIH3T3 cell line was obtained from the National Infrastructure of Cell Resource (NICR).

Cells were transfected using transfection reagent polyethylenimine linear (PEI) MW40000 (Yeasen, 40816ES02). In brief, plasmid DNA was mixed with PEI in Opti-MEM (Gibco, 31985-070) at a DNA: PEI mass ratio of 1:3. The mixture was incubated for 20 min at room temperature to allow DNA-PEI complex formation, then added to cells that had been pre-seeded to reach optimal confluency.

2.2 CuAAC click reaction and in-gel fluorescence analysis

Cell lysates were incubated with 75 μM TAMRA-azide (Confluore, BCA-27), a cocktail of 1 mM $CuSO_4$ and 2 mM BTTAA (GreenChem, GLMK-15041), and 2 mM sodium ascorbate (Solarbio, 134-03-2) for 30 min at 37 ℃ in the dark. The reaction was stopped by adding 5 × SDS sample buffer (250 mM Tris-HCl (pH 6.8), 10% SDS, 0.5% bromophenol blue, 50% glycerol, 5% β-mercaptoethanol) and boiled at 95 ℃ for 10 min. The proteins were resolved in a 10% SDS-PAGE acrylamide gel, and fluorescence imaging was performed using a fluorescent image analyzer (Amersham Typhoon 5) with the Cy3 channel. The gels were then stained by Coomassie Brilliant Blue to demonstrate equal loading.

2.3 Protein labeling in cell lysates using VC probes

Cells were lysed with 1% NP-40 (Biosharp, 9016-45-9) lysis buffer with 1% protease inhibitor cocktail (Biosharp, BL612A) or 2% SDS with 1% protease inhibitor cocktail and 0.1% UltraNuclease (Yeasen, 20156ES60). Protein concentration was

determined using a BCA protein assay kit (Biosharp, BL521A).

For the standard labeling reaction, the lysate (3 mg/mL) was incubated with 1 mM **VC-1** or 200 μM **VC-2** at 37 ℃ for 3 h. For competition assays, the lysate was first incubated with excess sodium ascorbate (NaVC, Solarbio, 134-03-2) for 1 h, followed by incubation with probe under the same conditions.

After incubation, proteins were precipitated using a methanol and chloroform solution (aqueous phase: methanol: chloroform=4:4:1) and were resuspended in 2% SDS buffer. Following resuspension, the samples were processed for CuAAC click reaction and in-gel fluorescence analysis.

2.4 Metabolic labeling in mammalian cells with VC-2

Cells were incubated with **VC-2** (200 μM) for 1 h, harvested and lysed in 1% NP-40 buffer with 1% protease inhibitor cocktail (Biosharp, BL612A). The concentration of the protein was determined by the BCA protein assay kit (Biosharp, BL521A). For competition experiments, cells were pre-treated with NaVC at indicated concentrations for 16 h, and then co-incubated with the **VC-2** (200 μM) and NaVC (4 mM) for another 1 h. Cell lysates (3 mg/mL) were processed for CuAAC click reaction and in-gel fluorescence analysis.

To analyse the turnover of **VC-2** protein labeling, cells were labeled with 200 μM **VC-2** for 1 h and then washed, treated with 0.4 μM TSA (Selleck, 9950S) or 2 mM NAM (Selleck, 72340-100G) or 20 μM TMG (MCE, HY-12588) for the indicated time periods.

2.5 Chemoproteomic profiling of vitcylated proteins

For *in vitro* labeling, HEK293T cell lysates were preincubated with 5 mM NaVC at 37 °C for 2 h, followed by incubation with 1mM **VC-1** for an additional 3 h. For live-cell labeling, HEK293T cells were pretreated with 4 mM NaVC for 16 h. The medium was then replaced with fresh culture medium containing with 4 mM NaVC and 400 μM **VC-2**, followed by incubation for a further 2 h. In both experiments, an equivalent volume of DMSO was used as the vehicle control. Three independent biological replicates were performed for each condition.

Cells were harvested and resuspended in ice-cold lysis buffer (PBS supplemented

with 1% (v/v) protease inhibitor cocktail) and lysed by three cycles of snap-freezing in liquid nitrogen followed by thawing at 37 °C. Lysates were clarified by centrifugation at 14,000g for 15 min at 4 °C, and protein concentrations were determined using a BCA assay according to the manufacturer's instructions (Biosharp, BL521A). All samples were normalized to 2 mg/mL.

Protein samples (1 mL) were subjected to click chemistry by incubation with Biotin-azide (100 μM, MedChemExpress, 908007-17-0), $CuSO_4$ (1 mM), BTTAA (2 mM, GreenChem, GLMK-15041), and sodium ascorbate (2 mM, NaVC, Solarbio, 134-03-2) for 30 min at 37 °C in the dark. Proteins were precipitated using methanol/chloroform (aqueous:methanol:chloroform, 4:4:1) and resuspended in 1% SDS. Samples were diluted with PBS to a final SDS concentration of 0.4% and incubated overnight at 4°C with pre-washed streptavidin-coated agarose beads (Thermo Fisher Scientific, P88816) on a rotator.

Beads were washed three times with PBS and resuspended in PBS containing 6M urea and 10 mM dithiothreitol (Solarbio, 3483-12-3), followed by incubation at 37 °C for 30 min. Iodoacetamide (20 mM, Solarbio, 144-48-9) was then added, and samples were incubated for an additional 30 min at 37 °C in the dark. Samples were diluted with PBS to reduce the urea concentration below 1 M, and proteins were digested overnight (12 – 16 h) at 37 °C with trypsin (Meizhiyuan, P01001) at a 1:100 enzyme-to-protein ratio. Digestion was quenched by addition of trifluoroacetic acid (Sigma, 76-05-1), and peptides were desalted prior to mass spectrometry analysis.

2.6 LC-MS/MS analysis

LC-MS/MS analysis was performed on an Ultimate 3000 RSLCnano system coupled to an Orbitrap Exploris™ 480 mass spectrometer equipped with a Nanospray Flex ion source (all Thermo Fisher Scientific, Bremen, Germany). Peptides were dissolved in 0.1% formic acid (FA) in water and loaded onto a trap column (75 μm × 2 cm, 2 μm C18; Thermo, #164535) and separated on an analytical column (75 μm × 25 cm, 2 μm C18; Thermo, #164941) at a flow rate of 300 nL/min. Mobile phase A was 0.1% FA in water, and mobile phase B was 0.1% FA in 80% acetonitrile. Separation was achieved using a linear gradient from 10% to 28% B over 66 min, followed by 28%

to 32% B over 12 min and a final increase to 99% B over 3 min.

Data was acquired in a data-dependent acquisition mode, switching between full-scan MS and MS/MS scans. Spray voltage was set to 2.1 kV and the ion transfer capillary temperature was 320 °C. Full-scan MS spectra were collected from m/z 350 to 1,500 at a resolution of 60,000 (at m/z 200) with an AGC target of 3×10^6 and a maximum injection time of 50 ms. Precursors with charge states 2^+ to 6^+ were isolated with a 1.6 m/z window and fragmented by higher-energy collisional dissociation (HCD) at 30% normalized collision energy. MS/MS spectra were acquired at a resolution of 15,000 (at m/z 200) with an AGC target of 1×10^5 and a maximum injection time of 22 ms. Dynamic exclusion was set to 50 s.

All raw mass spectrometry data were processed using the MaxQuant (version 1.6.1.0). Database searching was performed against the *Homo sapiens* reference proteome downloaded from UniProt (https://www.uniprot.org/).[1] The following parameters were applied: precursor mass tolerance was set to 20 ppm for the first search and 6 ppm for the main search, with a minimum peptide length of five amino acids. Trypsin was specified as the protease, allowing cleavage N-terminal to proline and up to two missed cleavages. Carbamidomethylation of cysteine was set as a fixed modification; oxidation of methionine, N-terminal acetylation, and other relevant adducts were set as variable modifications. The MS/MS match tolerance was 50 ppm, with the top 10 peaks per 100 Da considered for matching. Peptide-spectrum matches and protein identifications were filtered at a false discovery rate (FDR) of 1%. Mass spectrometry data are provided in Supplementary Table 1-2.

2.7 LC-MS/MS and PRM-based targeted analysis of Lysine Vitcylation-p1

In vitro vitcylation and vitcylation-p1 reactions of the synthetic peptide Ac-YAPVAKDLASR were performed under defined biochemical conditions. Briefly, reactions were carried out in a total volume of 30 μL containing 50 mM Tris-HCl (pH 8.0), 2 mM NaVC (for vitcylation) or 2 mM **VC-1** (for vitcylation-p1), and synthetic Ac-YAPVAKDLASR at a final concentration of 0.05 mg/mL. Reaction mixtures were incubated at 37 °C for 6 h to allow modification to proceed. After completion of the reaction, peptides were desalted using C18 ZipTips (Millipore), dried under vacuum,

reconstituted in 0.1% formic acid, and subjected to mass spectrometric analysis.

For detection of protein vitcylation-p1 modifications, a cell-based enrichment and in-gel digestion workflow was employed. HEK293T cells were transiently transfected with Flag-tagged expression plasmids encoding STAT1, FTO, ALDH1B1, IMPDH1, ALDH9A1, or GSTO1 and cultured for 36 h, followed by treatment with **VC-2** for 2 h to label vitcylation-p1-modified proteins. Cells were harvested and lysed in buffer supplemented with protease inhibitors. After clarification by centrifugation, Flag-tagged proteins were affinity-purified using anti-Flag magnetic beads. Bound proteins were eluted by boiling in SDS-PAGE loading buffer, resolved by SDS-PAGE, and visualized by Coomassie Brilliant Blue staining. Protein bands corresponding to the Flag-tagged proteins were excised and subjected to in-gel tryptic digestion. Briefly, gel pieces were destained, dehydrated, reduced with tris(2-carboxyethyl) phosphine hydrochloride (TCEP), alkylated with chloroacetamide (CAA), and digested overnight at 37°C with sequencing-grade trypsin. Peptides were sequentially extracted with 0.1% formic acid, pooled, dried, and reconstituted for LC-MS/MS analysis.

Prior to mass spectrometric analysis, peptide samples were separated on a Vanquish™ Neo UHPLC system using a reversed-phase C18 analytical column coupled online to a Thermo Scientific Orbitrap Astral mass spectrometer through a nano-electrospray ionization source. Peptides were first trapped on a desalting column and subsequently separated on the analytical column using a linear gradient of solvent B (0.1% formic acid in 80% acetonitrile) against solvent A (0.1% formic acid in water) at a constant nano-flow rate.

For FTO, ALDH1B1, IMPDH1, ALDH9A1, and GSTO1, vitcylation-p1 modifications were identified by conventional LC-MS/MS analysis. For identification of endogenous GAPDH vitcylation, cell lysates were subjected to conventional proteomic LC-MS/MS analysis. The acquired MS/MS data were searched against the human proteome database. Lysine vitcylation-p1 (+214.04774 Da) and lysine vitcylation (+175.0242 Da) were specified as variable modifications for the respective analyses. Methionine oxidation (+15.99491 Da) and protein N-terminal acetylation (+42.01056 Da) were included as additional variable modifications, whereas cysteine

carbamidomethylation (+57.02146 Da) was specified as a fixed modification.

For synthetic Ac-YAPVAKDLASR vitcylation, vitcylation-p1 and STAT1 K298 vitcylation-p1, targeted validation was performed by parallel reaction monitoring (PRM). The Orbitrap Astral mass spectrometer was operated in PRM mode. Each acquisition cycle consisted of an initial full MS1 scan acquired in the Orbitrap analyzer over an m/z range of 380-980 at a resolution of 240,000, with an automatic gain control (AGC) target of 1×10^6 and a maximum injection time of 5 ms. Targeted PRM scans were subsequently acquired for predefined precursor ions using quadrupole isolation. For synthetic Ac-YAPVAKDLASR vitcylation-modified and vitcylation-p1-modified peptides, precursor ions at m/z 704.34746 (z = 2) and 723.85923 (z = 2), respectively, were monitored. For the STAT1 K298 vitcylation-p1-modified peptide, the precursor ion at m/z 636.81463 (z = 2) was targeted. Fragmentation was performed by higher-energy collisional dissociation (HCD) with a normalized collision energy (NCE) of 25–28. MS/MS spectra were acquired at high resolution with an AGC target of 2×10^5 and a maximum injection time of 10 ms. The MS/MS scan range was dynamically adjusted according to the precursor ion m/z to ensure comprehensive acquisition of all relevant fragment ions. PRM acquisition was scheduled based on peptide retention times to maximize sampling across chromatographic peaks. Diagnostic fragment ions (b and y ions) extracted from the PRM data were used for selective confirmation of STAT1 K298 vitcylation-p1 as well as the corresponding *in vitro*-modified synthetic peptides.

2.8 Plasmid construction

Total RNA was extracted following the instructions of Total RNA Extraction Reagent (ABclonal, RK30129). The reverse transcription was adapted from protocols of ABScript II cDNA First-Strand Synthesis Kit (ABclonal, RK20400). The proteins of interest (STAT1, FTO, GSTO1, ALDH9A1, ALDH2, IMPDH1 and GAPDH) were cloned into a pCMV vector by amplifying their full-length coding sequences from cDNA templates with primers encoding an N-terminal Flag tag. The ALDH1B1 and LUC7L2 plasmids were purchased from Miaoling Plasmid (P48427; P51960). The primers used for cDNA cloning are listed in Supplementary Table 9.

2.9 Site-directed mutagenesis

The GAPDH K194R mutant was generated by PCR-based site-directed mutagenesis using the wild-type GAPDH expression plasmid as the template and Phanta Max Super-Fidelity DNA Polymerase (Vazyme, P505-d1). Mutagenic primers carrying the desired nucleotide substitution were designed to replace Lys194 with arginine. The PCR product was transformed into competent *Escherichia coli* DH5α (TOBOBIO, CC96102-02) for plasmid propagation. Individual colonies were screened, and the presence of the intended K194R substitution and the absence of additional mutations within the coding region were confirmed by DNA sequencing. The primers used for mutagenesis are listed in Supplementary Table 9.

2.10 Generation of GSTP1 knockout Huh7 cells

GSTP1 knockout Huh7 cells were generated using a CRISPR-Cas9 lentiviral system. Independent sgRNAs targeting human GSTP1 were cloned into the lentiCRISPR v2 vector by ligation of annealed oligonucleotides using *T4* DNA ligase (TAKARA, Cat# 2011A). The lentiCRISPR v2 vector was kindly provided by Prof. Fan Yao (Huazhong Agricultural University). The sgRNA sequences used in this study are listed in Supplementary Table 9.

For lentivirus production, HEK293T cells were co-transfected with the lentiCRISPR v2-sgRNA construct together with the packaging plasmids psPAX2 (Addgene, 12260) and pMD2.G (Addgene, 12259). Virus-containing supernatants were collected after transfection, clarified to remove cell debris, and used to transduce Huh7 cells. Following transduction, cells were selected with puromycin (2 μg/mL; Aladdin, P113126) to enrich for sgRNA-expressing populations. Independent GSTP1-knockout cell populations generated with multiple distinct sgRNAs were expanded and used for downstream experiments. GSTP1 depletion was confirmed by western blotting before subsequent labeling and functional analyses.

2.11 Immunoprecipitation and immunoblot assays

HEK293T cells were transfected with plasmids expressing Flag-tagged proteins for 36–48 h, metabolically labeled with **VC-2** (200 μM) for another 1 h, and harvested. For competition experiments, cells expressing the indicated Flag-tagged proteins were pre-treated with 4 mM sodium ascorbate for 16 h, and then co-incubated with the **VC-**

2 (200 μM) and 4 mM sodium ascorbate for another 1 h.

Cells were lysed on ice for 30 min in 1% NP-40 (Biosharp, 9016-45-9) lysis buffer with 1% protease inhibitor cocktail (Biosharp, BL612A). The resulting cell lysates were centrifuged at 14,000 g for 15 min at 4 ℃ to remove cellular debris. Protein concentration was determined using a BCA protein assay kit (Biosharp, BL521A). Equal amounts of cell lysates were incubated with anti-Flag beads (Genscript, L00425) for 2–4 h at room temperature with rotation or on a rotator at 4 ℃ overnight. The beads were washed with 1% NP-40 buffer three times and resuspended in 1% NP-40 buffer. Then the samples were processed for CuAAC click reaction. The reaction was stopped by adding 5 × SDS sample buffer (250 mM Tris-HCl (pH 6.8), 10% SDS, 0.5% bromophenol blue, 50% glycerol, 5% β-mercaptoethanol) and boiled at 95 ℃ for 10 min. Then proteins were resolved in a 10% SDS-PAGE acrylamide gel (Epizyme, PG212) for Western blot analysis and in-gel fluorescence imaging.

2.12 Western blot analysis

Proteins were separated by 10% SDS-PAGE and transferred to polyvinylidene difluoride (PVDF) membranes (Baseniao, BSN3250S). Subsequently, the membranes were blocked with 5% milk in TBST for 1 h at room temperature and then washed three times with TBST for 5 min each. The membranes were incubated with primary antibodies overnight at 4 ℃ or for 2 h at room temperature, and then washed three times with TBST for 5 min each. The primary antibodies used in this study were anti-Flag (ABclonal, AE092, 1:20,000 dilution), anti-GSTP1 (Selleck, G13B3, 1:2,500 dilution), anti-GAPDH (Proteintech, 10494-1-AP, 1:50,000 dilution) and anti-α-Tubulin (Proteintech, 11224-1-AP, 1:20,000 dilution). Then the membranes were exposed for 1 h at room temperature to corresponding HRP-conjugated secondary antibodies. The secondary antibodies were anti-rabbit IgG-HRP (Proteintech, SA00001-2, 1:20,000 dilution) and anti-mouse IgG-HRP (Proteintech, SA00001-1, 1:20,000 dilution). After washing, the protein signal was visualized using ECL (Biosharp, BL523B) and detected by eBlot imaging system.

2.13 VC-1 labeling of overexpressed proteins in cell lysates

HEK293T cells were transfected with plasmids expressing Flag-tagged proteins

for 36–48 h and harvested. Cells were lysed on ice for 30 min in 1% NP-40 (Biosharp, 9016-45-9) lysis buffer with 1% protease inhibitor cocktail (Biosharp, BL612A). The resulting cell lysates were centrifuged at 14,000 g for 15 min at 4 ℃ to remove cellular debris. Protein concentration was determined using a BCA protein assay kit (Biosharp, BL521A). Equal amounts of cell lysates were incubated with anti-Flag beads (Genscript, L00425) for 2–4 h at room temperature with rotation or on a rotator at 4 ℃ overnight. The beads were washed with PBS three times and resuspended in PBS. Then the samples were incubated with 1 mM **VC-1** at 37 ℃ for the indicated time periods. After incubation, the samples were processed for CuAAC click reaction and in-gel fluorescence analysis.

2.14 Sample Preparation for Stoichiometry Measurement

HEK293T cells were transfected with plasmids expressing Flag-tagged proteins for 36-48 h, metabolically labeled with **VC-2** (200 μM) for another 1 h, and harvested. Cells were lysed on ice for 30 min in 1% NP-40 (Biosharp, 9016-45-9) lysis buffer with 1% protease inhibitor cocktail (Biosharp, BL612A). The resulting cell lysates were centrifuged at 14,000 g for 15 min at 4 ℃ to remove cellular debris.

Cell lysates were incubated with freshly prepared click reaction cocktail containing 100 μM Biotin-azide, a cocktail of 1 mM $CuSO_4$ and 2 mM BTTAA (GreenChem, GLMK-15041), and 2 mM NaVC (Solarbio, 134-03-2) for 30 min at 37 ℃ in the dark. Proteins were precipitated using methanol/chloroform (aqueous: methanol: chloroform, 4:4:1) and resuspended in 1% SDS. Samples were diluted with PBS to a final SDS concentration of 0.4%. Protein concentration was determined using a BCA protein assay kit (Biosharp, BL521A).

Then samples were divided equally into input (300 μL, 2–3 mg/mL) and pull-down (300 μL, 2–3 mg/mL) groups. The pull-down group was incubated with pre-washed streptavidin-coated agarose beads (Thermo Fisher Scientific, P88816) overnight at 4 ℃ or for 4–6 h at room temperature on a rotator. Beads were washed three times with PBS and resuspended to the same volume as the starting lysates (300 μL). Meanwhile, a fraction of the input sample was diluted to 1/10–1/100 of the initial concentration using SDS sample buffer. Equal volumes of these serially diluted inputs and the pull-down

eluates were subsequently analyzed by immunoblotting.

2.15 Immunofluorescence microscopy

HeLa cells were cultured on sterilized coverslips and incubated with **VC-2** (200 μM, 400 mM stock solution in DMSO) in culture medium. The same volume of DMSO was used as the vehicle control. After 1 h of labeling at 37 ℃, the cells were washed once with PBS, fixed with 4% paraformaldehyde fixative (Biosharp, BL539A) for 10 min at room temperature, and then washed twice with PBS. Cells were permeabilized with 0.1% Triton X-100 (BioFRoxx, 9002-93-1) in PBS for 10 min at room temperature, blocked with 2% FBS (Gibco, A5256701) in PBS for 30 min at room temperature, and washed with PBS (3 × 5 min with gentle agitation). The cells were incubated in PBS with a freshly premixed click reaction cocktail (75 μM TAMRA-azide, a cocktail of 1 mM $CuSO_4$ and 2 mM BTTAA, and 2 mM NaVC) for 30 min at 37 ℃ in the dark. After gentle washes three times with PBS, the cells were incubated with primary antibodies of Fibrillarin (Selleck, F3066, 1:50) overnight at 4 °C. The cells were washed three times with PBS (3 × 5 min with gentle agitation) and incubated with secondary antibodies conjugated with fluorescent dyes (Proteintech, S00013-1, 1:400) for 1 h at room temperature. The cells were washed three times with PBS (3 × 5 min with gentle agitation). Cells were sealed with antifade mounting with DAPI (P0131, Beyotime Biotechnology) and imaged on a confocal microscope (Nikon, CSU-W1).

For inhibitor studies, cells were treated with 10 μg/mL Actinomycin D (GLPBIO, GC16866) and 200 μM **VC-2** for 1 h, then fixed for confocal microscopic imaging.

2.16 FACS-based CRISPR screening

The CRISPR screen library (Human CRISPRko Library-Whole Genome Pro, lentiCRISPR v2-Puro backbone, SciShare, SSLP047) and the second-generation packaging plasmids psPAX2 (Addgene, 12260) and pMD2.G (Addgene, 12259) were gifts from Prof. Fan Yao's laboratory (Huazhong Agricultural University). Individual library constructs were packaged into lentiviral particles by co-transfecting HEK293T cells with these packaging plasmids. Huh7 cells were then transduced with lentiCRISPR v2-Puro particles at an MOI of 0.3 to ensure single integrants per cell, followed by selection with 2 μg/mL puromycin for 3 days to generate a stable Cas9-

expressing population.

Cas9-expressing Huh7 cells were incubated with 200 μM **VC-2** for 1 h at 37 °C, then collected and fixed in 80% methanol with gentle agitation for 10 min. After permeabilization with 0.1% Triton X-100 (BioFRoxx, 9002-93-1) in PBS for 10 min at room temperature and blocking with 2% FBS in PBS for 10 min, cells were resuspended in PBS and incubated with a freshly prepared click reaction cocktail (75 μM TAMRA-azide, a cocktail of 1 mM $CuSO_4$ and 2 mM BTTAA, and 2 mM NaVC) at 37 °C for 30 min in the dark. Following the reaction, cells were washed three times (5 min each with gentle agitation) with PBS containing 1% Tween-20 and 0.5 mM EDTA, rinsed twice with PBS supplemented with 1% FBS, and resuspended in the same buffer. Labeled cells were analyzed and sorted by FACS based on red fluorescence intensity, collecting populations corresponding to the top 5%, bottom 5%, and middle 50% of the distribution (10 million cells total).

Genomic DNA was extracted from the sorted cell pellets using the FastPure Cell/Tissue DNA Isolation Mini Kit (Vazyme, DC102-01). The sgRNA-encoding regions were amplified by PCR with Green Taq Mix (Vazyme, P131-02/03) and vector-specific primers (sequences provided in Supplementary Table 9). Each 50 μL reaction contained 1 μg of genomic DNA template and was run under the following cycling conditions: 25 cycles of 95 ℃ for 15 s, 58 ℃ for 15 s, and 72 ℃ for 30 s. PCR products from each sample were pooled and purified using a DNA Gel Extraction Kit (Simgen, 2001250) according to the manufacturer's protocol. The resulting libraries were sequenced on an Illumina NovaSeq X Plus platform (Kindstar Sequenom), achieving an average coverage of approximately 100× per sgRNA. Genome-wide screening data were analyzed using MAGeCK (version 0.5.9.4).[2,3] Complete screening results are provided in Supplementary Tables 7 and 8.

2.17 GAPDH activity assay

Recombinant human GAPDH protein was incubated with 500 μM NaVC in 50 mM Tris-HCl buffers of different pH values at 37°C for 2 h. After incubation, GAPDH enzymatic activity was measured by monitoring the rate of NADH oxidation, as reflected by the decrease in absorbance at 340 nm over time. GAPDH activity was

determined according to the manufacturer's instructions (ScienCell GAPDH Activity Assay Kit, Cat. #8148).

For cellular assays, cells overexpressing FLAG-tagged GAPDH WT or K194R were treated with vehicle or 5 mM NaVC for 2 h. FLAG-tagged GAPDH was immunoprecipitated with anti-FLAG antibody, and GAPDH activity was subsequently measured as described above.

2.18 Flow cytometry

HEK293T cells were harvested, washed twice with cold PBS, and resuspended in PBS containing 2% fetal bovine serum (FBS). Cells were stained with LIVE/DEAD™ Fixable Aqua Dead Cell Stain (Thermo Fisher Scientific) according to the manufacturer's instructions. Cells were then incubated with anti-human HLA antibody (clone W6/32, BioLegend) for 30 min on ice. Following surface staining, cells were fixed and permeabilized, and intracellular phospho-STAT1 (Tyr701) was stained with anti-human phospho-STAT1 (Y701) antibody (clone A17012A, BioLegend). After staining, cells were washed with PBS containing 2% FBS and analyzed on a BD flow cytometer. Flow cytometry data were analyzed using FlowJo software.

2.19 RNA-seq and data analysis

Genomic DNA and total RNA were co-extracted from the same sample using a column-based purification kit. Briefly, up to 1×10^7 snap-frozen cells were homogenized in 600 µL Buffer RLT Plus by bead-beating (65 Hz, 60 s) and incubated at room temperature for 5 min. After centrifugation at 14,000 g for 3 min, the supernatant was loaded onto an AllPrep DNA spin column and centrifuged at 10,000 g for 30 s. The flow-through was mixed with one volume of 70% ethanol and applied to a RNeasy spin column for RNA purification. The column was washed with 700 µL Buffer RW1 and twice with 500 µL Buffer RPE, with centrifugation at 10,000 g for 30 s per wash. RNA was eluted in 30 µL RNase-free water after a final drying spin and centrifugation at 16,000 g for 2 min. RNA integrity was assessed prior to downstream analysis.

RNA sequencing libraries were constructed from total RNA after quality assessment. Poly(A)$^+$ RNA was selected using oligo(dT) beads and fragmented. cDNA was synthesized, end-repaired, A-tailed, and ligated to adapters. Following PCR

amplification and quality control, libraries were circularized and amplified via rolling circle replication to generate DNA nanoballs (DNBs). Sequencing was performed on a DNBSEQ platform with combinatorial Probe-Anchor Synthesis (cPAS).

Quality control of raw sequencing reads in FASTQ format was performed using FastQC (https://www.bioinformatics.babraham.ac.uk/projects/fastqc/).[4] Trimming and adapter removal were carried out with fastp (v0.23.2)[5] to retain high-quality reads. Clean paired-end reads were aligned to the Ensembl reference genome GRCh38 using HISAT2 (v2.2.1).[6] The resulting SAM files were sorted, indexed, and converted to BAM format using SAMtools (v1.14).[7] Read counts per gene were generated with featureCounts from the Subread package (v2.0.1). Differentially expressed genes (DEGs) were identified using DESeq2 (v1.28.1),[8] with thresholds set at P-value < 0.05 and $|\log_2(\text{fold change})| > 1$. Alternative splicing events between groups were detected with rMATS (v4.1.2). Using default parameters and the GRCh38 genome annotation, rMATS was applied to the aligned BAM files to systematically identify five major splicing event types: skipped exon (SE), mutually exclusive exon (MXE), retained intron (RI), alternative 5' splice site (A5SS), and alternative 3' splice site (A3SS). RNA-seq counts and alternative splicing event data were provided in Supplementary Tables 4-5.

2.20 Bioinformatic Analysis

The subcellular localization of vitcylated proteins was predicted using WoLF PSORT, a subcellular localization prediction program (https://wolfpsort.hgc.jp/).[9] Gene Ontology (GO) enrichment analysis was conducted with the R package clusterProfiler (v4.6.2), and the results were visualized using enrichplot (v1.18.4).[10]

2.21 Statistical Analysis

Statistical analysis was performed with GraphPad Prism (v8.0.2). Statistical comparisons of flow cytometric data for pSTAT1 and HLA signals, as well as GAPDH enzymatic activity assay results in HEK293T cells, were performed using two-way ANOVA. For other analysis, unpaired two-tailed Student's t-test (for normally distributed data) was used to compare two conditions. Quantitative data are expressed as means ± SEM. Differences with $P < 0.05$ were considered statistically significant;

ns, not significant; * $P < 0.05$; ** $P < 0.01$; *** $P < 0.001$; **** $P < 0.0001$.

3. Supplementary Figures

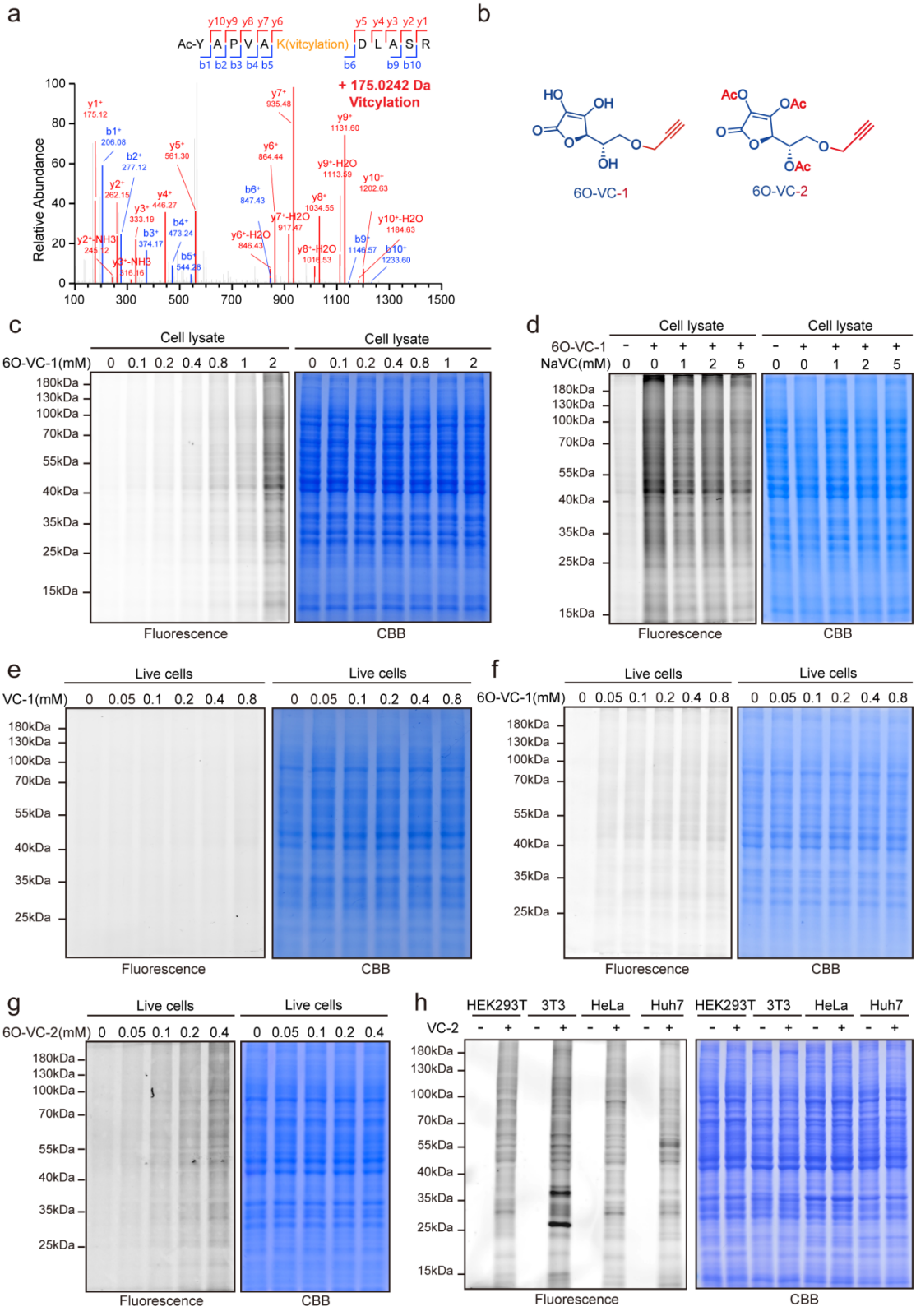


Fig. S1 Native vitamin C adduct formation and benchmarking of C6-O-propargyl

regioisomeric reporters.

a) Representative MS/MS spectrum of Ac-YAPVAKDLASR carrying the vitamin C-derived lysine modification with a mass shift of +175.0242 Da. The modified lysine is highlighted in orange, and annotated b- and y-type fragment ions support site localization.

b) Chemical structures of **6O-VC-1** and **6O-VC-2**.

c) Concentration-dependent labeling of HEK293T cell lysates by **6O-VC-1**. Lysates were treated with the indicated concentrations of **6O-VC-1** (3 h, 37°C). CBB staining served as a total-protein loading control.

d) NaVC competition of **6O-VC-1** labeling in HEK293T cell lysates. Lysates were pre-incubated with the indicated concentrations of NaVC (1 h, 37°C), followed by the addition of **6O-VC-1** for additional 3 h at 37°C.

e) Direct treatment of intact HEK293T cells with **VC-1** for 1 h produced minimal detectable labeling across the tested concentration range. Fluorescence labeling was detected after CuAAC with TAMRA-azide, and CBB staining served as a total-protein loading control.

f) Direct treatment of intact HEK293T cells with **6O-VC-1** for 1 h produced limited labeling across the tested concentration range. Fluorescence labeling was detected after CuAAC with TAMRA-azide, and CBB staining served as a total-protein loading control.

g) Concentration-dependent labeling of intact HEK293T cells by the O-acetylated C6-O pro-probe **6O-VC-2** for 1 h.

h) **VC-2**-derived (200 μM, 1 h) protein labeling in HEK293T, NIH/3T3, HeLa, and Huh7 cells under matched treatment conditions. Fluorescence labeling was detected by CuAAC with TAMRA-azide, and CBB staining served as a total-protein loading control.

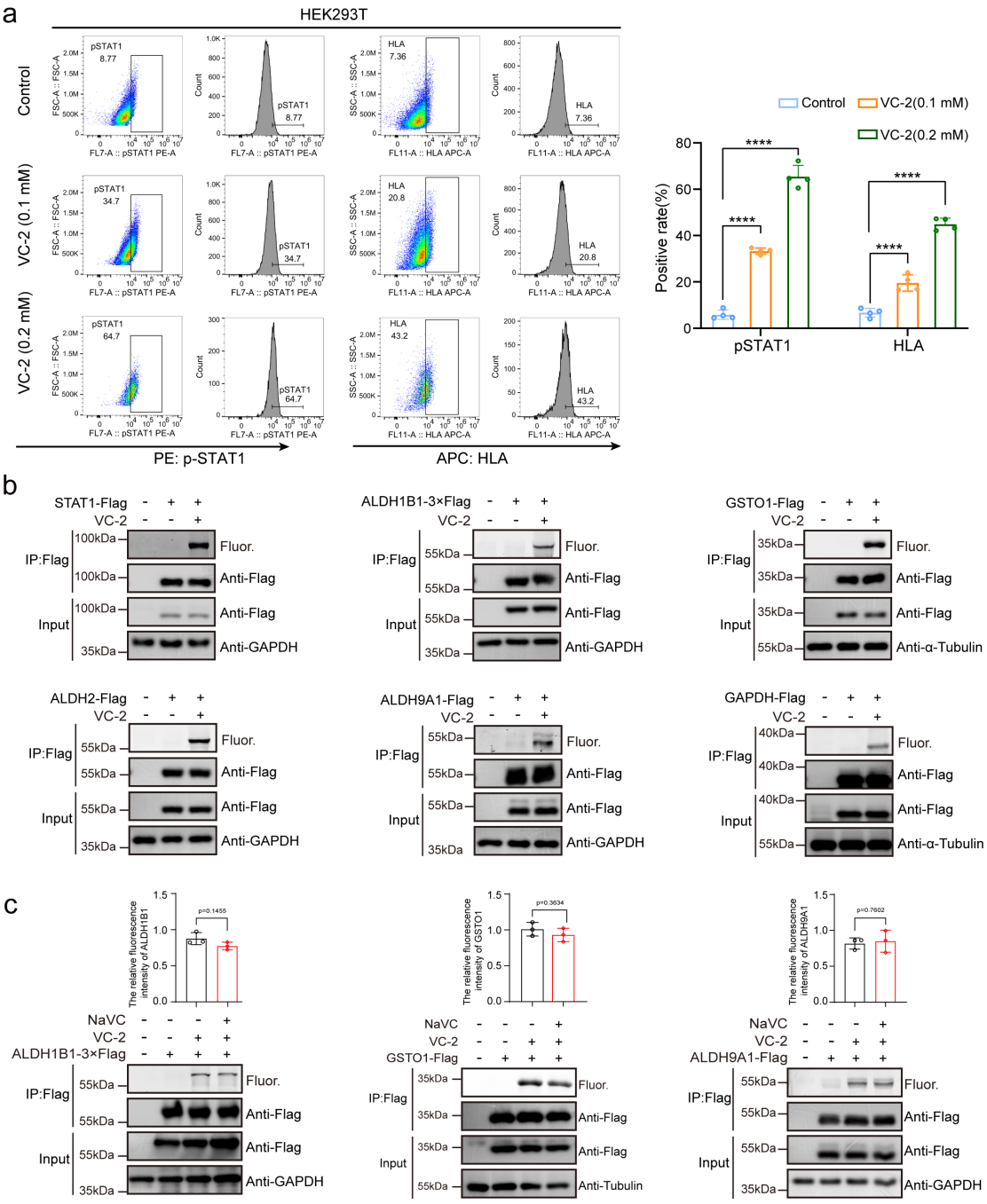


Fig. S2 Functional and biochemical analyses of representative VC-probe-enriched candidates.

a) Flow-cytometric analysis of pSTAT1 and HLA signals in HEK293T cells treated with DMSO, 0.1 mM **VC-2**, or 0.2 mM **VC-2**. Representative flow-cytometry plots and quantification of positive cells are shown. Data are presented as mean ± SEM from three independent biological replicates. Statistical significance was evaluated using Two-way ANOVA. Differences with $P < 0.05$ were considered statistically significant, **** $P < 0.0001$.

b) Immunoprecipitation-coupled fluorescence validation of representative VC-probe-enriched candidate proteins. HEK293T cells expressing the indicated Flag-tagged proteins were treated with 200 μM **VC-2** for 1 h, followed by anti-Flag immunoprecipitation, CuAAC with TAMRA-azide, and in-gel fluorescence analysis. Anti-Flag immunoblots show immunoprecipitated and input protein levels. Representative blots from three independent experiments are shown

c) Vitamin C competition of **VC-2**-derived labeling for selected candidate proteins. HEK293T cells expressing the indicated Flag-tagged proteins were treated with **VC-2** (200 μM, 1 h) in the absence or presence of excess NaVC (4 mM, 16 h) followed by anti-Flag immunoprecipitation, on-beads CuAAC with TAMRA-azide, and in-gel fluorescence analysis. Fluorescent signals were normalized to the immunoprecipitated protein signal. Data are shown as mean ± SEM from three independent biological replicates. *P* values are indicated above the bar graphs and were calculated using unpaired two-tailed Student's t-test.

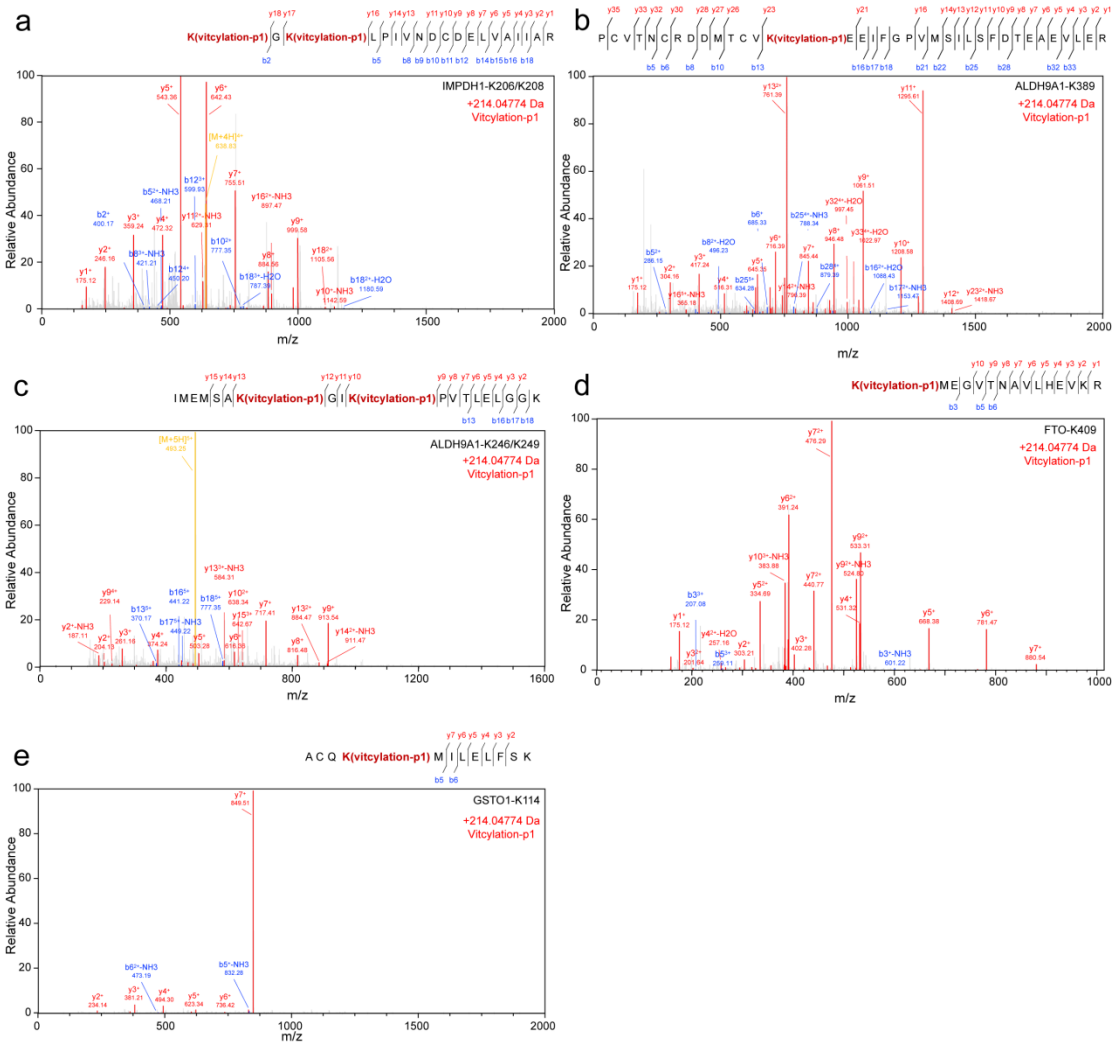
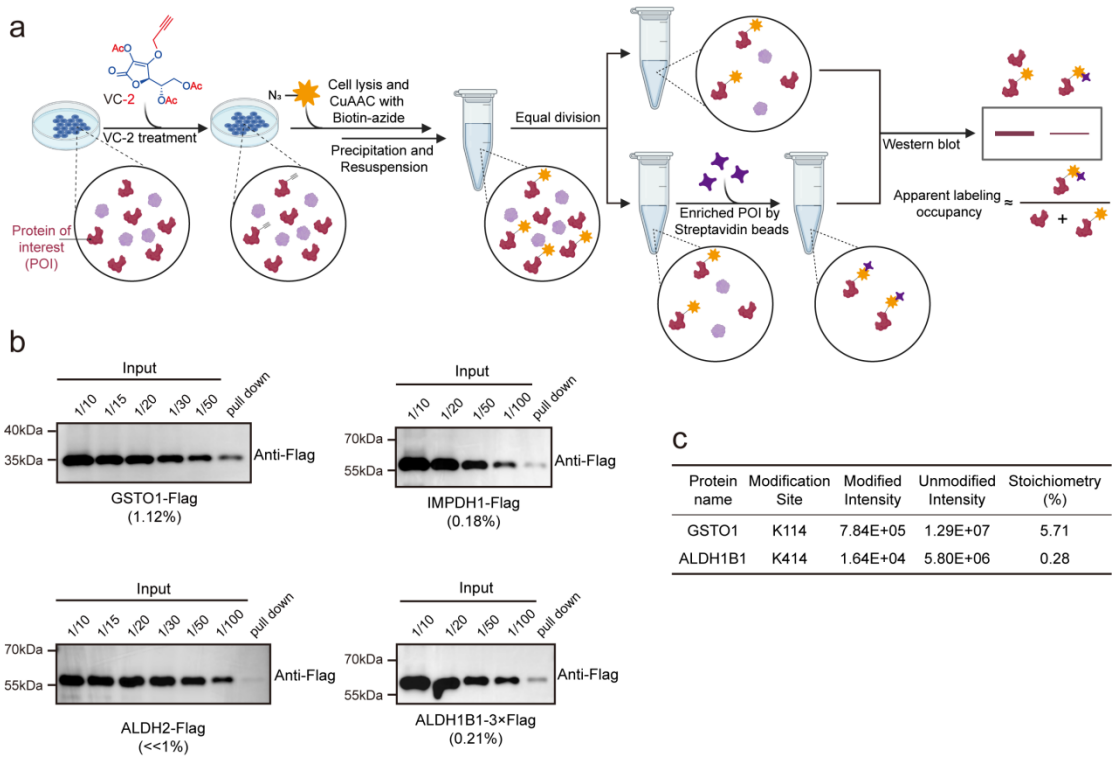


Fig. S3 Site-level LC-MS/MS identification of VC-reporter-derived lysine adducts on representative candidate proteins.

a-e) Representative MS/MS spectra of VC-probe modified peptides are shown for: a) IMPDH1 Lys206/Lys208; b) ALDH9A1 Lys389; c) ALDH9A1 Lys246/Lys249; d) FTO Lys409; and e) GSTO1 Lys114, identified in VC-2-treated HEK293T cells expressing the indicated FLAG-tagged proteins The modified lysines are highlighted in red, and annotated b- and y-type fragment ions support site localization. The database-search variable modification originally designated “Vitcylation-p1” corresponds to a VC-reporter-derived lysine adduct with a mass shift of +214.0477 Da.



c

Protein name	Modification Site	Modified Intensity	Unmodified Intensity	Stoichiometry (%)
GSTO1	K114	7.84E+05	1.29E+07	5.71
ALDH1B1	K414	1.64E+04	5.80E+06	0.28

Fig. S4 Apparent occupancy analysis of representative VC-probe-enriched candidates.

a) Workflow for estimating apparent protein-level labeling occupancy. After **VC-2** (200 μM) labeling and CuAAC with biotin-azide, samples were divided into serially diluted input fractions and a streptavidin-enriched fraction. Western blot signals from the enriched fraction were compared with serial input dilutions to estimate the fraction of each protein population carrying at least one VC-probe-derived adduct. Workflow created with BioRender.com.

b) Apparent protein-level labeling occupancy of representative candidates in HEK293T cells.

c) MS based direct quantification of modification stoichiometry for GSTO1 and ALDH1B1.

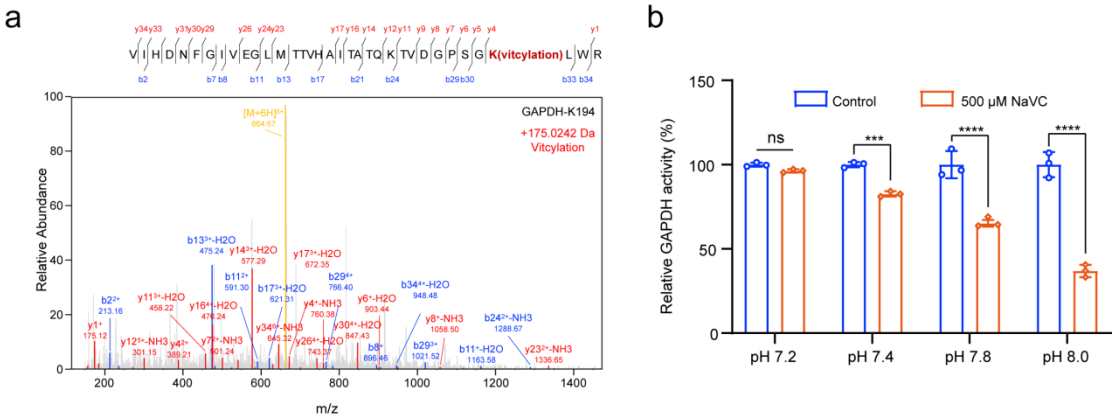


Fig. S5 LC-MS/MS identification and impact of the Vitamin C on GAPDH.

a) Representative MS/MS spectrum of GAPDH carrying the vitamin C-derived lysine modification with a mass shift of +175.0242 Da. The modified lysine is highlighted in red, and annotated b- and y-type fragment ions support site localization.

b) Effect of 500 μM NaVC treatment on GAPDH enzymatic activity under the indicated pH conditions. Data are shown as mean ± SEM from three independent experiments. Statistical significance was evaluated using Two-way ANOVA. Differences with $P < 0.05$ were considered statistically significant. ns, not significant; *** $P < 0.001$; **** $P < 0.0001$.

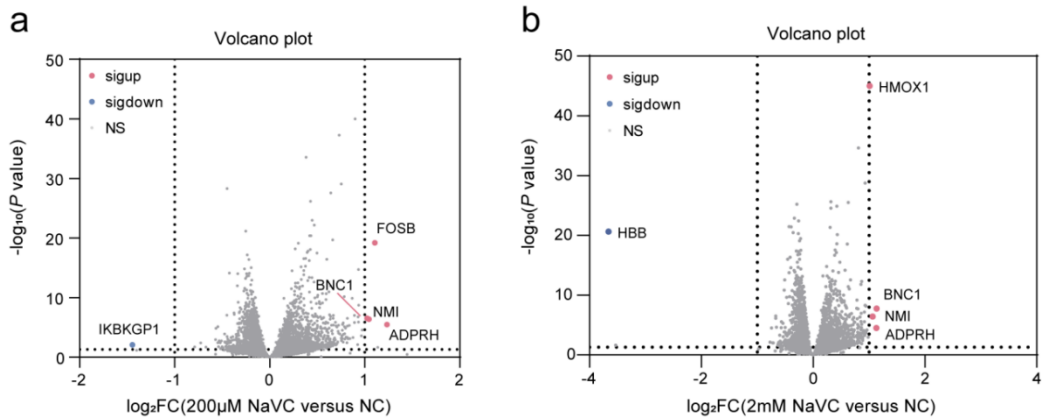


Fig. S6 Volcano plots of differentially expressed genes (DEGs) from RNA-seq analysis of HEK293T cells treated with NaVC for 12 h.

a) NaVC (200 μM) versus H_2O control; **b)** NaVC (2 mM) versus H_2O control. Genes with a fold change ≥ 2 and a *P* value < 0.05 are considered significantly differentially expressed. *P* values from DESeq2 Wald test were corrected by Benjamini-Hochberg (FDR).

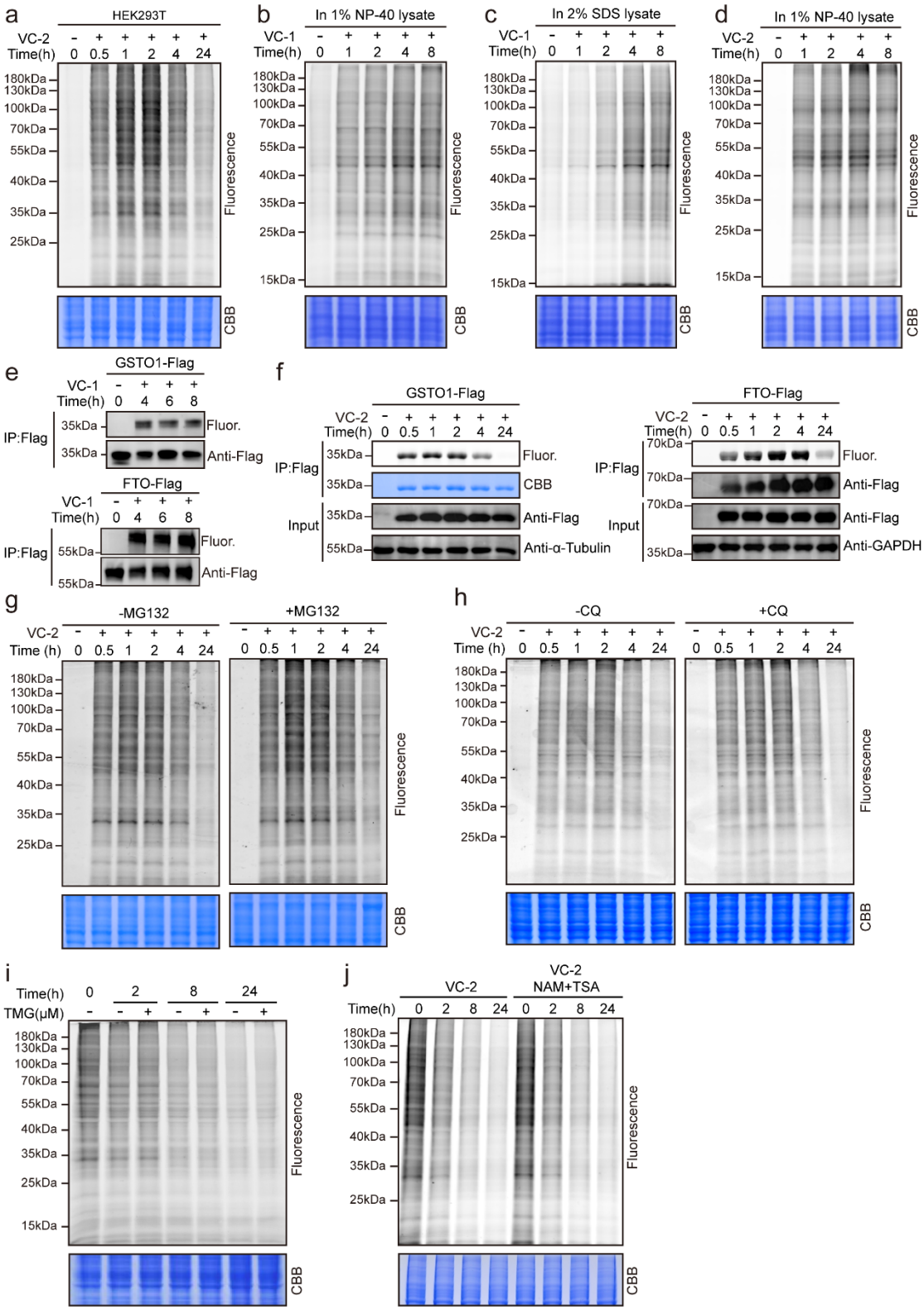


Fig. S7 Characterization of VC-2-derived labeling dynamics.

a) Time-dependent protein labeling with **VC-2** (200 μM) in HEK293T cells.

b–c) Stability of **VC-1** labeling in HEK293T cell lysates under native and denaturing conditions. HEK293T cell lysates were incubated with **VC-1** in b) 1% NP-40 or c) 2%

SDS-containing buffers for the indicated times at 37 °C.

d) Time-dependent **VC-2** labeling in HEK293T cell lysates.

e–f) Stability of **VC-1** (1 mM) or **VC-2**-derived (200 μM) labeling e) *in vitro* or f) in-cell from HEK293T cells expressing the indicated Flag-tagged proteins.

g–h) Effect of proteasomal/lysosomal inhibition on **VC-2**-derived labeling dynamics. HEK293T cells were treated with **VC-2** (200 μM) alone or HEK293T cells were pre-treated with g) MG132 (10 μM) or h) CQ (25 μM) for 2 h, followed by co-incubation with VC-2 (200 μM) for the indicated times.

i) Effect of the O-GlcNAcase inhibitor Thiamet G (TMG) on **VC-2**-derived labeling dynamic. After labeling with **VC-2** (200 μM, 1h), HEK293T cells were washed and treated for the indicated durations in the presence or absence of TMG (20 μM).

j) Effect of HDAC/sirtuin inhibition using trichostatin A (TSA) and nicotinamide (NAM) on **VC-2**-derived labeling dynamics. After labeling with **VC-2** (200 μM), HEK293T cells were washed and treated for the indicated durations in the presence or absence of TSA (0.4 μM) and NAM (2 mM).

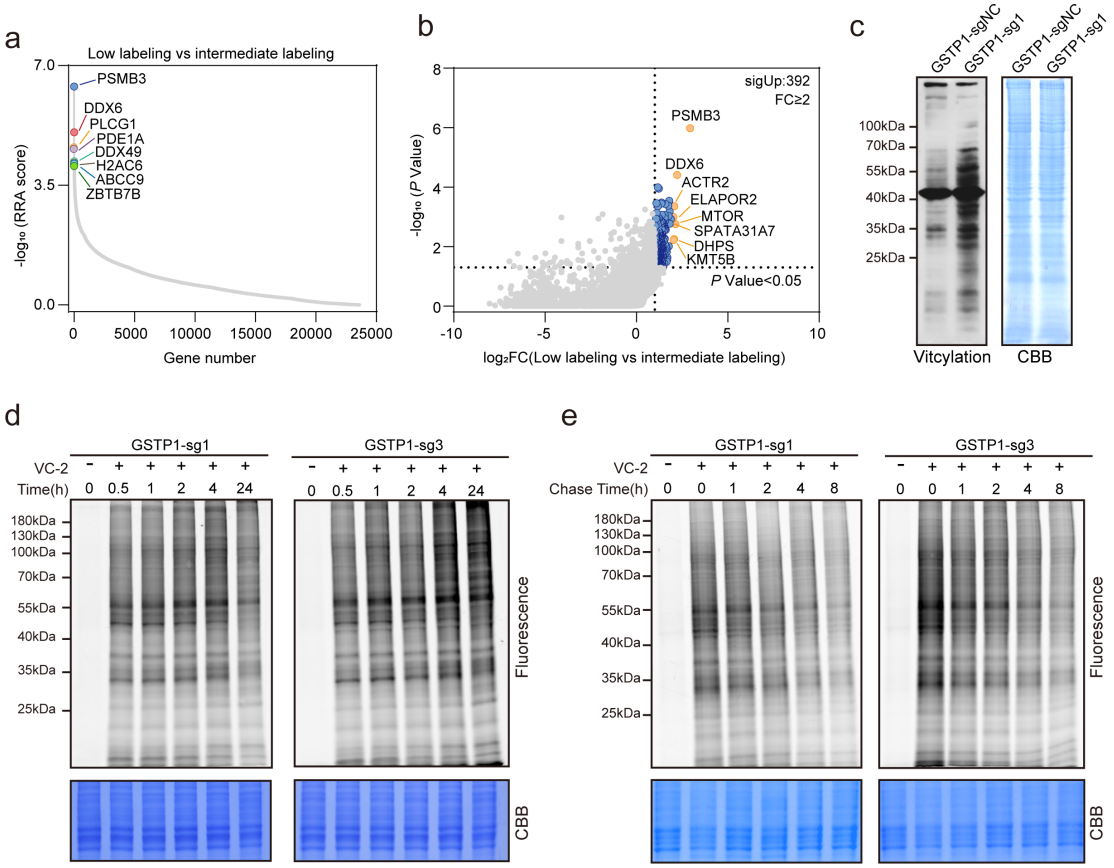


Fig. S8 CRISPR screen and GSTP1-dependent regulation of VC-2-derived labeling dynamics.

a) Robust rank aggregation (RRA) analysis of genes enriched in the low labeling population.

b) Volcano plot showing CRISPR screening hits from the low-labeling population. The x-axis represents gene-level $\log_2$ fold change (LFC) of low labeling versus unchanged populations. The y-axis shows the $-\log_{10}(P \text{ value})$ as calculated by MAGeCK.

c) GSTP1 knockout increases vitcylation levels of Huh7 cells, as detected by an in-house generated pan-vitcyllysine antibody.

d) Time-dependent protein labeling with **VC-2** (200 μM) in *GSTP1* KO Huh7 cells.

e) Pulse-and-chase analysis of vitcylation dynamics in *GSTP1* KO Huh7 cells.

4. Supplementary Tables

Table S1. Protein-level database-search and quantitative output from the **VC-1** chemoproteomics experiment. All database search information is listed. See the associated excel file.

Table S2. Protein-level database-search and quantitative output from the **VC-2** chemoproteomics experiment. All database search information is listed. See the associated excel file.

Table S3. GO enrichment analysis of vitcylated proteins. See the associated excel file.

Table S4. RNAseq counts. All database search information is listed. See the associated excel file.

Table S5. Vitamin C-dependent alternative splicing events. All database search information is listed. See the associated excel file.

Table S6. GO enrichment analysis of alternatively spliced transcripts. See the associated excel file.

Table S7. CRISPR results (TOP VS Middle). All database search information is listed. See the associated excel file.

Table S8. CRISPR results (Bottom VS Middle). All database search information is listed. See the associated excel file.

Table S9. Primer list. See the associated excel file.

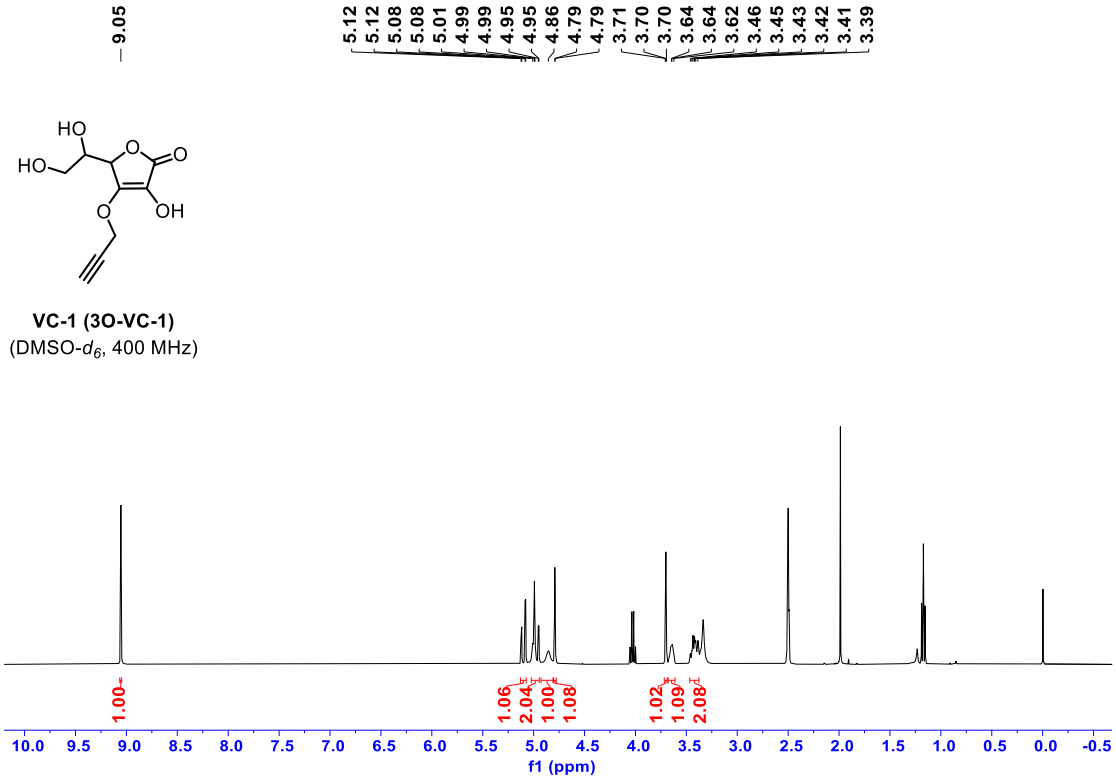
5. Source Data

Source Data Figure. Unprocessed western blots and/or gels. See the associated PDF file.

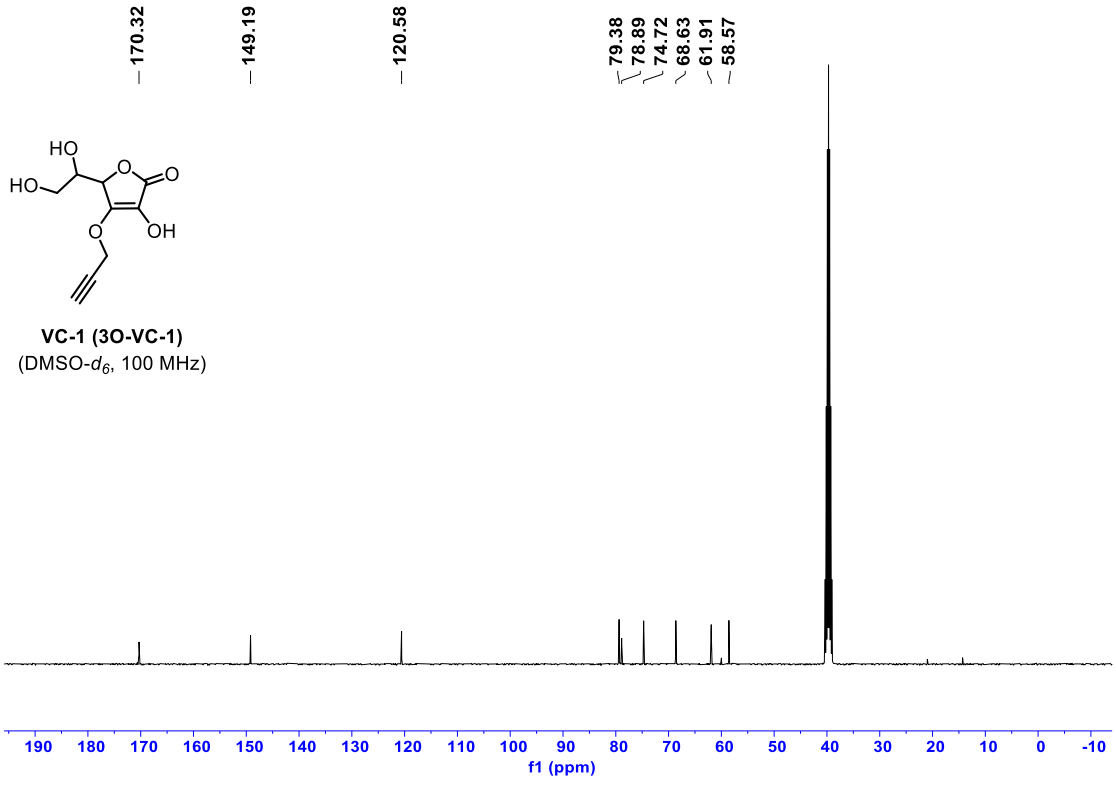
Statistical Source Data. See the associated excel file.

6. NMR Spectra, HPLC and HRMS Reports

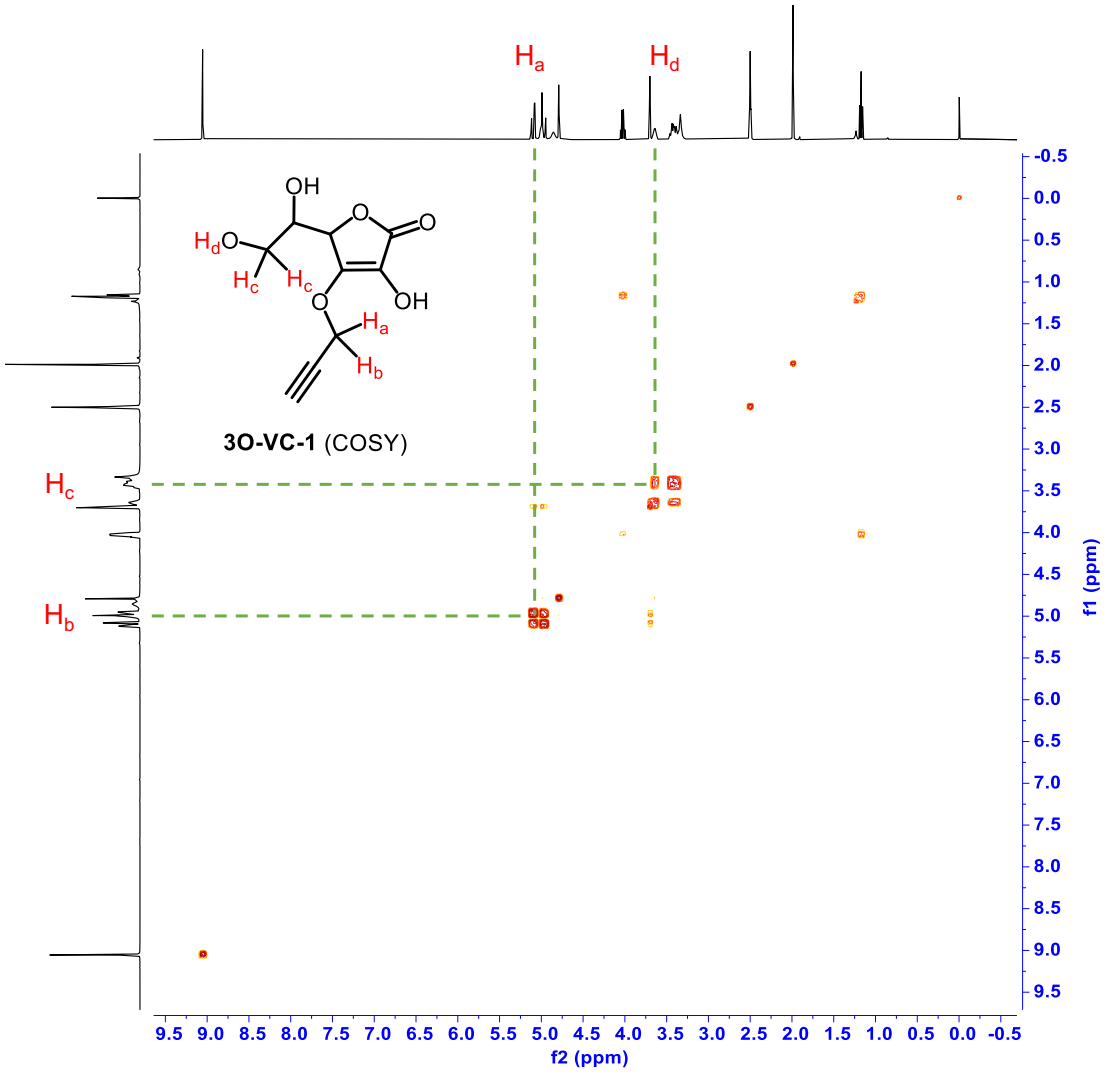
6.1 NMR Spectra

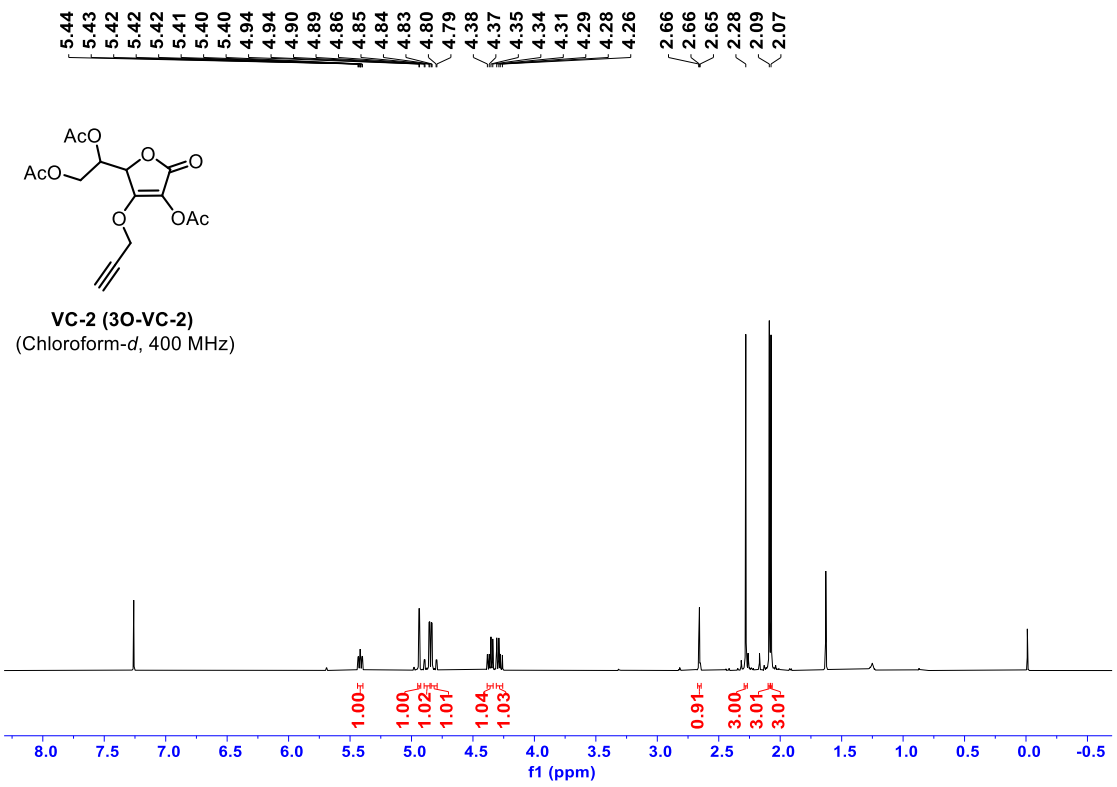


VC-1 (3O-VC-1)
(DMSO-d_6, 400 MHz)

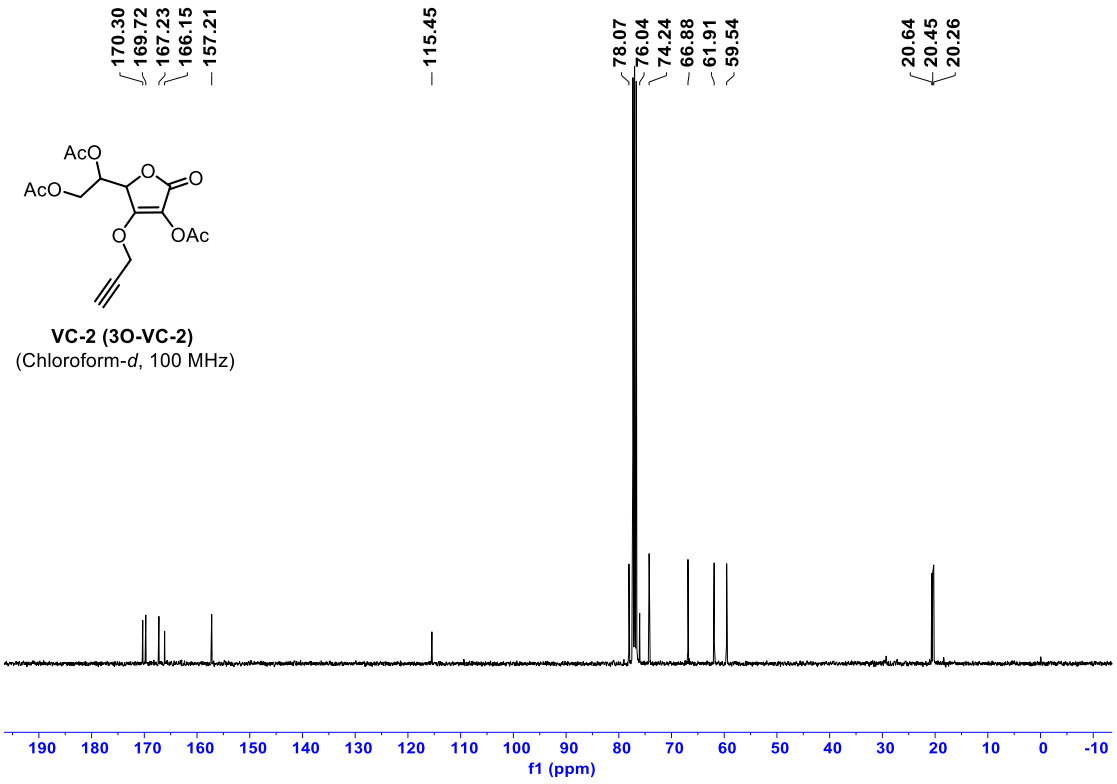


VC-1 (3O-VC-1)
(DMSO-d_6, 100 MHz)

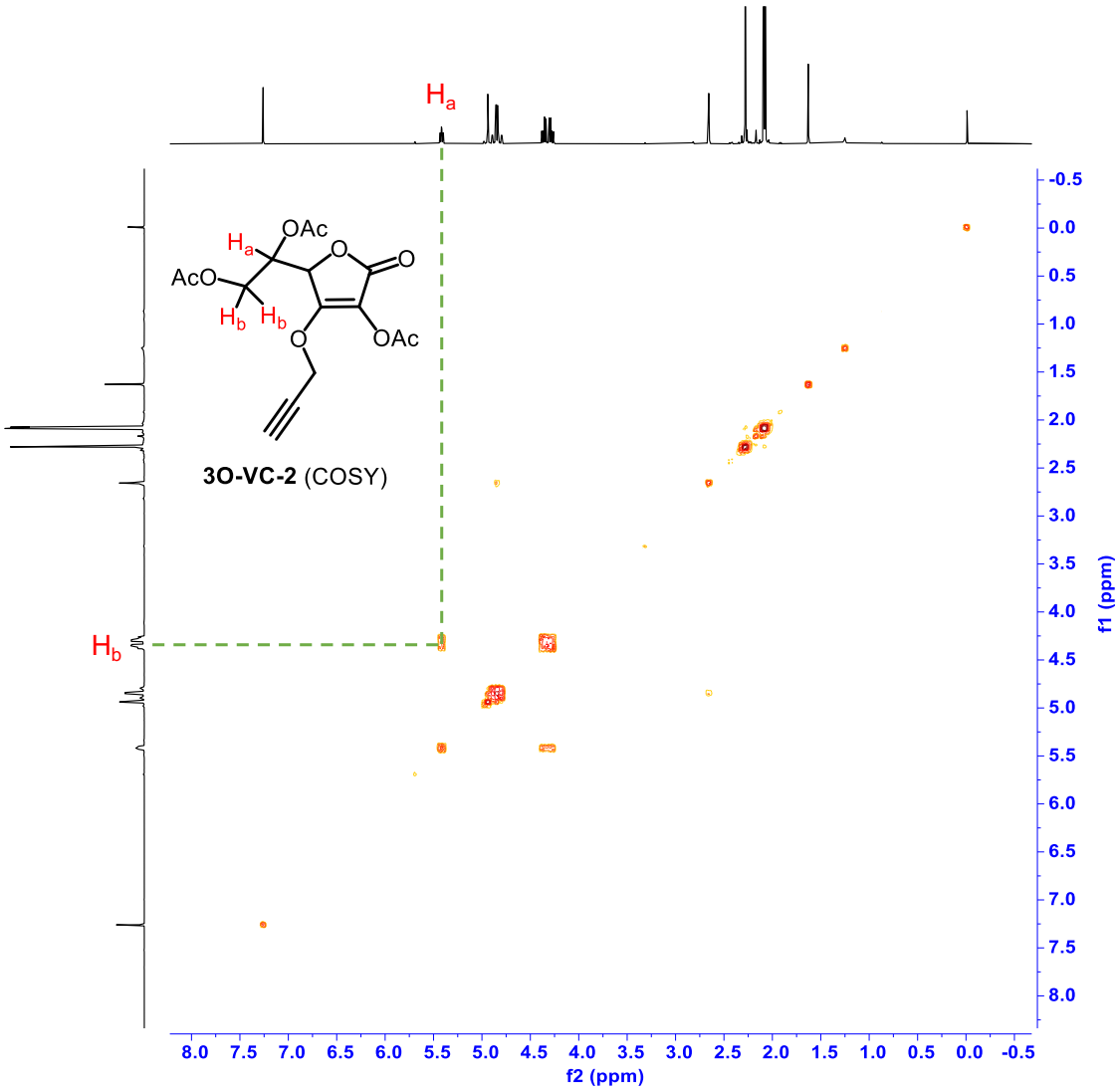

Ha
Hd
OH
O
O
Hd
O
Hc
Hc
OH
O
Ha
Hb
3O-VC-1 (COSY)
Hc
Hb
-0.5
0.0
0.5
1.0
1.5
2.0
2.5
3.0
3.5
4.0
4.5
5.0
5.5
6.0
6.5
7.0
7.5
8.0
8.5
9.0
9.5
f1 (ppm)
9.5 9.0 8.5 8.0 7.5 7.0 6.5 6.0 5.5 5.0 4.5 4.0 3.5 3.0 2.5 2.0 1.5 1.0 0.5 0.0 -0.5
f2 (ppm)

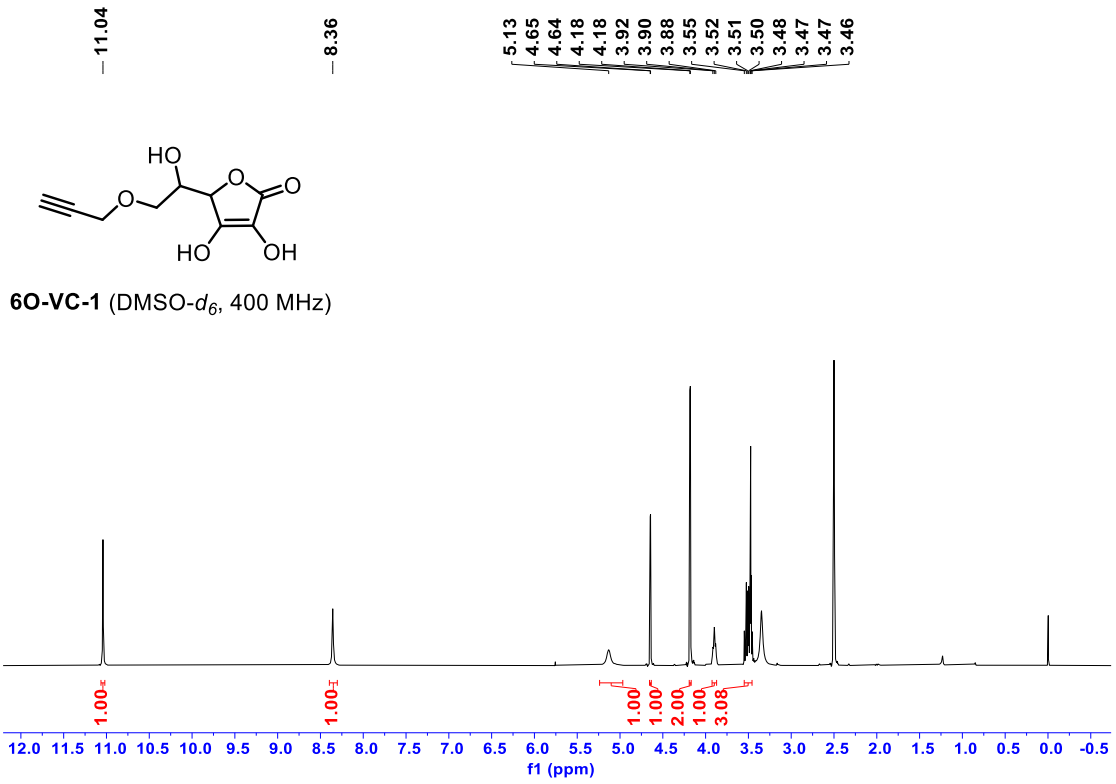


VC-2 (3O-VC-2)
(Chloroform-*d*, 400 MHz)

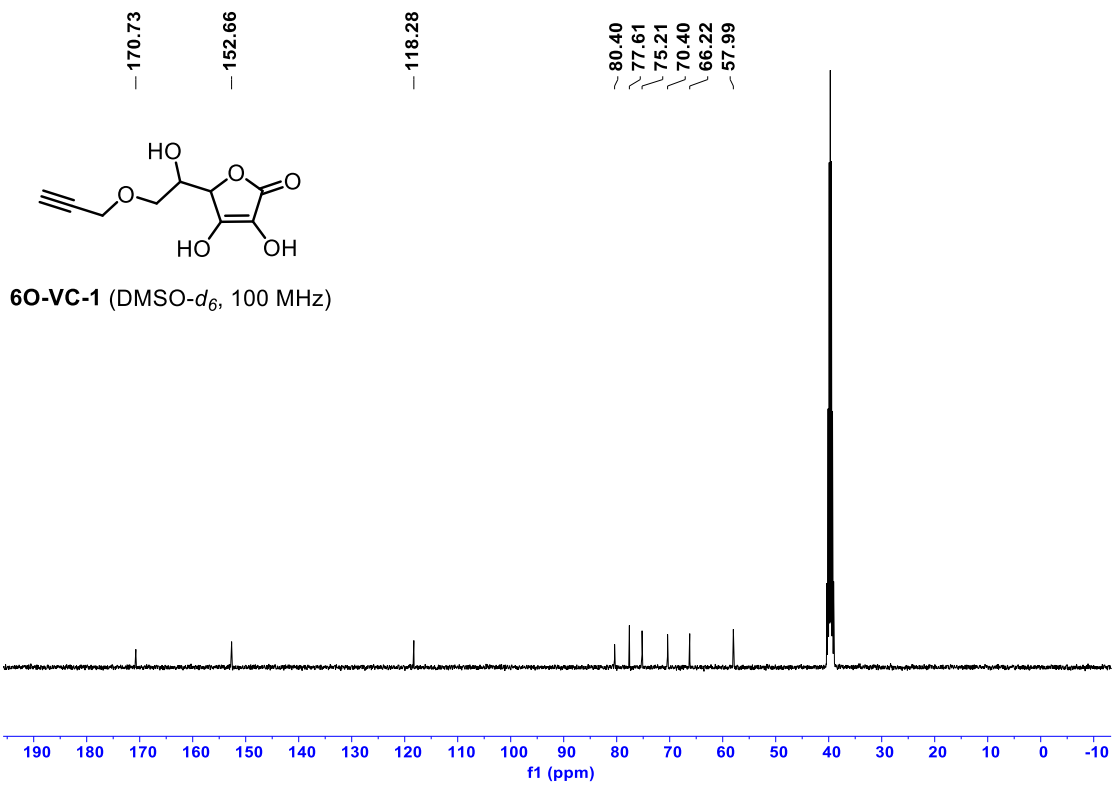


VC-2 (3O-VC-2)
(Chloroform-*d*, 100 MHz)

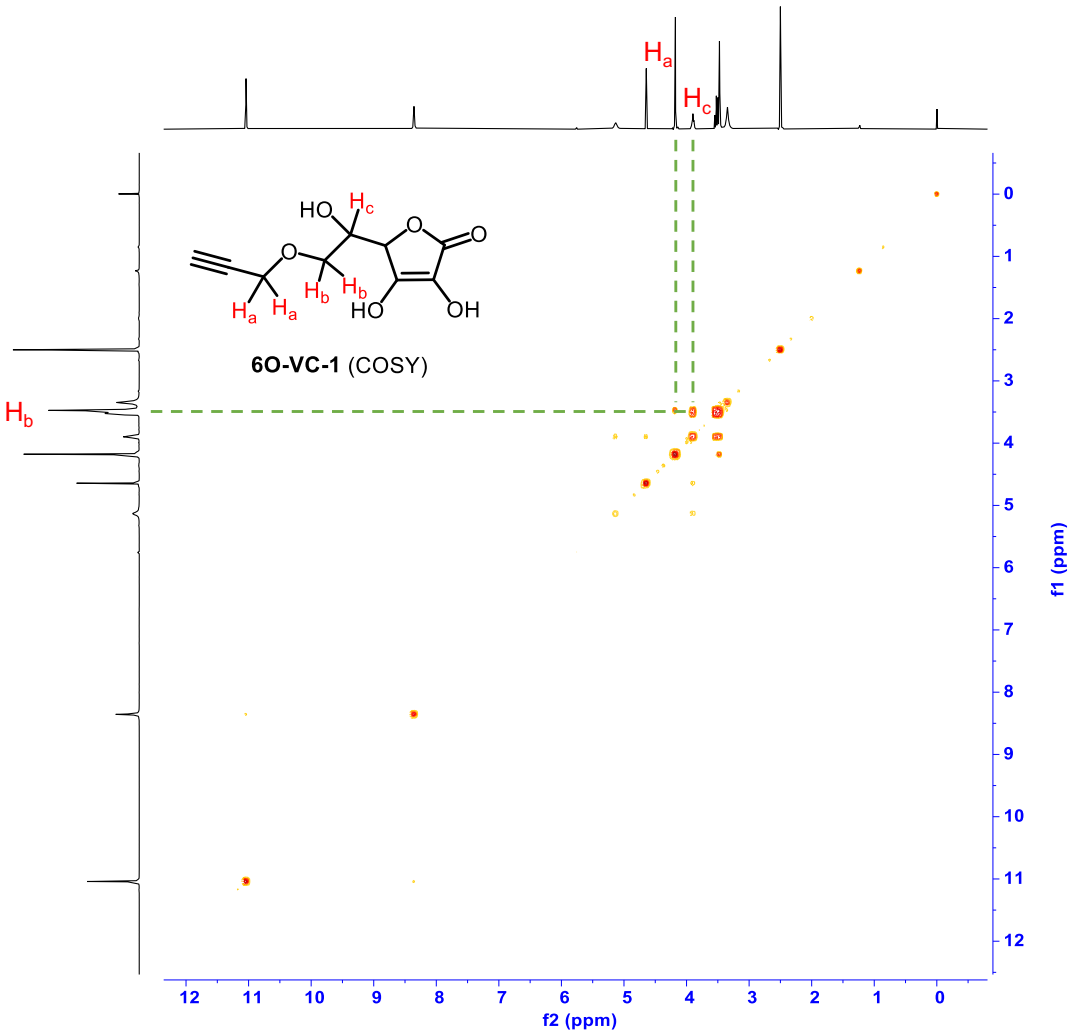

Ha
Hb
OAc
AcO
Ha
Hb Hb
O
O
O
OAc
3O-VC-2 (COSY)
f1 (ppm)
f2 (ppm)
-0.5 0.0 0.5 1.0 1.5 2.0 2.5 3.0 3.5 4.0 4.5 5.0 5.5 6.0 6.5 7.0 7.5 8.0
8.0 7.5 7.0 6.5 6.0 5.5 5.0 4.5 4.0 3.5 3.0 2.5 2.0 1.5 1.0 0.5 0.0 -0.5

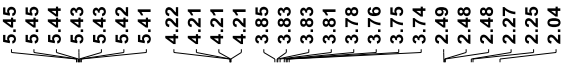


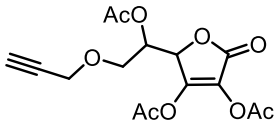
6O-VC-1 (DMSO-d_6, 400 MHz)



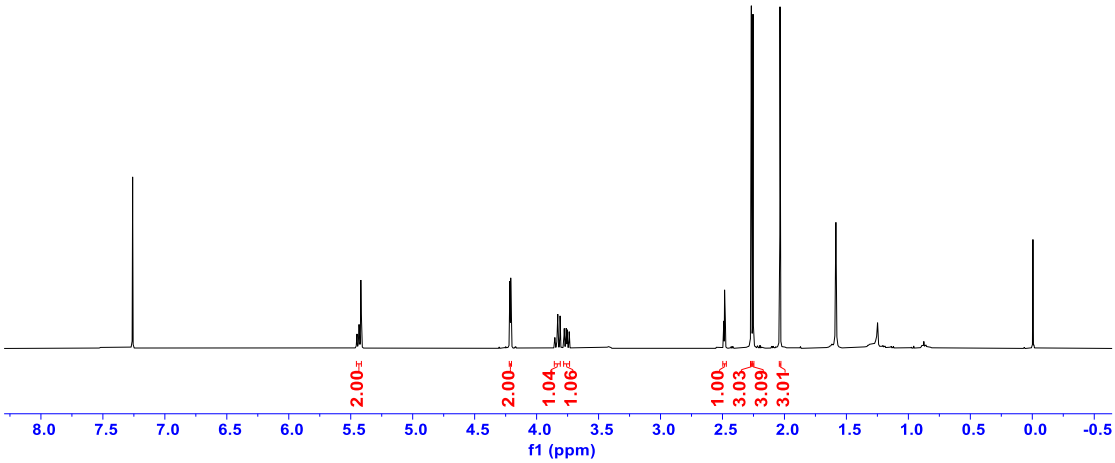
6O-VC-1 (DMSO-d_6, 100 MHz)


Ha
Hc
HO
Hc
O
O
O
Hb
Hb
Ha
Ha
HO
OH
6O-VC-1 (COSY)
Hb
f1 (ppm)
f2 (ppm)
0
1
2
3
4
5
6
7
8
9
10
11
12

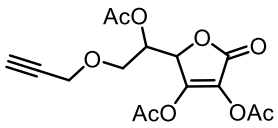




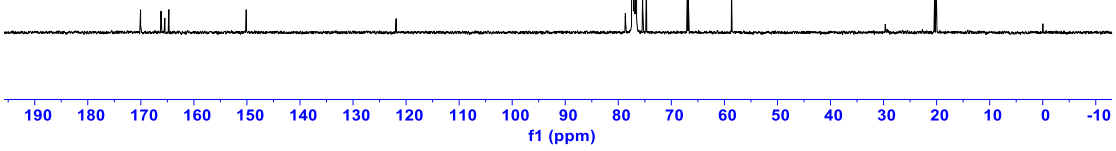
6O-VC-2 (Chloroform-*d*, 400 MHz)

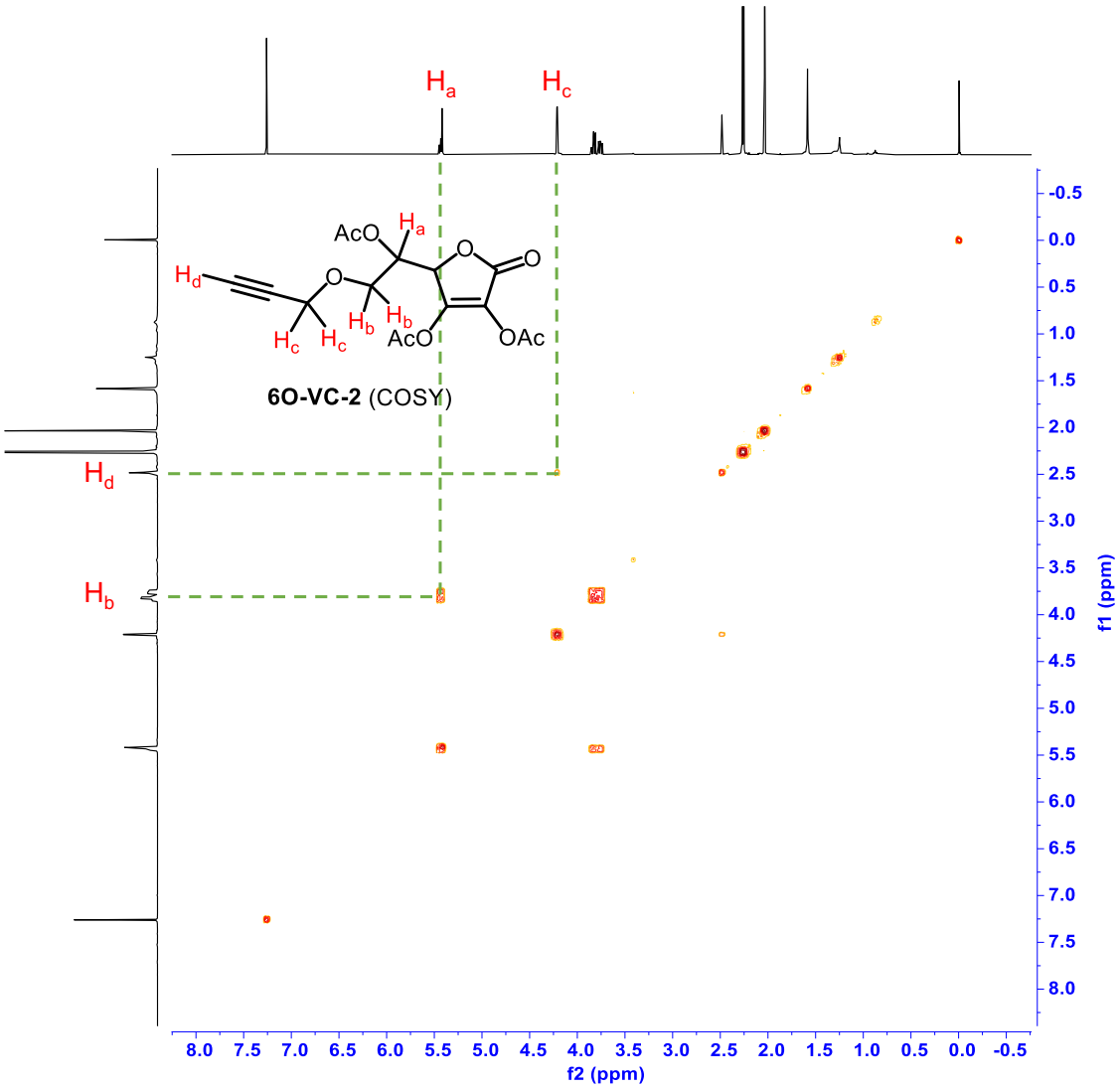






6O-VC-2 (Chloroform-*d*, 100 MHz)

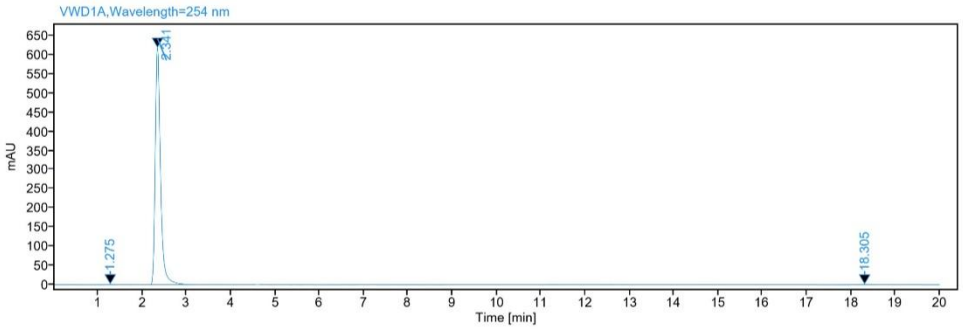



Ha
Hc
AcO
Ha
Hd
O
O
Hb
Hb
Hc
Hc
AcO
OAc
6O-VC-2 (COSY)
Hd
Hb
f1 (ppm)
f2 (ppm)

6.2 HPLC and HRMS Analysis Reports

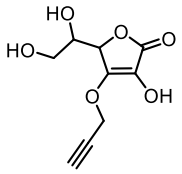
Single Injection Report

Data file:	3O-VC1.dx		
Sequence Name:	SingleSample	**Project Name:**	Entrust
Sample name:	3O-VC1	**Operator:**	admin
Instrument:	HPLC-1260-2	**Injection date:**	2026-07-10 17:36:48+08:00
Inj. volume:	2.000	**Location:**	P1-C3
Acq. method:	For.all_03.amx	**Type:**	Sample
Processing method:	3D UV Quantitative_DefaultMethod(MAX).pmx	**Sample amount:**	0.00
Manually modified:	None		



Signal: VWD1A,Wavelength=254 nm

RT [min]	Type	Width [min]	Area	Height	Area%	Name
1.275	BB	0.39	10.36	1.32	0.20	
2.341	BB	1.14	5101.83	618.63	99.37	
18.305	BB	1.40	21.95	0.88	0.43	
		Sum	**5134.14**			

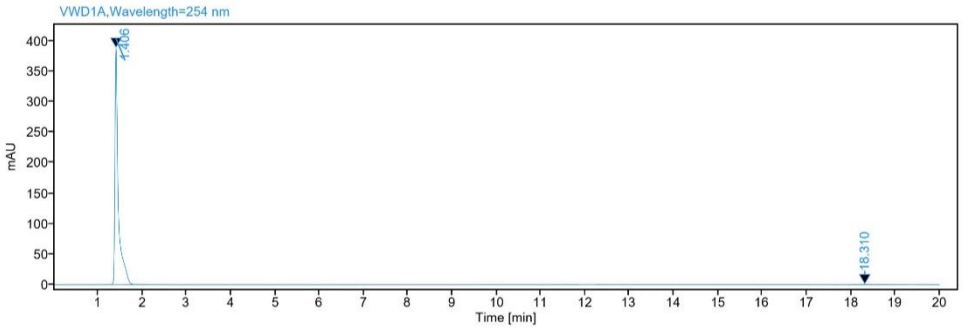


VC-1 (3O-VC-1)
HPLC purity: 99%

/Entrust/Report Templates/Short_Area.rdl [Rev. 42] Printed: 2026-07-10 18:37:57+08:00 Page 1 of 1

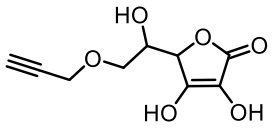
Single Injection Report

Data file:	6O-VC1..dx		
Sequence Name:	SingleSample	**Project Name:**	Entrust
Sample name:	6O-VC1.	**Operator:**	admin
Instrument:	HPLC-1260-2	**Injection date:**	2026-07-10 18:18:24+08:00
Inj. volume:	3.000	**Location:**	P1-C4
Acq. method:	For.all_03.amx	**Type:**	Sample
Processing method:	3D UV Quantitative_DefaultMethod(MAX).pmx	**Sample amount:**	0.00
Manually modified:	None		



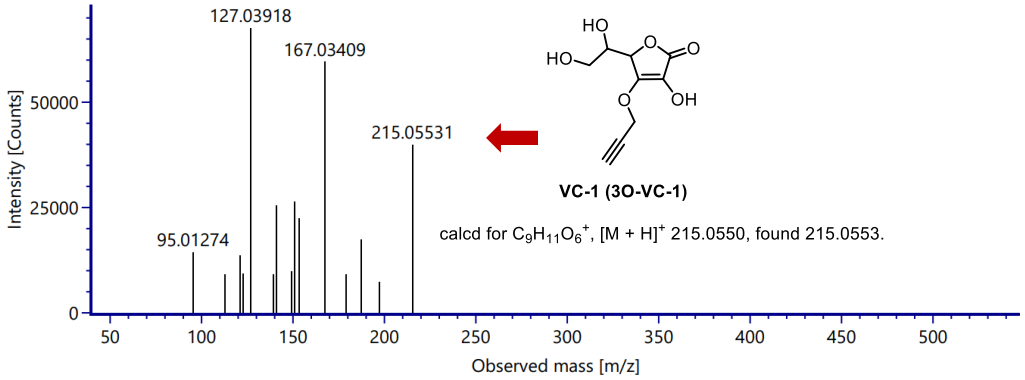
Signal: VWD1A,Wavelength=254 nm

RT [min]	Type	Width [min]	Area	Height	Area%	Name
1.406	VB	0.87	2066.46	388.62	99.06	
18.310	BB	1.40	19.65	0.77	0.94	
		Sum	**2086.11**			

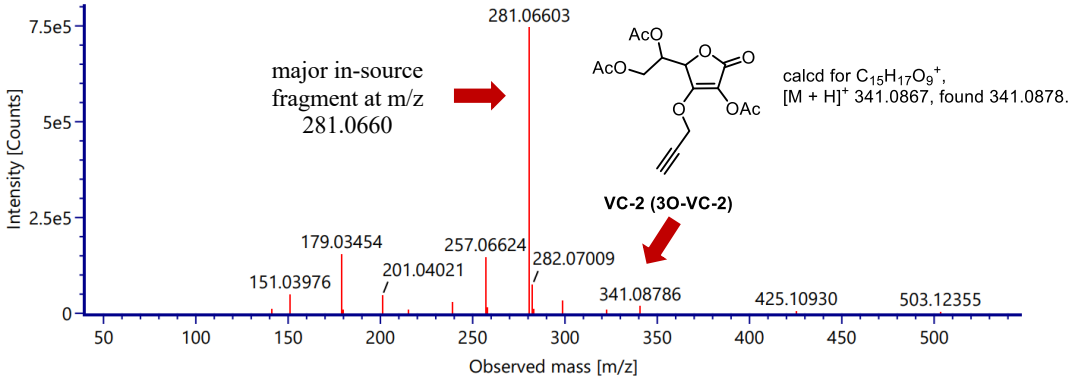


6O-VC-1
HPLC purity: 99%

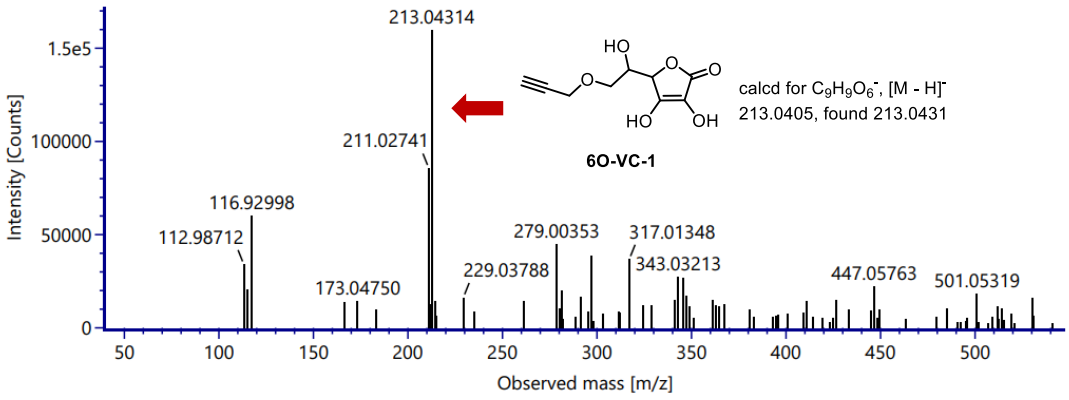
Item name: 3O-VC1-APCI **Channel name: Low energy : Time 1.4440 +/- 0.0598 minutes**



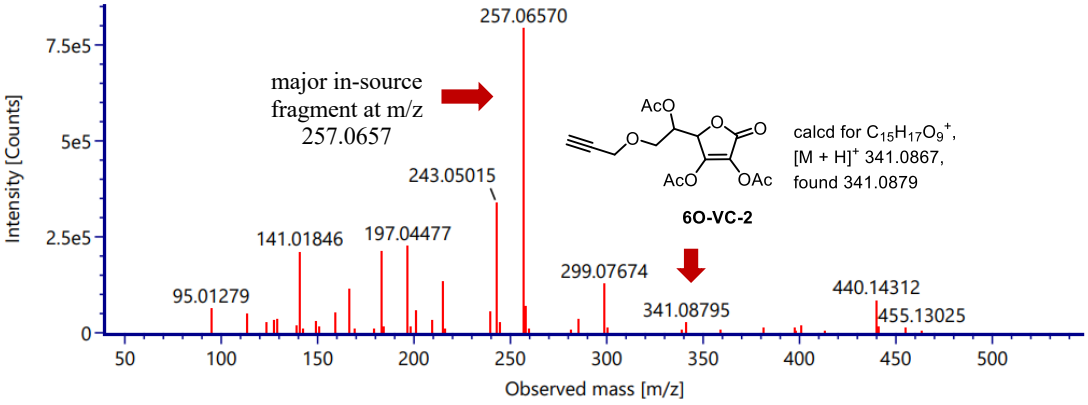
Item name: 3O-VC2-APCI **Channel name: Low energy : Time 5.4255 +/- 0.0571 minutes**



Item name: 6O-VC1-ESI- **Channel name: Low energy : Time 1.8832 +/- 0.0666 minutes**



Item name: 6O-VC3-50ug-APCI **Channel name: Low energy : Time 5.1831 +/- 0.0794 minutes**



7. Reference

[1] E. H. Bowler-Barnett, J. Fan, J. Luo, M. Magrane, M. J. Martin, S. Orchard, "UniProt and mass spectrometry-based proteomics—a 2-way working relationship" *Mol. Cell. Proteom. : MCP* **2023**, *22*, 100591.

[2] B. Wang, M. Wang, W. Zhang, T. Xiao, C.-H. Chen, A. Wu, F. Wu, N. Traugh, X. Wang, Z. Li, S. Mei, Y. Cui, S. Shi, J. J. Lipp, M. Hinterndorfer, J. Zuber, M. Brown, W. Li, X. S. Liu, "Integrative analysis of pooled CRISPR genetic screens using MAGeCKFlute" *Nat. Protoc.* **2019**, *14*, 756–780.

[3] W. Li, H. Xu, T. Xiao, L. Cong, M. I. Love, F. Zhang, R. A. Irizarry, J. S. Liu, M. Brown, X. S. Liu, "MAGeCK enables robust identification of essential genes from genome-scale CRISPR/Cas9 knockout screens" *Genome Biol.* **2014**, *15*, 554.

[4] S. W. Wingett, S. Andrews, "FastQ screen: a tool for multi-genome mapping and quality control" *F1000Research* **2018**, *7*, 1338.

[5] S. Chen, Y. Zhou, Y. Chen, J. Gu, "fastp: an ultra-fast all-in-one FASTQ preprocessor" *Bioinformatics* **2018**, *34*, i884–i890.

[6] D. Kim, B. Langmead, S. L. Salzberg, "HISAT: A fast spliced aligner with low memory requirements" *Nat Methods* **2015**, *12*, 357–360.

[7] P. Danecek, J. K. Bonfield, J. Liddle, J. Marshall, V. Ohan, M. O. Pollard, A. Whitwham, T. Keane, S. A. McCarthy, R. M. Davies, H. Li, "Twelve years of SAMtools and BCFtools" *Gigascience* **2021**, *10*, giab008.

[8] M. I. Love, W. Huber, S. Anders, "Moderated estimation of fold change and dispersion for RNA-seq data with DESeq2" *Genome Biol.* **2014**, *15*, 550.

[9] P. Horton, K.-J. Park, T. Obayashi, N. Fujita, H. Harada, C. J. Adams-Collier, K. Nakai, "WoLF PSORT: protein localization predictor" *Nucleic Acids Res.* **2007**, *35*, W585–W587.

[10] G. Yu, L.-G. Wang, Y. Han, Q.-Y. He, "clusterProfiler: An R package for comparing biological themes among gene clusters" *OMICS* **2012**, *16*, 284–287.